Journal of Materials Chemistry A

Accepted Manuscript

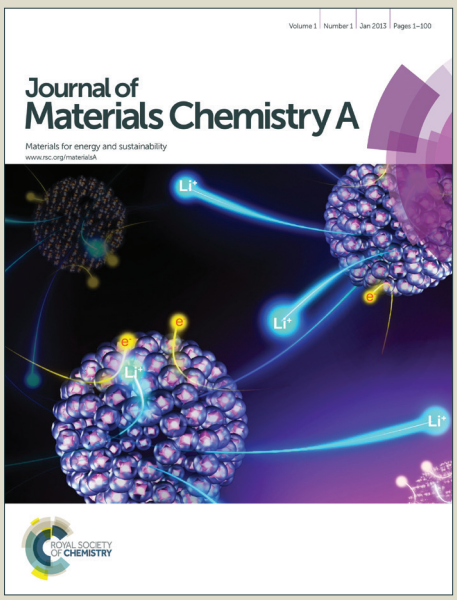

ROYAL SOCIETY OF CHEMISTRY

www.rsc.org/materialsA

Emerging trends in superhydrophobic surface based magnetic materials: fabrications and their potential applications

Saravanan Nagappan and Chang-Sik Ha*

Department of Polymer Science and Engineering, Pusan National University, Busan 609-735, Republic of Korea.

* Tel.: +82-10-48441-7066; Fax: +82-51-514-4331; E-mail: csha@pnu.edu

Abstract

Superhydrophobic surfaces have become an emerging field over the last few decades. Recently, these surfaces have attracted considerable attention in wide variety of applications due to the smart and self-cleaning ability of the surface. On the other hand, the switchable surface properties, self-healing and robust mechanism for mechanical abrasion make these superhydrophobic surfaces more reliable for practical applications and commercialisation in coating industries. More recently, superhydrophobic surfaces induced by magnetic fields or magnetic particles have also emerged as new area for a range of applications, such as oil spill capture and separation, catalysis, sensors, liquid marbles type microfluidic devices, magnetic resonance imaging (MRI) contrast agents, and superhydrophobic magnetic fluids. This review covers the fabrications of superhydrophobic surface based magnetic materials (SSBMMs), such as superhydrophobic magnetic surfaces, nanoparticles, liquid marbles, sponges and foams, bulk materials, aerogels, fabrics and papers, elastomer actuators, micro-fluids, anisotropic particles (tri-patch magnetic supraparticles), and their past, present and future applications.

Saravanan Nagappan received his B. Sc in Chemistry (2006, Madras University, Chennai, India), M.Sc in Chemistry (2008, Thiruvalluvar University, Vellore, India), M. Tech in Polymer Science and Engineering (2010, Anna University, Chennai, India). Then, he moved to Pusan National University, Korea in 2010 and would get a doctoral degree under the guidance of Prof. Chang-Sik Ha in February of 2015. He is working on organic-inorganic hybrid materials for amphiphobic and anti-stain coatings. He is also interested in functional polymers and magnetic hybrid materials for a range of applications, bio-inspired polymer hybrid materials for superhydrophobic, superhydrophilic, superamphiphobic, and superoleophilic coatings, and their vast applications in a wide variety of fields.

Chang-Sik Ha received his B.S. in Chemical Engineering from Pusan National University, Korea and his M.S. in Chemical Engineering from the Korea Advanced Institute of Science and Technology (KAIST), Daejeon, Korea. He obtained his Ph.D. at the KAIST in 1987. He has been a Professor at the Department of Polymer Science and Engineering, Pusan National University since 1982. He served as the Vice President of Pusan Nation University and the President of the Society of Adhesion and Interfaces, Korea. He is now a director of the Pioneer Research Center for Nanogrid Materials, the National Research Foundation of Korea. He was elected to both the Korean Academy of Science and

Technology (KAST) and the National Engineering Academy of Korea (NEAK) in 2004. He has served as an editorial board member of several international journals including the Editor-in-Chief of the Macromolecular Research (2008-2011) and the Associate Editor of the Advanced Porous Materials and the Composite Interfaces. He has received many awards including the Samsung Polymer Science Award from the Polymer Society of Korea and the Scientist of the Month Award from the Ministry of Science and Technology, Korea. His research interests include materials for drug delivery systems; mesoporous materials and nanostructured materials; functional polymers; organic/inorganic nanohybrid materials; bio-inspired materials for superhydrophobic and superoleophobic coatings. He has 50 patents, 22 books, and more than 650 publications in refereed journals.

1. Introduction

Superhydrophobic surfaces are inspired by a wide variety biological systems, such as lotus leaf (front side), rice leaf, wheat leaf, *Ailanthus altissima* (Tree of Heaven) leaf (rear side), geckos, butterfly wings, shark skin, carp scales, water strider, mussel, nacre, and Clam shell.[1-9] The example of nature may lead to the creation of micro-nano hierarchical structures on biological surfaces that resist water droplets on the surface and make the surface clean forever (self-cleaning).[10] Based on these bio-inspirations, several studies have attempted to mimic the surface topography of biological systems to form robust superhydrophobic and self-cleaning coatings.[11,12] Recently, highly robust, self-healing and switchable surface properties have attracted considerable attention to the production of superhydrophobic surfaces.[11-15] The above properties are very important for the commercialisation of materials for practical applications. On the other hand, the development of these properties is quite difficult. Therefore, care is needed when designing and fabricating these surfaces. Superhydrophobic surfaces are switchable under circumstances, such as pH, light (ultra-violet (UV), plasma, and laser), temperature, and electrochemical treatments. These all depend on the type of materials used for coating applications.[16-21]

Several metal precursors, polymers, silane precursors, siloxane based materials, and various substrates, such as glass, nanofibers, silica wafer, membranes, papers, textile fabrics, sponges, foams, and aerogels, etc., have been used to fabricate superhydrophobic surfaces.[1,22-32] Fig. 1 gives an example of superhydrophobic surfaces using polymer hybrids based on polymethylhydroxysiloxane (PMHOS)/nature leaf powder mixtures.[1] More recently, considerable attention has been paid to the development of superhydrophobic surface based magnetic materials (SSBMMs) on a range of substrates, such as sponges, foams, aerogels, glass,

magnetic particles, and liquid marbles (Fig. 2). These surfaces are used widely for the selective removal and separation of oils from water surfaces or under water, catalysis, sensors and biomedical applications, elastomeric actuators, magnetic fluid device fabrications, and other applications (Fig. 2). The main reason for use of these SSBMM is the easy separation of the material or substrate using a permanent magnet and the recyclability without any loss of material. To the best of the authors' knowledge, this is the first review to focus more deeply on the fabrication and emerging trends in a wide range of applications using SSBMMs. Based on a literature survey, the applications of SSBMMs have not been well established in wider applications compared to the superhydrophobic surfaces used in a range of applications (Fig. 3A and B). The growth and development of these SSBMMs have emerged for wider applications (Fig. 3B). More details of these properties, fabrications, and their applications of SSBMMs are provided in this review.

Superhydrophobicity is defined generally by the surface wettability.[33-36] Surfaces with a contact angle (CA) lower than 90° and 5° (or almost zero) are called hydrophilic and superhydrophilic surfaces, respectively. On the other hand, the surfaces with contact higher than 90° and 150° are called hydrophobic and superhydrophobic surfaces, respectively. In most cases, superhydrophobic surfaces show lower contact angle hysteresis (CAH) based on the surface properties. When superhydrophobic surfaces exhibit a very low CAH (< 10°-5°) the surfaces can show a very high contact angle (>170°). CAH is defined from their dynamic contact angles (DCAs), such as from the advancing and receding contact angles.[35-40] In another case, CAH is also defined from the subtraction of the advancing CA (θ_a) by the receding CA (θ_r).[39,40]

$$CAH = \theta_a - \theta_r \quad (1)$$

The extreme non-stick and self-cleaning properties of superhydrophobic substrates are quite useful in daily life.[41] The applications of these substrates are emerging in a wide range of applications based on the chemical compositions and properties.

2.0. Magnetic properties of various materials

Several metal ions exhibit partial magnetic properties due to the presence of unpaired electrons in the electronic configuration. On the other hand, Fe-based materials can generate strong magnetic moments due to the presence of a larger number of unpaired electrons in the orbital shells and positive net magnetic moments. The magnetic properties of a material are classified into several types based on the types of magnetisms such as diamagnetism, paramagnetism, ferromagnetism, anti-ferromagnetism, ferrimagnetism, and superparamagnetism, etc.[42-44]

Diamagnetism is a weak and non-permanent magnetism in magnetic materials. The orbital shells of a material filled completely by electrons show that there is no net magnetic moment in the material. The material does not show any dipoles in the absence of magnetic field, which illustrates the non-magnetic property of the material. Meanwhile, dipoles are induced in the presence of magnetic field and aligned towards the opposite direction of the applied field direction. Based on this approach, the material shows negative magnetic moments when exposed to the permanent magnet field, so that magnetic susceptibility also becomes negative. Paramagnetic materials show the presence of some unpaired electrons in the orbital shells, so that the electron can easily exchange between the orbital shells in the presence of some external quencher. The materials are magnetized partially and showed the positive net magnetic moment and magnetic susceptibility by applying permanent magnet field. On the other hand, the net magnetic moment becomes weaker due to the non-interaction of individual magnetic moment.

As a consequence, the net magnetic moment of the materials becomes zero in the absence of permanent magnetic field.

On the other hand, ferromagnetic materials can show strong magnetic properties to the permanent magnet due to the presence of large number of unpaired electrons in the materials. The multi-domains of electrons in the materials are parallel to each others in the presence of external magnetic field which helps to maintain the magnetic property of the materials for longer time even in the absence of permanent magnet, so that the net magnetic moment and susceptibility of those materials also becomes positive. Anti-ferromagnetic materials are similar to the ferromagnetic materials. However, the magnetic domains are exactly in the opposite direction of the applied magnetic field. This is due to anti-parallel coupling with neighbouring atoms or ions which results to cancel out the net magnetic moment in the materials. Anti-ferromagnetic materials show no magnetic property in the absence of magnetic field, whereas the materials show small net magnetic moment under the applied magnetic field. Ferrimagnetic materials are also similar to the ferromagnetic materials. It differs from the net magnetic moments. An incomplete cancellation and anti-parallel directions of the spin moments in the magnetic domains result to the net magnetic moments. Ferrimagnetic materials also show permanent magnetic property in some materials based on the properties of the materials.

In most cases, superparamagnetic materials act like a ferromagnetic material. When the particle size of ferromagnetic materials is reduced to the size of less than 10 nm, the electronic domains in the individual particles try to assemble to each other. Then, the materials do not have stronger interaction between them due to their smaller size. The electronic domains in each single particle are parallel to each other, so that the materials also maintain the magnetic property for short time in the absence of permanent magnet and show positive net magnetic moment and

susceptibility. The materials show much weaker magnetic property than that of ferromagnetic materials.

2.1. Fabrication of superhydrophobic surface based magnetic materials (SSBMMs)

Superhydrophobic surfaces prepared by using magnetic materials can generate strong magnetic properties on the surface.[45-47] Pogreb *et al.*[48] developed a novel hierarchical SSBMM by two stage processes with the support of a laser beam and permanent magnet on the polymer substrate. In the first stage, they spread large scale metallic (Ni 17Cr 4Fe 4Si 3.5B 1C) magnetic nanoparticles (100 μm) on polymethylpetene (TPX) film on the top of a permanent magnet followed by surface irradiation under laser light. During this treatment, metallic particles generate heat that melts the TPX at 200-230 °C. This molten polymer film covered the metallic magnetic particles and exhibited hydrophobic (120-135°) surface properties. In the second stage, the surface was treated in a similar manner using small scale metallic (Fe, 1-5 μm) magnetic particles. Through this two stage process, a twin scale hierarchical surface was generated by depositing small scale metallic magnetic particles on large scale metallic magnetic particles. This dual hierarchical structure showed a superhydrophobic contact angle (153°) with lower hysteresis (15°) on the surface. Zhu *et al.*[49] developed a novel conducting and magnetic superhydrophobic surface by an electrospinning technique using polyvinyl alcohol (PVA) and ferrous acetate ($FeAc_2$). The materials were mixed at various weight percentages and electrospun into nanofibers. The obtained nanofibers were calcined at 600 °C for 8 h in an Ar atmosphere to produce carbon nanofibers (CNFs). The obtained CNFs exhibited excellent conductivity (3.4 S cm^{-1} at 50 wt.% $FeAc_2$), magnetic properties (ferromagnetic) and superhydrophobicity (156° ± 2.6° at 40 wt.% $FeAc_2$). They also reported an increase in conductivity and magnetic properties

of the multifunctional CNFs by the increase in the weight percentage of $FeAc_2$. Wang *et al.*[50] also prepared multifunctional magnetic superhydrophobic surfaces by electrospinning using poly(vinylidine fluoride) (PVDF) as the basic material for the nanofibers. A pre-synthesised fluorinated core/shell magnetic microsphere was dispersed with PVDF under ultrasonication and electrospun into nanofibers (Fig. 4). The obtained nanofibers exhibited superparamagnetic properties and stable superhydrophobicity (152.4° ±0.4°) under strong acids and bases. Table 1 lists the recent developments of SSBMMs and their potential properties.

In a similar manner, a superparamagnetic and superhydrophobic coating surface was fabricated by the graft polymerisation of a core/shell magnetite nanoparticles (MNPs) (Fe_3O_4@SiO_2@MPS) surface using 2,2,3,4,4,4-hexafluorobutyl acrylate (HFBA) on a copper wafer substrate using casting method.[51] The casted copper wafer substrates showed a CA 154.6° with a saturation magnetisation value of 44.0 emu/g. In another method, Zhang *et al.*[52] synthesised superhydrophobic (157°) and superparamagnetic films by the atom transfer radical polymerisation (ATRP) of core/shell maghemite nanoparticles (Fig. 5). On the other hand, stable biomimetic SSBMM was fabricated by forming copper (Cu)-ferrite nanorods on a copper substrate that is treated further by a fluorinated silane precursor (dodecafluorooctatriethoxysilane (FOS-12)).[53] The Cu-ferrite produces crystal nanorods film on a copper substrate by increasing the growth time (Fig. 6). By increasing the growth time from a few hours to 24 h, the number of crystal nanorods decreased and their size and mean distance between the nanorods increased. The 'dagger-like' nanorod crystals (1 h) will become sword-like nanorod crystals within 8 h of immersion and a submicrorods crystal structure developed at 24 h. The magnetisation of the substrate was dependent mainly on the cu-ferrite nanorod size. The saturation magnetisation of the film increased with increasing growth time of the Cu-ferrite nanorods. On the other hand, the

increased Cu-ferrite nanorods film would produce a partially smooth surface that reduces the surface CA from superhydrophobic (156.5° ± 2.1° at 10 h of immersion) to hydrophobic (142° ± 2.4° at 24 h of immersion).

2.1.1. Superhydrophobic magnetic nanoparticles

Recently, novel bio-inspired magnetic nanoparticles were synthesised by mimicking the surface of mussels.[54] They developed this mussel-inspired surface using silica nanoparticles with a range of particle sizes as the core material, which was modified by a surface treatment with dopamine, silver nanoparticles and 1H,1H,2H,2H-perfluorodecanethiol. The obtained nanoparticles exhibited superhydrophobic properties. The surface wettability was changed partially depending on the size of the silica nanoparticles cores (171.0° ± 2.0° at 500 nm, 166.8° ± 2.1° at 200 nm and 156.8° ± 1.4° at 300 nm) used for synthesis. Based on this idea, they also developed liquid marble-magnetic nanoparticles using carbonyl iron particles as the core material (Fig. 7). The magnetic nanoparticles obtained exhibited superhydrophobicity (159.6°), and almost complete oil wettability (~0°). The magnetic nanoparticles can be controlled remotely by the help of a permanent magnet. Using this idea, the applications of magnetic nanoparticles can be useful for a range of applications. The mussel-inspired magnetic nanoparticles exhibited oil marble properties by spreading the particles on oil spills over the water surface. This shows that using a permanent magnet, oils can be separated and recycled without any loss of magnetic nanoparticles. Fang *et al.*[55] fabricated magnetically-induced temporary superhydrophobic coatings by a simple approach in a one-pot process based on the Fig. 8. In the first step, magnetite nanoparticles were prepared by a co-precipitation method using ferrous and ferric chloride, which was dissolved in water in a beaker in one-pot followed by the addition of an

aqueous ammonia solution. The obtained magnetite nanoparticles were surface functionalised further by the addition of tridecafluorooctyl triethoxysilane (FAS), ethanol, and water in one-pot. The obtained fluorinated magnetite nanoparticles exhibited hydrophobic properties. To create superhydrophobicity using this material, fluorinated magnetite nanoparticles were deposited on a range of substrates by keeping the permanent magnet below the substrate. The hydrophobic particles (124.6° ± 2.1° on a glass substrate) exhibited temporary superhydrophobicity (172.8° ± 0.2° on glass substrate) on a range of substrates using this technique. The saturation magnetisation of pure magnetite nanoparticles was approximately 65.20 emu/g at 300 K. On the other hand, the surface-functionalised magnetic nanoparticles exhibited partially-reduced magnetisation (53.10 emu/g at 300 K). The reduced magnetisation of the magnetic nanoparticles was mainly due to the surface functionalisation of FAS. The formation of smooth layers on the outer surface of magnetite nanoparticles by fluorinated silica particles would reduce the magnetisation and increase the surface properties from hydrophilic (38.9° ± 1.2° of pure magnetite nanoparticles on glass substrate) to hydrophobic and superhydrophobic. Several magnetic nanoparticles have also been synthesised and functionalised with a range precursors to enhance the surface properties of those materials.[56-58]

2.1.2. Superhydrophobic magnetic liquid marbles

Aussillous *et al.*[59,60] proposed the first concept of the formation of liquid marbles by a hydrophobic material. Liquid marbles are prepared by rolling a water droplet on the hydrophobic micro or nanoparticles surface.[59-62] Water can generate the layer formation of particles over the water surface because of the electrostatic attractions among the particle surfaces by their highly active functional groups (Fig. 9). Liquid marbles maintain the surface properties up to the

separation of hydrophobic particles on the surface. Liquid marbles are used widely in a range of applications, such as oil adsorption and separation, gas separation, identification of water on the water/vapour interface, and in the synthesis of solid polyelectrolyte microspheres.[63-68] Recently, liquid marbles using monodisperse poly(methylsilsesquioxane) (PMSQ) particles have been developed (Fig. 9).[63] A liquid drop was rolled gently on a PMSQ powder bed to create monolayers of powder on the water surface. The excess deposited powders were removed by transferring the liquid marbles to a n-octadecyltrimethoxysilane (OTS) modified silicon wafer substrate followed by gentle rolling and cleaning the liquid marbles on the surface. The obtained liquid marbles exhibited stable surface properties until the loss of particles on the surface. On the other hand, the freezing properties of the liquid marbles have been studied.[69-71] These studies found that the liquid marbles can delay the freezing time of a water drop due to the formation of layers of particles on the water drop surface. Similarly, some studies were also carried out to measure the evaporation rate of liquid marbles.[72,73] Magnetic liquid marbles were prepared based on these concepts with superhydrophobic properties. Zhang *et al.*[74] synthesised magnetic liquid marbles using core/shell magnetic nanoparticles followed by surface functionalisation of the shell by grafting with a block copolymer (poly(2-vinylpyridine-*b*-dimethylsiloxane, (P2VP- *b* -PDMS)) (Fig. 10). The surface was treated further with a photoacid generator (PAG). Owing to the presence of PAG on the polymer-core/shell magnetic nanoparticles surface, the surface can be tuned easily under acids and UV light. Under these conditions, PAG protonates the adjacent P2VP blocks and generates hydrophilic groups on the surface of the particles, which form a thin layer on the surface of the water drop. The hydrophobic property remaining on the particles maintains the stability of liquid marbles. Based on the mechanism, the magnetic liquid marbles were controlled remotely using a permanent magnet.[74-76] Zhao *et al.*[75] examined the movements

of magnetically-activated liquid marbles on a glass substrate by placing a permanent magnet at one side of the substrate and moving the magnetic liquid marble slowly by the movement of a permanent magnet. The magnetic liquid marbles (the mass of magnetic powders on the droplet (0.18 mg)) was moved a distance of ~14 mm with the support of an external magnetic field (0.02 T). The authors also explained the role of the particles size on the development of stable magnetic liquid marbles.[77] Nanoparticles can produce more robust liquid marbles than microparticles. This is because of the uniform deposition of nanoparticles on the surface of the water drop, which reduces the liquid/air boundary and maintains the stability for a longer period of time. They used very small (10 nm) and highly hydrophobic Fe_3O_4 magnetic nanoparticles.[77] The particles obtained exhibited highly durable liquid marble properties because of the reduced interface between the liquid and air. In another method, highly stable superhydrophobic magnetic liquid marbles were developed using fluorinated decylpolyhedral oligomeric silsesquioxane (FD-POSS)/Fe_3O_4 nanoparticles.[76] A thin bed was prepared using a FD-POSS/Fe_3O_4 nanoparticles powder, the surface exhibited superhydrophobicity to water (171.1°) and superamphiphobicity to dimethyl sulphoxide (DMSO), toluene, hexadecane, and ethanol with a contact angle of 166.2°, 155.7°, 154.4°, and 142.8°, respectively (Fig. 11). The FD-POSS/Fe_3O_4 magnetic liquid marbles were adjusted by opening and closing the marbles. During this stage, a range of water colours were also encapsulated to the check the chemiluminescence properties of the liquid marble surface. The hexadecane magnetic liquid marble displayed various colours on the surface, which confirms the highly durable surface property of the liquid marbles. The stable superhydrophobic magnetic liquid marbles were attributed to the formation of low surface energy FD-POSS on the surface of Fe_3O_4 nanoparticles. They also examined the chemiluminescence reaction in magnetic liquid marbles by the addition of hydrogen peroxide in a single liquid marble and bis(2,4,6-

trichlorophenyl)oxalate and dye in another liquid marble. A chemiluminescence reaction occurred in the liquid marble when the two liquid marbles joined to form a single liquid marble, which can be observed from the optical images (Fig. 11). In a similar manner, the authors also conducted other chemical reactions successfully in magnetic liquid marbles, such as acid-base reactions, nanoparticles synthesis and photochemical polymerisation. The chromatography study showed the direct purification of the reaction product by a chromatographic alumina sheet. In a similar fashion, Janus particles are also attracted considerable attention to develop magnetic liquid marbles. In general, Janus particles are fabricated by the formation of anisotropic colloidal particles in water/oil interface or pickering emulsion method using polymers or inorganic nanoparticles, polymer/inorganic hybrid system.[78,79] Similarly, the Janus particles have been also fabricated by layer-by-layer self-assembly, photo-polymerization in micro-fluidic channel, and surface coating by deposition of evaporated metal particles, etc.[78,79] The surface properties of the colloidal particles were modified by using various types of surfactants, compatibilizers, stabilizers, etc. The size and shape of the Janus particles can also be varied based on the use of surfactants, compatibilizers, and stabilizers in the inorganic, polymeric and polymer-inorganic systems.[78,79] Based on these approaches, a multi-compartment bio-inspired Janus particles were prepared by using silica nanoparticles (250 nm), α-Fe_2O_3 nanoparticles and ethoxylated trimethylolpropane triacrylate (ETPTA) (Fig. 12).[80] The Janus particles were prepared by dissolving silica nanoparticles with α-Fe_2O_3 in ethanol and mixing them with ETPTS followed by the complete removal of ethanol from the magnetic nanoparticles. The obtained suspension was mixed with a photoinitiator (0.25% v/v 2-hydroxy-2-methylpropiophenone) under ultrasonication and were capped with 5 wt.% poly(vinyl alcohol) (PVA) and 1 wt.% ethyleneoxide propyleneoxide tri-block copolymer (Pluronic F108). The capping agents were

removed completely by an acid wash and the particles were treated with O_2 plasma for 30 seconds. The treated amphiphilic particles were modified further with fluorosilane and wax to create the Janus particles. The obtained Janus particles exhibited magnetic liquid marble properties and could be useful for optical reflective spectroscopy. Several other studies have also been carried out for the preparation of SSBMMs, and their properties and various applications were analyzed.[81-86]

2.1.3. Superhydrophobic magnetic sponges and foams

Superhydrophobic sponges and foams were fabricated using a simple approach by a surface treatment with pristine melamine, polyurethane, carbon nanotube (CNT) sponges, or other foams by a dip coating method.[1,87-94] On the other hand, melamine and polyurethane sponges have attracted considerable interest for various applications, such as cleaning vessels to oils and organic solvent absorption/adsorption, and separations. Because of the flexible, economically viable and thermally stable properties under optimal conditions, the sponges can be applied easily to a range of fields. The simple surface modifications of the sponge also lead to enhanced properties of the substrate. Zhou *et al.*[87] developed a novel Fe^{2+} ion induced superhydrophobic polyurethane (PU) sponge using 1H,1H,2H,2H-perfluorooctyltriethoxysilane (PTES) and pyrrole monomer as the surface modifier. The PU sponge was cleaned in acetone and water before a surface treatment (Fig. 13a). The pre-cleaned sponge was dip-coated in a ferric chloride/PTES solution dissolved in ethanol (Fig. 13b). The dip-coated sponge was covered further by vaporisation of the pyrrole monomer, which was polymerised at room temperature by the continuous exposure of pyrrole vapour on the substrate (Fig. 13c). The pyrrole monomer was oxidised in the presence of Fe^{3+} ions and provided polypyrrole (Fig. 13d), whereas at the same

time, Fe^{3+} ions were reduced to Fe^{2+} ions (Fig. 13e). The prepared substrate showed superhydrophobic and superoleophilic properties (Fig. 13). In 2003, Maspoch *et al.*[90] introduced the concept for the fabrication of a porous magnetic solid by mixing copper atoms with polychlorinated triphenylmethyl tricarboxylate (PTMTC) as an organic radical ligand. A selective magnetic sponge was formed by enhancing the network structure of the porous solid. Based on this concept, a new model was designed for developing a magnetic sponge with an alkanedithiol-bridged network using nano magnets (Fig. 14).[91] A switchable magnetic sponge was developed via an ON and OFF mechanism of an applied magnetic field. By changing the applied magnetic field, the magnetic sponge can expand or compress their framework.[91] The alkanedithiol, such as icosane-1,20-dithiol (C_{20} dithiol) and triacontane-1,30-dithiol (C_{30} dithiol), were used in that study with magnetic Co-Pd alloy nanoparticles as a network connector of the alkanedithiol to create a bridged network of magnetic sponges. Recently, ultralight superhydrophobic magnetic foam was fabricated by modifying the PU sponge under an acid wash followed by acrylic acid (Fig. 15).[94] This acrylic acid-modified sponge was dipped into a range of solutions, such as $Fe(NO_3)_3$, $Co(NO_3)_2$ and $Ni(NO_3)_2$, respectively, and sintered at 400 °C for 1 h in an Ar atmosphere. Ultralight weight magnetic foams of Fe_2O_3/C, Co/C and Ni/C foams were prepared using this technique. The magnetic foams underwent a further surface treatment using 2% (v/v) of methyltrichlorosilane to induce superhydrophobicity. The density of the foams can vary depending on the acrylic acid and metal ions loading. The modified foam exhibited superhydrophobic (152° for water), superoleophilic (0° for lubricating oil) and superparamagnetism properties. Owing to the ultralight weight, the superhydrophobic and superoleophilic properties of the modified foam can be used to separate a larger amount of oils

through the pore channels. The superhydrophobicity of the foam prevent the water (surface tension 72.8 mN/m) from passing through the pore channels of the foam.

2.1.4. Superhydrophobic magnetic aerogels and films

An aerogel is a type of light weight material that is normally prepared by sol-gel techniques using a silane precursor followed by the complete removal of solvents under reduced pressure.[95] Silica-based aerogels have a large surface area (55-1200 m^2/g), high porosity (80-99.8%), high thermal insulation value (0.005 W/m K), fire resistance, ultra-low dielectric constant (k = 1.0–2.0), low density (~0.0003 g/cm^3), and lower refractive index (~1.05).[96] Owing to the extreme properties of the silica aerogel, the applications of the aerogel are used widely in a range of applications, such as supercapacitors, thermal insulations, catalytic supports, and acoustic barriers. Recently, superhydrophobic aerogels and superhydrophobic aerogels based magnetic materials have also attracted keen interest for the development of aerogels for a variety of applications.[97-109] Hamdeh *et al.*[98] and Long *et al.*[99] examined the magnetic properties of zinc-ferrite aerogel powders and nanocrystalline magnetic mesoporous aerogels. The iron oxide (FeOx) based nanocrystalline mesoporous aerogels were prepared by sol-gel method by using ferric chloride and epoxide-based proton scavenger under various calcination conditions. The magnetic property of the prepared magnetic aerogel was measured by vibrating sample magnetometry (VSM) (Fig. 16).[99] Amorphous nature of the as-prepared magnetic material showed weak paramagnetic property with no saturation or coercivity (Fig. 16). Similarly, the magnetic materials calcined in air at 260 °C and 320 °C also showed weak paramagnetism and less crystalline properties (Fig. 16). The authors found that the magnetic materials calcined in argon gas or argon/air mixture at 260 °C and 370 °C showed the formation of nanocrystalline

mesoporous aerogel with superparamagnetic property (Fig. 16). On the other hand, the particle size and the magnetic properties of the prepared aerogels were depended strongly on the calcination condition and their structural behaviour. The magnetic aerogel prepared at 370 °C in argon gas showed stronger magnetic property even though the particle size was quite higher in size (~18.5 nm, saturation magnetization 57 emu/g) as compared with the material prepared at 260 °C in argon (~7 nm, 44 emu/g) (Fig. 16). Olsson *et al.* prepared a highly flexible cellulose-based magnetic aerogel.[100] Initially, a bacterial cellulose hydrogel was prepared using a bacterial strain (*Acetobacter xylinum FF-88*) in a cell culture medium containing 5 vol.% of coconut milk and 8 vol.% of sucrose. The obtained hydrogel was treated with a 10 vol.% NaOH solution, and washed with distilled and Milli-Q water followed by freeze drying. The obtained cellulose aerogel was treated further by immersing it into a $FeSO_4/CoCl_2$ solution for 15 min. and heated it at 90 °C for 3 h. The dried aerogel was further soaked in a NaOH and KNO_3 solutions at 90 °C for 6 h. The aerogel was washed with Milli-Q water and freeze dried to obtain elastic and ferromagnetic aerogel nanocomposites. Liu *et al.*[101] also prepared highly flexible magnetic aerogel using similar method with $FeCl_3$ and $CoCl_2$ and cellulose hydrogel membranes. Based on these approaches, a range of magnetically-induced aerogels were prepared successfully. Recently, a new method for producing superhydrophobic surface based magnetic films by an aerogel-assisted chemical vapour deposition method (AACVD) using a range of metal nanoparticles, such as Fe_3O_4, Co, Ti, Ni, and Au nanoparticles, was developed.[103] The nanoparticles were hydrophobised using oleic acid or trimethoxy(octadecyl) silane (OTMS). A Sylgard® 184 Silicone Elastomer solution was prepared by dissolving in chloroform followed by the slow addition of a variety of hydrophobised nanoparticles solutions. The obtained solution was used to prepare a superhydrophobic magnetic film by AACVD. The Fe_3O_4 nanoparticles

exhibited superparamagnetic properties in the colloidal suspension as well in the aerogel assisted film with a magnetisation saturation of 42.2 emu/g, which is due mainly to the small crystallite size (<20 nm) of Fe_3O_4. The metal nanoparticle-loaded superhydrophobic films could be used for the photodegradation of organic dyes. The dye can be adsorbed on the surface of the superhydrophobic film because of the presence of a larger surface area on the surface. The adsorbed organic dye is degraded further by the photocatalytic properties of Ti and other metal nanoparticles. The superhydrophobic films can be removed easily from solution using an external magnet because of the magnetic properties of the superhydrophobic film. The magnetically-induced superhydrophobic film can be recycled for the continuous degradation of organic dyes in water.

2.1.5. Superhydrophobic magnetic fabrics and papers

A fabric or paper prepared with superhydrophobic properties exhibited another interesting surface property due to the use of the matrix surface for various applications, such as self-cleaning textile fabrications, filtrations, and the separation of oils and solvents, micro-nanoparticles and bio-molecules, electrochemical energy storage, etc..[110-115] In most cases, the electrospinning technique has been used for the development of superhydrophobic fabrics.[114] This was attributed to the creation of micro and nanostructures over larger areas by the electrospinning of a polymer solution. The hydrophobicity of the polymer fabrics (hydrophobic polymer) can impart superhydrophobic surface properties based on the nanofiber architecture or the surface treatment with hydrophobic materials or the loading of hierarchical nanoparticles with a polymer solution. Richard *et al.*[111] developed a novel superhydrophobic cotton fabric using a simple method with zinc hydroxide and stearic acid solutions through a solution

immersion method. The obtained superhydrophobic fabric exhibited relatively low cost and non-toxic properties. Bayer *et al.*[117] developed a new type of cellulose fabric with a combination of superhydrophobic and magnetic properties. First, spherical superparamagnetic $MnFe_2O_4$ nanoparticles were synthesised by dissolving 2 mmol of iron (III) acetylacetonate [$Fe(acac)_3$], 1.25 mmol of manganese (II) acetylacetonate [$Mn(acac)_2$], 10 mmol of hexadecanediol, 6 mmol of dodecylamine, and 6 mmol of dodecanoic acid in a round bottomed flask with 20 mL of benzyl ether under a nitrogen atmosphere at various temperatures (140 °C, 210 °C and 300 °C) and times (600, 120, 60 min.). The magnetic nanoparticles were washed with a mixture of isopropanol, ethanol and acetone, and dispersed in toluene. In the second stage, a functionalised hydrophobic cellulose fibre sheet was prepared using 5 wt.% ethyl-2-cyanoacrylate (ECA) monomer in acetone using a solution cast or dip-coating method. The functionalised sheet surface was treated further with yellow carnauba Wax flakes (150 nm) or PTFE particles, and the ECA monomer was polymerised at room temperature. The surface property of the functionalised cellulose sheet increased steadily and become saturated at certain concentrations by increasing the weight percentage of wax or PTFE particles. The results showed that PTFE particles play a key role in producing superhydrophobicity on a cellulose fabrics sheet than the use of carnauba wax. Optical images of the water droplet on the modified cellulose substrate and Fig. 17 (a-c) shows their surface morphology. Magnetic cellulose sheets were prepared by immersing the cellulose sheet in a ECA/$MnFe_2O_4$ nanoparticle solution and polymerised at room temperature. $MnFe_2O_4$ nanoparticle-loaded cellulose sheets exhibited hydrophobic properties and superparamagnetic properties due to the extremely smaller nanoparticles of $MnFe_2O_4$ and the motion on the paper was monitored easily by a permanent magnet (Fig. 17A).

2.1.6. Superhydrophobic surfaces and magnetic fluids

Micro-fluidic devices can be fabricated by surface patterning techniques using laser, ion irradiation, sealing, rapid prototyping, lithography, and replica molding, etc.[79] The transportation of macro or micro or nanofluids in a controlled manner requires an external force to transport the fluids.[118,119] This might need more energy or incur high cost for maintenance, storage and transport. Several approaches to fluid transportation in controlled wetting phenomena, such as liquid drop movement on a surface using external gradient and capillary rise and fall technique, have been carried out.[120-122] The wetting phenomenon of a fluid on the substrate was controlled by treating the surface with various techniques, such as surface chemical treatment, light and pH. The movement of the fluid droplet was also controlled in a systematic manner based on these concepts. Two external forces were used for the transport of fluid drops, such as asymmetric lateral vibrations and thermal gradient controlled by laser beam.[118-122] Recently, superhydrophobic surfaces have attracted increasing interest in this field due the extremely high surface non-wetting and self-cleaning properties. Water or other fluids can be easily transportable in a controlled manner using the superhydrophobic surface, which might reduce power consumption, external stimuli and cost. Several engineers have designed suitable coating materials and methods for fluid transportation. Recently, an attempt for the tracking of fluid motion on a superhydrophobic surface by an external magnet was conducted. The fluid motion might depend on the magnetic properties of the fluids. Gómez *et al.*[118,119] examined the paramagnetic fluid movement on a superhydrophobic surface. Spherical paramagnetic particles (diameter, 0.2 to 4.0 μm) were dispersed in water at various concentrations (0.1% -5%) and used as a fluid motion study. A permanent magnet was kept under a superhydrophobic surface (CA, 145° to 160°) followed by placing the magnetic nanoparticle-dispersed fluid on a surface (fluid

drop, 5 to 35 μL). The movements of magnetic fluids were monitored and controlled by the permanent magnet. The superhydrophobic surface exhibited excellent properties for fluid transport than other methods used for fluid transportation. This was attributed to the non-stick and self-cleaning properties of the superhydrophobic surface. The drop motion was dependent mainly on the concentration and size of the magnetic particles at the magnetic fluid. The authors concluded that drop motion was mainly due to the sliding of the droplet rather than to rolling on the superhydrophobic surface under an external magnetic field. In another case, the particle clusters at the sides of a droplet surface by an external magnet, which drives the fluid by capillary forces and strongly distorts the drop shape. Hong *et al.*[122] also examined the transportation of a superparamagnetic micro-fluid on the superhydrophobic surface. The fluid transport and adhesion of the superparamagnetic fluid were studied using an ON and OFF mechanism of the external magnetic field on the surface (Fig. 18). The superhydrophobic surface (~160°) was fabricated by the formation of a polystyrene (PS) nanotube layer on the porous alumina membrane template. A superparamagnetic magnetic drop (4 μL) was placed on the superhydrophobic surface, which was controlled by two permanent magnets at the top and bottom of the two superhydrophobic substrates at a constant distance of 2 mm (Fig. 18a). The external magnetic field was switched on the substrate at the top, which attracts the magnetic fluids towards the surface due to the strong magnetic field acting on the superhydrophobic surface (Fig. 18b and c). When the magnetic field was switched off on the top and switched on the bottom, the attracted magnetic fluid on the top of superhydrophobic surfaces pulls towards the bottom of the superhydrophobic surface (Fig. 18d and e). The results showed the controlled and magnetically driven fluids on the superhydrophobic surface by the permanent magnet (Fig. 18f). The movement of the ferrofluid on the superhydrophobic aluminium alloy substrate (162°)

under a constant external magnetic field was also studied.[123] Cheng *et al.* reported the tuneable adhesion of the superparamagnetic fluid on the superhydrophobic surface (157°) (Fig. 19).[124] When iron is magnetised, the surface will become a micro-magnetic field due to the presence of a small magnetic field remaining caused by the ferromagnetism of iron, which attracts the superparamagnetic droplet on the surface and nucleates the magnetic fluid partially on the surface. On the other hand, the surface completely resisted the penetration of a magnetic fluid on the surface before magnetisation or after demagnetisation (Fig. 19). This was attributed to the absence of a strong magnetic field and the presence of air layers on the superhydrophobic surface, which exhibited a Cassie-Baxter state on the surface. The rotation and movement of a viscous paramagnetic fluid on the superhydrophobic surface (~160°) was also studied by applying an external magnetic field to the bottom of the substrate.[125] The superhydrophobic surface was fabricated on a low density polyethylene (LDPE) surface, and used further by placing a magnetic fluid drop on the surface. The drop was moved slowly by moving the permanent magnet at the bottom of the superhydrophobic surface (Fig. 20). Owing to its paramagnetic properties, the fluid drop can rotate towards the opposite directions of the magnetic field applied to the superhydrophobic surface. Based on this concept, we can monitor the movements of paramagnetic fluid on the superhydrophobic surface. Zhu *et al.*[126] examined the simulation of non-linear deformation of a ferrofluid on a superhydrophobic surface under an applied magnetic fluid. Recently, Timonen *et al.*[127] examined the switchable static and dynamic self-assembly mechanisms of a magnetic fluid on a superhydrophobic surface (~175°) by an external magnet. When the permanent magnet was moved slowly towards the superhydrophobic surface, the mother magnetic fluid drops began to split into several daughter magnetic fluid

droplets because of the strong magnetic property developed on the fluid droplet. This could be switchable by moving the permanent magnet away and nearer to the superhydrophobic surface.

3.0. Emerging applications of superhydrophobic surface based magnetic materials (SSBMMs)

Superhydrophobic surfaces are used widely in a range of applications due to the non-stick and self-cleaning properties.[1,6,128-130] The stability of the superhydrophobic surface under external stimuli, such as temperature, light and pH, are important criteria to consider when using the substrates for practical applications. The cost of the final material is also an important consideration for practical uses. In most cases, fluorine-based precursors were used for a surface treatment to develop superhydrophobicity on the substrate surface.[131-134] The cost of the fluorine-based precursor lacks the use of materials for bulk applications. Superhydrophobic surfaces are generally used for oils and organic solvents absorption/adsorption and separation, self-cleaning coatings, drug delivery, and various bio-medical applications, solar cell, sensors, etc. Magnetic nanoparticles have several applications. By combining the superhydrophobic and magnetic properties, the obtained SSBMMs also have a range of applications, such as oil absorption/adsorption and separation, catalysis, sensors and bio-medical applications, micro-fluidic device fabrication, actuators, and other applications. The magnetic properties of superhydrophobic materials allowed easy separation of the particles after the absorption/adsorption using a permanent magnet. The applications of SSBMMs have emerged in recent days due to the necessity of the controlled motion of fluids, improving the recyclability of materials for longer period of time and reducing the processing cost.

3.1. Oil-spill capture and separation

Recently, a novel bio-inspired superhydrophobic hybrid micro-nanocomposites suspension was developed using lotus leaf powder, polymethylhydroxysiloxane and phenyl substituted silica ormosils.[1] A suspension of the above mixture exhibited superhydrophobicity on a variety of substrates through the evaporation of solvents. The suspension was also loaded on a melamine sponge (pre-cleaned in water/ethanol/acetone mixture before use) and treated with polydimethylsiloxane (PDMS)/chloroform at room temperature and 100 °C. The obtained hybrid sponge also exhibited superhydrophobicity and the selective absorption of various oils and organic solvents (Fig. 21).[1] The absorbed oils and organic solvents were collected by simply squeezing the absorbent and collecting the oils and solvents in a glass beaker. The absorbed oil was purified by mixing with hexane and in a rotary evaporator under mild conditions. The hybrid micro-nanocomposite sponges were recycled approximately 15 times after the absorption of larger amounts of oils and organic solvents.[1] Recycling of the material, absorption of larger amounts of oils and purification of the absorbed oils are important considerations for using a superhydrophobic absorbent. Several light weight sponges, foams and aerogels, and membranes have also been used for the absorption of oils and solvent spills in water.[135-141] SSBMMs also have many more applications for the sorption and separation of oils from water.[54,93,94,,97,112,142-146] This is because of the self-driven properties of magnetic particles or surfaces under a permanent magnet and high stability to pHs and temperatures, which might assist in the easy separation of oil sorbed on the substrate or material from oil spills.

Highly hydrophobic core-shell Fe_2O_3@C nanoparticles were prepared using terephthalic acid, which was modified by lithium hydroxide and iron (II) sulphate hexahydrate ($FeSO_4.7H_2O$).[135] The material was carbonised in a quartz tube at 600 °C for 6 h. The resulting

Fe_2O_3@C nanoparticles were treated further with vinyltriethoxysilane and used to capture oil spills on the water surface. The magnetic nanoparticles were poured on the outer surface of the oil bed followed by the selective separation of the oil-absorbed magnetic nanoparticles from the water using an external magnetic field (Fig. 22). In another method, Gui *et al.*[142] developed a novel magnetically-induced hydrophobic CNT sponge (>145°) by chemical vapour deposition (CVD) using ferrocene and dichlorobenzene as precursors. The resulting magnetic sponge exhibited highly stable properties at a range of pH and maintained their hydrophobicity under strong acidic and basic pH conditions. This simple way of preparing hydrophobic sponges has been used widely for oil absorption. Owing to the magnetic properties of the hydrophobic surface, the sponge substrate can be recycled several times for the sorption and separation of oils from water. A small piece of a magnetic sponge was placed on the oil spill and the sponge was removed within a few minutes using a permanent magnet (Fig. 23). The sorbed oils were removed from the sorbent by heat treatment and collected by mechanical compression. The Me-CNT sponge was recycled again for the absorption larger quantities of oil. The Me-CNT sponge was repeated more than 1000 times for oil absorption. This excellent absorption behaviour of the Me-CNT sponge allowed the hydrophobic magnetic sponge to be used in larger scale oil absorption applications. In a similar manner, a magnetically induced superhydrophobic bulk material was prepared by the simple mixing of PTFE with MWCNT (diameter, 30-50 nm and length 30 μm) and pre-synthesised Fe_3O_4 nanoparticles in 30 mL chloroform at 60 °C.[143] The solvent was removed completely by evaporation and the remaining PTFE/MWCNT was poured into a mould and hot pressed (pressure-11.5 KPa) for 30 min. at 390 °C. The bulk material surface exhibited superhydrophobicity with a CA ~158° (Fig. 24). The superhydrophobicity of the magnetically-induced surface was stable under strong acidic and basic pH values, and higher

temperatures. Owing to the bulk properties of the superhydrophobic surface, the matrix can absorb larger amounts of oils from a spill on the water surface and be removed easily through the help of a permanent magnet. The absorbed oil was removed by burning the bulk material (Fig. 24). The superhydrophobic property of the bulk material was maintained even after burning the oil absorbed bulk matrix. The stable superhydrophobicity of the matrix surface might be due to the high thermal stability of the bulk material. Consequently, the superhydrophobic based magnetic bulk material was also recycled for several times.

Calcagnile *et al.*[93] also developed a novel magnetically-driven superhydrophobic foam using PU foam as the starting substrate, which was modified further using submicrometer polytetrafluoroethylene (PTFE) particles and colloidal superparamagnetic iron oxide nanoparticles (NPs). They incorporated different types of magnetic nanoparticles into the sponge with the support of PTFE. The wettability of the hybrid-loaded and surface-treated foam exhibited superhydrophobicity with a CA greater than 160° and lower hysteresis. The hysteresis of the PU/PTFE and PU/NPs/PTFE hybrid foams was 7.23° ± 2.31° and 5.53° ± 2.21°. The hybrid PU/NPs/PTFE foam also exhibited superoleophilic and superparamagnetic properties. The superhydrophobic, superoleophilic and superparamagnetic properties of the foam can be traced easily on the water surface. The motion of the hybrid foam can be controlled using a permanent magnet. This self-driven magnetic foam is also useful for the adsorption of larger amounts of oils from a water surface. The fabricated foam exhibited the selective absorption of oil from the water surface. The superhydrophobic foam can also be used in the separation of oil by a simple filtering technique. Similarly, a magnetically-driven superhydrophobic and super durable polyester material surface was fabricated by dip coating the substrate in a pre-prepared hybrid nanocomposites solution.[112] The nanocomposite solution was prepared by the

polymerisation of tetraethoxysilane (TEOS) and n-hexadecyltriethoxysilane (HDTES) in the presence of Fe_3O_4. The magnetic-driven superhydrophobic surface (>150°) exhibited excellent water resistance, good absorption for oil (superoleophilic), and long- term chemical stability. The obtained properties highlight the potential of the surface treated polyester material for the absorption and separation of oils, such as petrol or gasoline, diesel and crude oil from water. The magnetic superhydrophobic polyester substrate was also recycled 10 times without significant loss of the total absorbent capacity. The superhydrophobicity was also maintained on the substrate with lower sliding angle before and after 10 times of oil absorption and separation. These results highlight the excellent properties of the surface-treated magnetic superhydrophobic polyester material. Recently, a novel metal (FeO, CoO, NiO, CuO and Ag) nanoparticle-loaded superhydrophobic sponge and textile fabrics were fabricated for the separation of oil from water.[113] The metal nanoparticle-loaded sponges and textile fabrics were treated with octadecylthiol to the bind the metal nanoparticles with a mercapto group. The octadecyl group on the outer surface makes the substrate superhydrophobic (>150°) due to the hydrophobicity of octadecylthiol and the formation of a hierarchical surface on the substrate by metal nanoparticles. The obtained superhydrophobic surface showed excellent water resistance, was stable in hot water (~85 °C), various surfactant solutions and ultrasonic treatments, and induced the excellent separation of oil and water. The applications of magnetically-induced and self-driven superhydrophobic surfaces are increasing dramatically for the absorption and separation of oils from water because of the excellent absorption behaviour and the easy removal of the absorbed absorbent using an external magnet as well as the possibility of recycling several times. These extreme properties illustrate the potential of a magnetic superhydrophobic matrix in bulk amounts for the mass-scale purification of oils for real practical applications.

3.2. Catalysis

Catalysts are classified mainly into two classes, homogeneous and heterogeneous catalysts.[147-149] In homogeneous catalysis, the catalytic phase is similar to that of the reactant phase. Therefore, the homogenous mixing of these two phases makes it easier for the material to convert the reaction product under the catalytic system. The complete separation of the mixed catalyst was quite difficult, which may lack the purity of the final product and in some applications. To avoid this problem, heterogeneous catalysts are used for reaction conversion. Heterogeneous catalysts are normally prepared by the grafting or covalently binding of the active molecules on the surface of a material or inside the pore channel. A heterogeneous catalyst had the drawback of a decrease in the product yield than the product obtained by a homogeneous catalyst. More recently, nanocatalysts and magnetically-induced nanocatalysts have been used widely for catalysis applications.[150,151] Several metal nanoparticle-loaded materials have been used for catalysis applications. The metal nanoparticle-loaded materials showed the fast conversion of the reaction with a higher yield.[152-154] In other cases, small nanoparticles, such as CoO, Mn_3O_4 and Co_3O_4, supported on SBA-15 and other meso and nanoporous materials exhibited better catalytic activity for the selective oxidation of ethylbenzene, toluene, and cyclohexane, and for the reduction n-nitro phenol than larger nanoparticles.[153-159] The magnetically-induced and metal nanoparticle-loaded materials can be much more applicable to catalysis applications because of the possibility of recycling the materials several times by the simple separation of materials by the assistance of an external magnet. Magnetic materials with hydrophilic properties have been used widely for catalysis because of easy dispersal of the nanocatalyst with the reactant. On the other hand, some hydrophobic and superhydrophobic materials have also been used for catalytic applications.[41,152-163] Shi *et al.*[152] synthesised a yolk shell superhydrophobic nanosphere catalyst

using gold nanoparticles for the reduction p-nitro phenol. Chen *et al.*[153] synthesised a variety of organic silane precursor-coated superhydrophobic cobalt nanocomposites for the selective oxidation of ethylbenzene. The nanocomposites showed hierarchical particles with a raspberry like structure and excellent catalytic properties for the oxidation of ethylbenzene. TiO_2 nanoparticles are well known for their photocatalytic and self-cleaning properties. Kamegawa *et al.*[154] used TiO_2 nanoparticles for the preparation of superhydrophobic and photocatalytic self-cleaning surfaces. TiO_2 nanoparticles were hydrophobised using PTFE by radio frequency magnetron sputtering (RF-MS) deposition on quartz and structured Ti substrates. Fig. 25 shows the surface morphologies of the pristine and modified substrates. The TiO_2 nanoparticles sputtered Ti substrate exhibited hydrophobic properties (CA ~ 107°). On the other hand, the PTFE-modified substrate showed enhanced surface non-wettability because of the deposition of the hydrophobic layer on the TiO_2 surface, which might affect the surface morphology and induce superhydrophobicity (168°) on the surface (Fig. 25). The obtained superhydrophobic surface exhibited self-cleaning properties due to self-oxidation of the surface under light by their photocatalytic property. Magnetic nanoparticles also showed a range of catalytic properties and recyclability because of the easy separation of the particles using a bar magnet. Sreedar *et al.*[155] synthesised propargylamines by coupling three components, such as aldehydes, alkynes and amines, via C-H activation using magnetically separable Fe_3O_4 nanoparticles as a catalyst. The authors also synthesised 5-substituted 1H-tetrazoles using magnetically separable $CuFe_2O_4$ nanoparticles as a catalyst.[156] The Fe_3O_4-supported palladium nanoparticles catalyst was also used for the fluoride-free Hiyama cross-coupling reaction of aryl halides with aryl siloxanes under aqueous conditions.[157] In another method, the Fe_3O_4@mesoporous SBA-15 nanoparticles were used as a catalyst for the photodegradation of malachite green dye in water.[158] Some other

metal nanoparticles, such as Au-, Ag- and Pt-loaded magnetic nanoparticles, were also used for the reduction of 4-nitro phenol to 4-amino phenol.[159] A light responsive ferromagnetic $Bi_7Fe_3Ti_3O_{21}$ catalyst was prepared for the photocatalytic degradation of Rhodamine B under the irradiation of a 20 W fluorescent lamp with wavelengths ranging from 400 to 760 nm at neutral pH.[164] The ferromagnetic $Bi_7Fe_3Ti_3O_{21}$ catalyst induced the easy decolouration of Rhodamine B using the catalyst. The light responsive catalyst was also recycled by centrifugation of the dispersed catalyst in an aqueous medium followed by a similar experiment.

More recently, SSBMMs were also used for catalysis applications. Zheng *et al.*[165] synthesised a novel biphasic Pickering emulsion and micelle catalyst with magnetically (Fe_3O_4)-induced hydrophobic polymer (polystyrene) nanospheres. A Pickering emulsion, such as water-in-oil or oil-in-water is normally used for the reduction of surface energy. In another case, the emulsion was also used for the self-assembly of nano or micro particles to form particle framework capsules. Based on this technique, the prepared magnetic micelle nanocatalyst was modified by 2,2,6,6-tetramethylpiperidine 1-oxyl (TEMPO) as a model oxidation catalyst. This TEMPO-grafted Fe_3O_4/PS nanoparticles surface formed a micelle-like architecture, and was used for the Montanari oxidation of alcohols (Fig. 26). Li *et al.*[166] fabricated a multifunctional ferromagnetic superhydrophobic film for the reduction of p-nitro phenol. The various types of synthesised superhydrophobic magnetic nanoparticles (Co, 152.2° ± 0.9°, Ni, 152.2° ± 0.9°, $Co_{75}Ni_{25}$ alloy, 156.3° ± 1.4°, and $Co_{50}Ni_{50}$ alloy, 153.5° ± 1.2°) exhibited an excellent catalytic effect for the reduction of p-nitro phenol. The ferromagnetic nanoparticles were recycled successfully 20 times for the reduction of p-nitro phenol. The results showed an almost similar trend for the reduction capacity at the first and 20th cycle, and confirmed the excellent catalytic properties of the magnetically-induced superhydrophobic films.

3.3. Sensors

Sensors are used widely for the detection of chemical compounds or bio-molecules or metal ions in mixed solutions.[167,168] Magnetic nanoparticle-based sensors are used widely in a range of applications, such as the sensing of metal ions, detection of antibodies, magnetic resonance imaging (MRI), and various other bio-medical applications. Superhydrophobic surfaces and materials have attracted recent attention for various sensing applications. Pang *et al.*[169] developed a novel, highly sensitive and flexible superhydrophobic strain gauge sensor using ultra-violet curable polyurethane acrylate (PUA). First, a replica was fabricated by exposure to UV light for several hours and two layers of Pt-coated PUA nanohair array were then placed in contact with the surface followed by sealing with a thin layer of PDMS and an oxygen plasma treatment on both sides. The resulting substrate showed a hierarchical surface morphology with superhydrophobic (160°) properties. The fabricated device was used to detect the physical force of a heartbeat and the dynamic motion of a small bouncing droplet. Yoon *et al.*[170] prepared well-ordered multi-functional spherical monodisperse nanoparticles with magnetic, superhydrophobic and sensing properties (Fig. 27). The multi-functional nano-sensor was prepared by the synthesis of a core material, such as aminopropyltrimethoxysilane (APS)-functionalised silica colloidal suspension, which was modified further by 2-bromo-2-methylpropionic acid (BMPA)/quantum dots (QD) and poly(amidoamine) (i.e. PAMA) dendrimers. In another step, the synthesised Fe_3O_4 nanoparticles was functionalised further using 2-bromo-2-methylpropionic acid (BMPA). The functionalised Fe_3O_4 nanoparticles were added to the surface of the core-shell sphere, and a layer by layer type of well-ordered multi-functional magnetic raspberry-type spherical particles were prepared (Fig. 27). The layer prepared by the layer hybrid substrate also showed superhydrophobic (153°) and photo luminescent properties under UV light.

3.4. Bio-medicals

Several environmental-friendly materials already existed for various types of bio-medical applications, such as drug and gene delivery, tissue engineering, cancer-therapy, dental, and bone regeneration applications.[171-173] Recently, superhydrophobic surfaces and SSBMMs have also attracted attention in various bio-applications, such as cell and protein adhesion and transport, blood typing, drug delivery, anti-bio adhesion, fluid transport, and the detection of antibodies.[174-179] Pernites *et al.*[176] fabricated colloidally-templated, superhydrophobic polythiophene films and examined the switchable adhesion behaviour of proteins and bacterial cells on the surface. The fabricated substrate exhibited stable superhydrophobicity under a wide range of pHs (pH 1 to 13) and temperatures of -10 °C to +80 °C with self-cleaning properties and a very low sliding angle 3° ± 1°. Protein and bacteria cell adhesion were examined by doping and dedoping of the superhydrophobic surface. A doping study was carried out using an electrochemical technique by immersing the superhydrophobic surface in aceteonitrile (ACN) with hexafluorophosphate (0.1 M TBAH) along with the reference (Ag/AgCl) and counter (Pt wire) electrodes followed by the application of a constant oxidation potential (1.5 V or 0 V) for 30 min. The undoped surface maintained its superhydrophobicity before and after coming in contact with the fibrinogen on the surface which results the resisting property of the superhydrophobic surface for the protein molecules adhesion on the surface. On the other hand, the doped superhydrophobic surface by applying an oxidation potential 1.05 V showed switchable surface properties, ranging from superhydrophobic to hydrophilic, as well as excellent adhesion of the fibrinogen by nucleating the protein on the porous gaps of the surface. The hydrophilic property becomes superhydrophobic after dedoping at the oxidation potential of 0 V. The results showed the excellent tuning properties of the superhydrophobic surface under an oxidation potential and

improved the adhesion behaviour for protein and bacteria cells. Song *et al.*[177,178] fabricated a superhydrophobic polystyrene (PS) substrate, which was treated with argon plasma at 30 W for 20 s and the surface was modified with 1H,1H,2H,2H-perfluorodecyltrimethoxysilane. Magnetic microparticles, chitosan and genipin-mixed magnetic hydrogel beads were prepared by dropping the hydrogel solution on the superhydrophobic surface (>150°). The resulting magnetic responsive hydrogel was freeze dried and used to examine the cell adhesion and expansion behaviour on the surface of the hydrogel beads. The magnetic responsive hydrogel beads exhibited good cytocompatibility, such as pristine chitosan. Moreover, the magnetic hydrogel beads were also easy fixed and transported from the culture medium with an external magnetic field, which results the use of a new system of the superhydrophobic surface for the preparation of uniform size biocompatible hydrogel beads. Nie *et al.*[179] prepared the superhydrophobic surface-based analytical platform (SSAP) on the inner wall surfaces of a polypropylene (PP) tube by a coating with bisphenol A-type polycarbonate (PC) particles on the surface. The authors also prepared magnetic particle-based bio-conjugates by mixing amine coated superparamagnetic nanoparticles (0.5 μm to 1 μm) in glutaraldehyde, which was modified further with Schistosoma *japonicum antigen* (sjAg) (Fig. 28). On the other hand, a modified gold nanoparticle-based bio-conjugate was also prepared by mixing Au nanoparticles with antibodies. They also reported three main advantages for the detection of antibodies using the superhydrophobic surface: 1) requirement of a small volume of a biomagnetic particle probe, reagents or samples and a shorter time; 2) efficient mixing and binding of antigen and antibodies via a self-circulating flowing mechanism; and 3) reusability of the system more than 300 times.[179] The potential advantages of this simple system for the detection of antibodies using superhydrophobic surface-based magnetic electrochemical immunoassays can be usable in a range of bio-molecule sensors.

3.5. Micro-fluidic devices and actuators

Micro-fluidic devices are an important classical type of application for controlled fluid transport and a reaction of small amounts of liquid or gas in micrometre-sized miniature channels. The applications of micro-fluidic devices are well established in various bio-medical applications, such as the detection of proteins, DNA amplification, biological cell manipulation, stem cells, drug delivery, single cell analysis, structural biology, electronic devices, and other applications.[180-190] This is because of the controlled flow of liquid or gas at the channel, which makes the device easily detect various types of bio-molecules. Superhydrophobic surfaces have attracted recent attention in the fabrication of micro-fluid devices due to the complete non-wetting property of the coated surfaces, which makes easy flow of the fluid on the substrate surface and reduces the loss of the sample during the experiment, which then increased the reusability of the sample.[191,192] Bormashenko *et al.*[193] fabricated liquid marble type superhydrophobic micro-fluidic devices on a poly(methyl methacrylate) (PMMA) substrate via a hot pressing (95 °C) technique using a hydrophobic PTFE nanopowder (100-200 nm). They examined the movement of ferrofluids on the superhydrophobic surface with the support of an external magnetic field. A ferrofluidics liquid marble was first prepared by dispersing the Fe_2O_3 nanoparticles in water. The resulting fluid was dropped slowly on the superhydrophobic surface using a micro-syringe and the ferrofluids were covered with layers of polyvinylidinefluoride (PVDF) beads (130 nm) and rolled on the polyethylene (PE) substrate. Fluid motion was controlled by an external magnetic field (permanent neodymium magnet, 0.5 T) applied to the bottom of the PE substrate. A thin polypropylene film was kept on the outer surface of the ferrofluids liquid marbles (Fig. 29) stacked on the PE substrate and moved slowly with the assistance of a magnetic field. The ferrofluids were easy magnetised by the magnetic field and

moved in the direction of the applied magnetic field. When a ferrofluid liquid marble moves on the substrate as a result of a permanent magnet, it also moves and rotates the PP film on the surface of the ferrofluids liquid marble towards the directions of the magnetic field, as indicated in Fig. 29. The results highlight the possibilities of the fabrication of magnetic ferrofluidic devices for a variety of applications. García *et al.*[194] also examined the movements of a magnetic fluid on the superhydrophobic surface. First, they synthesised polysiloxane-coated carbonyl-iron microparticles by mixing carbonyl-iron microparticles with tetraethoxyorthosilicate (TEOS) in the presence of ethyl alcohol and an ammonium hydroxide solution. The polysiloxane magnetic fluid was modified by doping with various biological fluids (8% bovine serum albumin (BSA), foetal bovine serum (VWR), and whole bovine blood supplemented with an anti-coagulant, K_3EDTA), and checked the movement of the magnetic biological fluid on the superhydrophobic surface. Similar to the Bormashenko *et al.*[193], this study also suggests the movement of magnetic biological fluids by the permanent magnet. In another method, Seo *et al.*[195] prepared superhydrophobic magnetic elastomer actuators for the controlled motion of fluid droplets. The superhydrophobic elastomer prepared with four coatings, such as the soft layer at the bottom, magnetic elastomer layer at the second followed by the hard elastomer coating. The top (fourth) layer consisted of a superhydrophobic coating that was fabricated by applying a pre-dissolved solution of isotactic polypropylene in p-xylene and a-butanone using a spray coating method. Based on these four layer coatings, the fabricated substrate showed robust superhydrophobicity (159° ± 1°) and very low hysteresis (2°) with magnetically active properties (Fig. 30). When a water drop was placed on the superhydrophobic elastomeric surface the surface formed a mini-bowl (or concave) shape on the substrate due to the elastic property of the surface. The droplet rolls on the concave bowl due to the gravitational force toward to centre of the bowl. On the

other hand, when a droplet is placed in the presence of an external magnetic field, the ferromagnetic elastomer coating activates the droplet on the concave shape bowl, and the move is towards the direction of the permanent magnet. The velocity at the movement of a droplet in the magnetically-induced superhydrophobic elastomer substrate by the presence of an external magnetic field could be higher than 8 cm/s. This simple idea gave the technical advantages of the use of a superhydrophobic magnetic elastomer substrate for controlled fluid transport and other applications.

3.6. Other applications

The applications of SSBMMs are also used for the synthesis of anisotropic magnetic nanoparticles, electromagnetic shielding, etc. Rastogi *et al.*[196] synthesised well-ordered anisotropic magnetic nanoparticles (Mickey mouse) using iron-nickel alloy (Iron 55% and Nickel 45%), which was modified by TEOS in the presence of an aqueous ammonia solution. The nanoparticles suspension was stabilised using PS latex to form a patchy magnetic supraparticles on the superhydrophobic surface. A variety of patchy magnetic supraparticles were prepared by applying rod magnets at different directions to engineer magnetic supraparticles with the desired shape, such as single, double and tri patchy magnetic particles (Fig. 31). Ding *et al.*[197] prepared SSBMM in a one-pot approach by mixing the Fe_3O_4 nanoparticles with silicone resin, curing agent and aminopropyltriethoxysilane (APS). The dispersant was cast on a glass or polycarbonate substrate using a drawdown rod and dried at ambient temperature for 1 week. The superhydrophobicity of the surface was mainly due to the amounts of Fe_3O_4 nanoparticles present in the dispersion. The cast substrate exhibited hydrophobic properties at lower levels of Fe_3O_4 nanoparticles in the dispersion. On the other

hand, the surface contact angle increased gradually with increasing Fe_3O_4 weight percentage and become superhydrophobic (156-158°) at more than 40 wt.% Fe_3O_4 nanoparticles. The SSBMM exhibited highly stable surface property and enhanced mechanical hardness compared to the pristine Fe_3O_4 nanoparticle-coated substrate. The magnetic superhydrophobic surface also showed a stable surface property under the QUV accelerated weathering test (QUV/se, Q-Panel, Co. Ltd., USA). QUV/se tester was used to test the surface property of a material under accelerated weathering conditions such as UV light, condensation, and solar eye irradiation control. The surface treated magnetic nanoparticles can show an electromagnetic shielding effect. The electromagnetic shielding effectiveness (SE%) was measured from the magnetic superhydrophobic surface. The pristine polysiloxane coating showed <3% SE% on the coated substrate, which indicated no shielding effect of the substrate. On the other hand, the Fe_3O_4 nanoparticles-loaded superhydrophobic coated substrate showed 60% SE% over the frequency range (10–3000 Hz), which indicated a higher electromagnetic shielding property of the superhydrophobic substrate. The results proved the excellent electromagnetic shielding property of the Fe_3O_4 nanoparticles on the superhydrophobic surface. Moreover, the higher reflection by the rough superhydrophobic surface was also responsible for the electromagnetic shielding. The enhanced electromagnetic shielding properties of the hierarchical superhydrophobic surface highlight the use of the substrate in self-cleaning coatings. SSBMMs are also useful in a range of applications through simple modifications of the surface properties.

.

4. Conclusions and Future Perspectives

This review deals with the recent approaches and their potential advantages and emerging applications of superhydrophobic surface based magnetic materials (SSBMMs) with broad way

of explaining the main concepts to synthesise and fabricate a new class of SSBMMs, such as magnetic nanoparticles, liquid marbles, sponges and foams, aerogels, fabrics and papers, and fluids for various applications, such as oil sorption and separation, catalysis, sensors, bio-medicals, micro-fluidic devices and actuators, anisotropic magnetic nanoparticles synthesis, and electromagnetic shielding. The wide ranges of applications by the SSBMMs are important because of the excellent recyclable property, ease of the control of motion by the external magnetic field and the ability to switch the surface property by the electrode potential. These smart ways of producing SSBMMs result highly stable surface properties under a wide range of conditions, such as temperature, pH, light, and acid/base solutions. The potential properties of the SSBMMs also show the emerging trends of the surface for various applications and the extreme breakthrough of the SSBMMs for a variety of other applications in the future.

Acknowledgements

This study was supported by the National Research Foundation of Korea (NRF) Grant funded by The Ministry of Science, ICT & Future Planning, Korea. Pioneer Research Center Program (2010-0019308/2010-0019482) and Brain Korea (BK) 21 Plus Program (21A2013800002).

Abbreviations

MRI	Magnetic resonance imaging (MRI)
SSBMMs	Superhydrophobic surface based magnetic materials
UV	Ultra-violet
PMHOS	Polymethylhydroxysiloxane
CA	Contact angle
CAH	Contact angle hysteresis
DCAs	Dynamic contact angles
θ_a	Advancing CA
θ_r	Receding CA
SAXS	Small angle X-ray scattering
TPX	Polymethylpetene
PVA	Polyvinyl alcohol
$FeAc_2$	Ferrous acetate
CNFs	Carbon nanofibers
PVDF	Poly(vinylidine fluoride)
MNPs	Magnetite nanoparticles
HFBA	2,2,3,4,4,4-hexafluorobutyl acrylate
FOS-12	Dodecafluorooctatriethoxysilane
PSVSF	polystyrene/silica/maghemite
FAS	Tridecafluorooctyl triethoxysilane
Fe_3O_4	Magnetite
PMSQ	Poly(methylsilsesquioxane)

1	OTS	n-Octadecyltrimethoxysilane
2	SEM	Scanning electron microscopy
3	FESEM	Field emission scanning electron microscopy
4	TEM	Transmission electron microscopy
5	P2VP- *b* -PDMS	Poly(2-vinylpyridine-*b*-dimethylsiloxane)
6	PAG	Photoacid generator
7	ETPTA	Ethoxylated trimethylolpropane triacrylate
8	Fe_2O_3	Iron (II) oxide
9	PVA	Poly(vinyl alcohol)
10	Pluronic F108	Ethyleneoxide propyleneoxide tri-block copolymer
11	FD-POSS	Fluorinated decylpolyhedral oligomeric silsesquioxane
12	DMSO	Dimethyl sulfoxide
13	EMIMTFB	1-ethyl-3-methylimidazolium tetrafluoroborate
14	TEOS	Tetraethoxysilane
15	CTAB	Cetyltrimethylammonium bromide
16	NH_4NO_3	Ammonium nitrate
17	SiO_2	Silica nanoparticles
18	RMPs	Stimuli-responsive magnetic particles
19	CNT	Carbon nanotube
20	PU	Polyurethane
21	PTES	1H,1H,2H,2H-Perfluorooctyltriethoxysilane
22	PTMTC	Polychlorinated triphenylmethyl tricarboxylate
23	C_{20} dithiol	Icosane-1,20-dithiol

1	C_{30} dithiol	Triacontane-1,30-dithiol
2	CVD	Chemical vapour deposition
3	PTFE	Polytetrafluoroethylene
4	NPs	Nanoparticles
5	$Fe(NO_3)_3$	Ferric nitrate
6	$Co(NO_3)_2$	Cobalt (II) nitrate
7	$Ni(NO_3)_2$,	Nickel (II) nitrate
8	VSM	Vibrating sample magnetometry
9	PPy	Polypyrrole
10	XRD	X-ray diffraction
11	TGA	Thermogravimetric analysis
12	AACVD	Aerogel assisted chemical vapour deposition method
13	OTMS	Trimethoxy(octadecyl) silane (OTMS)
14	$Fe(acac)_3$	Iron (III) acetylacetonate
15	$Mn(acac)_2$	Manganese (II) acetylacetonate
16	ECA	Ethyl-2-cyanoacrylate
17	PTFE	Polytetrafluoroethylene
18	PECA	Poly(ethyl-2-cyanoacrylate)
19	PS	Polystyrene
20	LDPE	Low density polyethylene
21	Me-CNT	Magnetic carbon nanotube
22	CVD	Chemical vapour deposition
23	HDTES	n-hexadecyltriethoxysilane

1	TEMPO	2,2,6,6-tetramethylpiperidine 1-oxyl
2	PUA	Polyurethane acrylate
3	APS	Aminopropyltrimethoxysilane
4	BMPA	2-bromo-2-methylpropionic acid
5	QD	Quantum dot
6	PAMA	Poly(amidoamine)
7	EB-MOS	Ethidium bromide-bridged alkoxysilane precursor
8	ACN	Acetonitrile
9	TBAH	Hexafluorophosphate
10	SSAP	Superhydrophobic surface-based analytical platform
11	PC	Polycarbonate
12	CV	Cyclic voltammetry
13	DNA	Deoxyribonucleic acid.
14	PMMA	Poly(methyl methacrylate)
15	PVDF	Polyvinylidinefluoride
16	PE	Polyethylene
17	BSA	Serum albumin
18	QUV/se	UV light, condensation, and solar eye irradiation control
19	SE	Shielding effectiveness
20		

References and Notes

1. S. Nagappan, J. J. Park, S. S. Park, W. K. Lee and C. S. Ha, *J. Mater. Chem. A*, 2013, **1**, 6761-6769.
2. S. Nagappan and C. S. Ha, *Macromol. Res.*, 2014, **22**, 843-852.
3. T. Darmanin and F. Guittard, *J. Mater. Chem. A*, 2014, **2**, 16319-16359.
4. K. Liu, X. Yao and L. Jiang, *Chem. Soc. Rev.*, 2010, **39**, 3240-3255.
5. Y. Liu and G. Li, *J. Colloid Interface Sci.*, 2012, **388**, 235-242.
6. K. Liu and L. Jiang, *Annu. Rev. Mater. Res.*, 2012, **42**, 231-263.
7. X. Liu, J. Zhou, Z. Xue, J. Gao, J. Meng, S. Wang and L. Jiang, *Adv. Mater.*, 2012, **24**, 3401-3405.
8. D. Zhong, Q. Yang, L. Guo, S. Dou, K. Liu and L. Jiang, *Nanoscale*, 2013, **5**, 5758-5764.
9. B. H. Kim, D. H. Lee, J. Y. Kim, D. O. Shin, H. Y. Jeong, S. Hong, J. M. Yun, C. M. Koo, H. Lee and S. O. Kim, *Adv. Mater.*, 2011, **23**, 5618-5622.
10. S. Nagappan, S. S. Park and C. S. Ha, *J. Nanosci. Nanotechnol.*, 2014, **14**, 1441-1462.
11. X. Yao, Y. Song and L. Jiang, *Adv. Mater.*, 2011, **23**, 719-734.
12. F. Xia and L. Jiang, *Adv. Mater.*, 2008, **20**, 2842-2858.
13. Q. Zhu, Y. Chu, Z. K. Wang, N. Chen, L. Lin, F. T. Liu and Q. M. Pan, *J. Mater. Chem. A*, 2013, **1**, 5386-5393.
14. H. Zhou, H. Wang, H. Niu, A. Gestos and T. Lin, *Adv. Funct. Mater.*, 2013, **23**, 1664-1670.
15. M. Liu and L. Jiang, *Adv. Funct. Mater.*, 2010, **20**, 3753-3764.
16. X. Yu, Z. Wang, Y. Jiang, F. Shi and X. Zhang, *Adv. Mater.*, 2005, **17**, 1289-1293.

17. H. S. Lim, D. Kwak, D. Y. Lee, S. G. Lee and K. Cho, *J. Am. Chem. Soc.*, 2007, **129**, 4128-4129.
18. A. Chaudhary and H. C. Barshilia, *J. Phys. Chem. C*, 2011, **115**, 18213-18220.
19. J. Byun, J. Shin, S. Kwon, S. Jang and J. K. Kim, *Chem. Commun.*, 2012, **48**, 9278-9280.
20. L. Chen, M. J. Liu, L. Lin, T. Zhang, J. Ma, Y. L. Song and L. Jiang, *Soft Matter*, 2010, **6**, 2708-2712.
21. R. B. Pernites, R. R. Ponnapati and R. C. Advincula, *Adv. Mater.*, 2011, **23**, 3207-3213.
22. V. A. Ganesh, S. S. Dinachali, A. S. Nair and S. Ramakrishna, *ACS Appl. Mater. Interfaces*, 2013, **5**, 1527-1532.
23. P. A. Levkin, F. Svec and J. M. J. Fréchet, *Adv. Funct. Mater.*, 2009, **19**, 1993-1998.
24. Y. Li, L. Li and J. Sun, *Angew. Chem. Int. Ed.*, 2010, **122**, 6265-6269.
25. D. J. Yang, J. P. Li, Y. Xu, D. Wu, Y. H. Sun, H. Y. Zhu and F. Deng, *Microporous Mesoporous Mater.*, 2006, **95**, 180-186.
26. S. Nagappan, D. B. Lee, D. J. Seo, S. S. Park and C. S. Ha, *J. Ind. Eng. Chem.*, 2014, Doi: 10.1016/j.jiec.2014.07.022.
27. H. Budunoglu, A. Yildirim, M. O. Guler and M. Bayindir, *ACS Appl. Mater. Interfaces*, 2011, **3**, 539-545.
28. R. Fürstner, W. Barthlott, C. Neinhuis and P. Walzel, *Langmuir*, 2005, **21**, 956-961.
29. H. Ogihara, J. Xie, J. Okagaki and T. Saji, *Langmuir*, 2012, **28**, 4605-4608.
30. Y. Liu, J. H Xin and C. H. Choi, *Langmuir*, 2012, **28**, 17426-17434.
31. H. Bi, X. Xie, K. Yin, Y. Zhou, S. Wan, L. He, F. Xu, F. Banhart, L. Sun and R. S. Ruoff, *Adv. Funct. Mater.*, 2012, **22**, 4421-4425.

32. Z. Niu, J. Chen, H. H. Hng, J. Ma and X. Chen, *Adv. Mater.*, 2012, **24**, 4144-4150.
33. W. Barthlott and C. Neinhuis, *Planta*, 1997, **202**, 1-8.
34. C. Neinhuis and W. Barthlott, *Annals Bot.*, 1997, **79**, 667-677.
35. C. Dorrer and J. Rühe, *Soft Matter*, 2009, **5**, 51-61.
36. Z. G. Guo, W. M. Liu and B. L. Su, *J. Colloid Interface Sci.*, 2011, **353**, 335-355.
37. J. F. Joanny and P. G. de Gennes, *J. Chem. Phys.*, 1984, **81**, 552-562.
38. C. W. Extrand, *J. Colloid Interface Sci.*, 1998, **207**, 11-19.
39. L. Gao and T. J. McCarthy, *J. Am. Chem. Soc.*, 2006, **128**, 9052-9053.
40. S. Nagappan, M. C. Choi, G. Sung, S. S. Park, M. S. Moorthy, S. W. Chu, W. K. Lee and C. S. Ha, *Macromol. Res.*, 2013, **21**, 669-680.
41. P. Ragesh, V. A. Ganesh, S. V. Nair and A. S. Nair, *J. Mater. Chem. A*, 2014, **2**, 14773–14797.
42. http://www.irm.umn.edu/hg2m/hg2m_b/hg2m_b.html
43. http://en.wikipedia.org/wiki/Magnetism
44. http://phys.thu.edu.tw/~hlhsiao/mse-web_ch20.pdf
45. X. M. Zheng, Q. B. Zhang and J. Wang, *Micro Nano Lett.*, 2012, **7**, 561-563.
46. X. Zhang, Y. Guo, Y. Liu, X. Yang, J. Pan and P. Zhang, *Appl. Surf. Sci.*, 2013, **87**, 299-303.
47. J. J. Zhang and Z. L. Lei, *Appl. Surf. Sci.*, 2012, **258**, 5080-5085.
48. R. Pogreb, G. Whyman, R. Barayev, E. Bormashenko and D. Aurbach, *Appl. Phys. Lett.*, 2009, **94**, 221902.
49. Y. Zhu, J. C. Zhang, J. Zhai, Y. M. Zheng, L. Feng and L. Jiang, *Chem. Phys. Chem.*, 2006, **7**, 336-341.

50. S. Wang, Q. W. Liu, Y. Zhang, S. D. Wang, Y. X. Li, Q. B. Yang and Y. Song, *Appl. Surf. Sci.*, 2013, **279**, 150-158.

51. Y. Fan, C. Li, Z. Chen, F. Ma and H. Chen, *Surf. Coat. Technol.*, 2012, **213**, 8-14.

52. L. D. Zhang, W. L. Liu, W.H. Xu, J.S. Yao, L. Zhao, X.Q. Wang and Y.Z. Wu, *Appl. Surf. Sci.*, 2012, **259**, 719-725.

53. Z. B. Huang, Y. Zhu, J. Zhang and G. F. Yin, *J. Phys. Chem. C*, 2007, **111**, 6821-6825.

54. L. Zhang, J. Wu, Y. Wang, Y. Long, N. Zhao and J. Xu, *J. Am. Chem. Soc.*, 2012, **134**, 9879-9881.

55. J. Fang, H. X. Wang, Y. H. Xue, X. A. Wang and T. Lin, *ACS. Appl. Mater. Interfaces*, 2010, **2**, 1449-1455.

56. M. Giardiello, T. O. McDonald, P. Martin, A. Owen and S. P. Rannard, *J. Mater. Chem.*, 2012, **22**, 24744-24752.

57. Y. Z. Voloshin, I. G. Belaya (Makarenko), A. S. Belov, V. E. Platonov, A. M. Maksimov, A. V. Vologzhanina, Z. A. Starikova, A. V. Dolganov, V. V. Novikov and Y. N. Bubnov, *Dalton Trans.*, 2012, **41**, 737-746.

58. J. V. I. Timonen, M. Latikka, O. Ikkala and R. H. A. Ras, *Nat. Commun.*, 2013, **4**, 2398.

59. P. Aussillous and D. Quéré, *Nature*, 2001, **411**, 924-927.

60. P. Aussillous and D. Quéré, *Proc. R. Soc. A*, 2006, **462**, 973-999.

61. G. McHale and M. I. Newton, *Soft Matter*, 2011, **7**, 5473-5481.

62. E. Bormashenko, *Curr. Opin. Colloid Interface Sci.*, 2011, **16**, 266-271.

63. S. Ogawa, H. Watanabe, L. M. Wang, H. Jinnai, T. J. McCarthy and A. Takahara, *Langmuir*, 2014, **30**, 9071-9075.

64. M. I. Newton, D. L. Herbertson, S. J. Elliott, N. J. Shirtcliffe and G. McHale, *J. Phys. D: Appl. Phys.*, 2007, **40**, 20-24.

65. C. Aberle, M. Lewis, G. Yu, N. Lei and J. Xu, *Soft Matter*, 2011, **7**, 11314-11318.

66. S. Fujii, S. Kameyama, S. P. Armes, D. Dupin, M. Suzaki and Y. Nakamura, *Soft Matter*, 2010, **6**, 635-640.

67. J. M. Chin, M. R. Reithofer, T. T. Y. Tan, A. G. Menon, E. Y. Chen, C. A. Chow, A. T. S. Hor and J. Xu, *Chem. Commun.*, 2013, **49,** 493-495.

68. T. Arbatan and W. Shen, *Langmuir*, 2011, **27**, 12923-12929.

69. A. Hashmi, A. Strauss and J. Xu, *Langmuir*, 2012, **28**, 10324-10328.

70. J. O. Marston, Y. Zhu, I. U. Vakarelski and S. T. Thoroddsen, *Powder Technol.*, 2012, **228**, 424-428.

71. D. Zang, K. Lin, W. Wang, Y. Gu, Y. Zhang, X. Geng and B. P. Binks, *Soft Matter*, 2014, **10**, 1309-1314

72. A. Tosun and H. Y. Erbil, *Appl. Surf. Sci.*, 2009, **256**, 1278-1283.

73. B. Laborie, F. Lachaussée, E. Lorenceau and F. Rouyer, *Soft Matter*, 2013, **9**, 4822-4830.

74. L. Zhang, D. Cha and P. Wang, *Adv. Mater.*, 2012, **24**, 4756-4760.

75. Y. Zhao, J. Fang, H. Wang, X. Wang and T. Lin, *Adv. Mater.*, 2010, **22**, 707-710.

76. Y. Xue, H. Wang, Y. Zhao, L. Dai, L. Feng, X. Wang and T. Lin, *Adv. Mater.*, 2010, **22**, 4814-4818.

77. Y. Zhao, Z. Xu, M. Parhizkar, J. Fang, X. Wang and T. Lin, *Microfluid. Nanofluid.*, 2012, **13**, 555-564.

78. J. Hu, S. Zhou, Y. Sun, X. Fang and L. Wu, *Chem. Soc. Rev.,* 2012, **41**, 4356–4378.

79. S. Lone and I. W. Cheong, *RSC Adv.*, 2014, **4**, 13322–13333.

80. Y. Zhao, H. Gu, Z. Xie, H. C. Shum, B. Wang and Z. Gu, *J. Am. Chem. Soc.*, 2013, **135**, 54-57.

81. S. Zhang, Y. Zhang, Y. Wang, S. Liu and Y. Deng, *Phys. Chem. Chem. Phys.*, 2012, **14**, 5132-5138.

82. Y. Li, Y. Hu, H. Jiang and C. Li, *Nanoscale*, 2013, **5**, 5360-5367.

83. M. Abkarian, S. Protiére, J. M. Aristoff and H. A. Stone, *Nature Commun.*, 2013, **4**, 1895.

84. Y. Hu, H. Jiang, J. Liu, Y. Li, X. Hou and C. Li, *RSC Adv.*, 2014, **4**, 3162-3164.

85. J. R. Dorvee, A. M. Derfus, S. N. Bhatia and M. J. Sailor, *Nat. Mater.*, 2004, **3**, 896-899.

86. E. Bormashenko, A. Musin, G. Whyman, Z. Barkay, A. Starostin, V. Valtsifer and V. Strelnikov, *Colloids Surf. A*, 2013, **425**, 15-23.

87. X. Y. Zhou, Z. Z. Zhang, X. H. Xu, X. H. Men and X. T. Zhu, *Ind. Eng. Chem. Res.*, 2013, **52**, 9411-9416.

88. L. Li, B. Li, L. Wu, X. Zhao and J. Zhang, *Chem. Commun.*, 2014, **50**, 7831-7833.

89. G. Férey, *Nat. Mater.*, 2003, **2**, 136-137.

90. D. Maspoch, D. Ruiz-Molina, K. Wurst, N. Domingo, M. Cavallini, F. Biscarini, J. Tejada, C. Rovira and J. Veciana, *Nature Mater.*, 2003, **2**, 190-195.

91. Y. Ito, A. Miyazaki, K. Takai, V. Sivamurugan, T. Maeno, T. Kadono, M. Kitano, Y. Ogawa, N. Nakamura, M. Hara, S. Valiyaveettil and T. Enoki, *J. Am. Chem. Soc.*, 2011, **133**, 11470-11473.

92. M. Cheng, G. Ju, C. Jiang, Y. Zhang and F. Shi, *J. Mater. Chem. A*, 2013, **1**, 13411-13416.

93. P. Calcagnile, D. Fragouli, I. S. Bayer, G. C. Anyfantis, L. Martiradonna, P. D. Cozzoli, R. Cingolani and A. Athanassiou, *ACS Nano*, 2012, **6**, 5413-5419.

94. N. Chen and Q. Pan, *ACS Nano*, 2013, **7**, 6875-6883.

95. N. Leventis, C. Chidambareswarapattar, A. Bang and C. Sotiriou-Leventis, *ACS Appl. Mater. Interfaces*, 2014, **6**, 6872-6882.

96. A. Soleimani Dorcheh and M. H. Abbasi, *J. Mater. Process. Technol.*, 2008, **199**, 10-26.

97. S. F. Chin, A. N. Binti Romainor and S. C. Pang, *Mater. Lett.*, 2014, **115**, 241-243.

98. H. H. Hamdeh, J. C. Ho, S. A. Oliver, R. J. Willey, G. Oliveri and G. Busca, *J. Appl. Phys.*, 1997, **81**, 1851-1857.

99. J. W. Long, M. S. Logan, C. P. Rhodes, E. E. Carpenter, R. M. Stroud and D. R. Rolison, *J. Am. Chem. Soc.*, 2004, **126**, 16879-16889.

100. R. T. Olsson, M. A. S. Azizi Samir, G. Salazar-Alvarez, L. Belova, V. Ström, L. A. Berglund, O. Ikkala, J. Nogués and U. W. Gedde, *Nat. Nanotechnol.*, 2010, **5**, 584-588.

101. S. Liu, Q. Yan, D. Tao, T. Yu and X. Liu, *Carbohydr. Polym.*, 2012, **89**, 551-557.

102. R. Xiong, C. Lu, Y. Wang, Z. Zhou and X. Zhang, *J. Mater. Chem. A*, 2013, **1**, 14910-14918.

103. V. Thiruvengadam and S. Vitta, *RSC Adv.*, 2013, **3**, 12765-12773.

104. S. M. Jones, M. S. Anderson, G. Dominguez and A. Tsapin, *Icarus*, 2013, **226**, 1-9.

105. J. S. Lee, S. K. Hong, N. J. Hur, W. S. Seo and H. J. Hwang, *Mater. Lett.*, 2013, **112**, 153-157.

106. C. R. Crick, J. C. Bear, P. Southern and I. P. Parkin, *J. Mater. Chem. A*, 2013, **1**, 4336-4344.

107. X. Zhang, L. Chen, T. Yuan, H. Huang, Z. Sui, R. Du, X. Li, Y. Lu and Q. Li, *Mater. Horiz.*, 2014, **1**, 232-236.

108. Y. F. Lin and J. L. Chen, *J. Colloid Interface Sci.*, 2014, **420**, 74-79.

109. S. Bullita, A. Casu, M. F. Casula, G. Concas, F. Congiu, A. Corrias, A. Falqui, D. Loche and C. Marras, *Phys. Chem. Chem. Phys.*, 2014, **16**, 4843-4852.

110. H. S. Lim, J. H. Baek, K. Park, H. S. Shin, J. Kim and J. H. Cho, *Adv. Mater.*, 2010, **22**, 2138-2141.

111. E. Richard, R. V. Lakshmi, S. T. Aruna and B. J. Basu, *Appl. Surf. Sci.*, 2013, **277**, 302-309.

112. L. Wu, J. P. Zhang, B. Li and A. Wang, *Polym. Chem.*, 2014, **5**, 2382-2390.

113. J. Li, L. Shi, Y. Chen, Y. B. Zhang, Z. G. Guo, B. L. Su and W. M. Liu, *J. Mater. Chem.*, 2012, **22**, 9774-9781.

114. C. Zhang, W. Zhou, Q. Wang, H. Wang, Y. Tang and K. S. Huid, *Appl. Surf. Sci.*, 2013, **276**, 377-382.

115. X. Chen, H. Zhu, C. Liu, Y. C. Chen, N. Weadock, G. Rubloff and L. Hu, *J. Mater. Chem. A*, 2013, **1**, 8201-8208.

116. M. Ma, Y. Mao, M. Gupta, K. K. Gleason and G. C. Rutledge, *Macromolecules*, 2005, **38**, 9742-9748.

117. I. S. Bayer, D. Fragouli, A. Attanasio, B. Sorce, G. Bertoni, R. Brescia, R. Di Corato, T. Pellegrino, M. Kalyva, S. Sabella, P. P. Pompa, R. Cingolani and A. Athanassiou, *ACS Appl. Mater. Interfaces*, 2011, **3**, 4024-4031.

118. A. Egatz-Gómez, S. Melle, A. A. García, S. A. Lindsay, M. Márquez, P. Domínguez-García, M. A. Rubio, S. T. Picraux, J. L. Taraci, T. Clement, D. Yang, M. A. Hayes and D. Gust, *Appl. Phys. Lett.*, 2006, **89**, 034106.

119. A. Egatz-Gómez, J. Schneider, P. Aella, D. Q. Yang, P. Domínguez-García, S. Lindsay, S. T. Picraux, M. A. Rubio, S. Melle, M. Marquez and A. A. García, *Appl. Surf. Sci.*, 2007, **254**, 330-334.

120. S. Daniel, M. K. Chaudhury and J. C. Chen, *Science*, 2001, **291**, 633-636.

121. K. Ichimura, S. K. Oh and M. Nakagawa, *Science*, 2000, **288**, 1624-1626.

122. X. Hong, X. F. Gao and L. Jiang, *J. Am. Chem. Soc.*, 2007, **129**, 1478-1479.

123. Z. G. Guo, F. Zhou, J. C. Hao, Y. M. Liang, W. M. Liu and W. T. S. Huck, *Appl. Phys. Lett.*, 2006, **89**, 081911.

124. Z. Cheng, L. Feng and L. Jiang, *Adv. Funct. Mater.*, 2008, **18**, 3219-3225.

125. J. Schneider, A. Egatz-Gómez, S. Melle, S. Lindsay, P. Domíinguez-García, M. A. Rubio, M. Márquez and A. A. García, *Colloids Surf. A*, 2008, **323**, 19-27.

126. G. P. Zhu, N. T. Nguyen, R. V. Ramanujan and X. Y. Huang, *Langmuir*, 2011, **27**, 14834-14841.

127. J. V. I. Timonen, M. Latikka, L. Leibler, R. H. A. Ras and O. Ikkala, *Science*, 2013, **341**, 253-257.

128. E. Bormashenko and Y. Bormashenko, *Langmuir*, 2011, **27**, 3266-3270.

129. X. Deng, L. Mammen, H. J. Butt and D. Vollmer, *Science*, 2012, **335**, 67-70.

130. S. Nagappan, H. Y. Park, A. R. Sung and C. S. Ha, *Compos. Interfaces*, 2014, **21**, 597-609.

131. H. Yabu and M. Shimomura, *Chem. Mater.*, 2005, **17**, 5231-5234.

132. H. Wang, Y. Xue, J. Ding, L. Feng, X. Wang and T. Lin, *Angew. Chem. Int. Ed.*, 2011, **50**, 11433-11436.

133. T. Dikić, W. Ming, R. A. T. M. van Benthem, A. C. C. Esteves and G. de With, *Adv. Mater.*, 2012, **24**, 3701-3704.

134. Y. Lai, Y. Tang, J. Gong, D. Gong, L. Chi, C. Lin and Z. Chen, *J. Mater. Chem.*, 2012, **22**, 7420-7426.

135. Q. Zhu, Q. Pan and F. Liu, *J. Phys. Chem. C*, 2011, **115**, 17464-17470.

136. J. Zhao, W. Ren and H. M. Cheng, *J. Mater. Chem.*, 2012, **22**, 20197-20202.

137. J. G. Reynolds, P. R. Coronado and L. W. Hrubesh, *J. Non-Cryst. Solids*, 2001, **292**, 127-137.

138. C. F. Wang and S. J. Lin, *ACS Appl. Mater. Interfaces*, 2013, **5**, 8861-8864.

139. Y. Tang, K. L. Yeo, Y. Chen, L. W. Yap, W. Xiong and W. Cheng, *J. Mater. Chem. A*, 2013, **1**, 6723-6726.

140. H. Sun, Z. Xu and C. Gao, *Adv. Mater.*, 2013, **25**, 2554-2560.

141. B. R. Solomon, M. N. Hyder and K. K. Varanasi, *Scientific Rep.*, 2014, **4**, 5504 (1-6).

142. X. Gui, Z. Zeng, Z. Lin, Q. Gan, R. Xiang, Y. Zhu, A. Cao and Z. Tang, *ACS Appl. Mater. Interfaces*, 2013, **5**, 5845-5850.

143. B. Ge, Z. Z. Zhang, X. T. Zhu, G. Ren, X. H. Men and X. Y. Zhou, *Colloids Surf. A*, 2013, **429**, 129-133.

144. Q. Zhu, F. Tao and Q. Pan, *ACS Appl. Mater. Interfaces*, 2010, **2**, 3141-3146.

145. L. P. Xu, X. Wu, J. Meng, J. Peng, Y. Wen, X. Zhang and S. Wang, *Chem. Commun.*, 2013, **49**, 8752-8754.

146. X. Y. Zhou, Z. Z. Zhang, X. H. Xu, X. Men and X. T. Zhu, *Ind. Eng. Chem. Res.*, 2013, **52**, 9411-9416.
147. L. Zhou, J. Xu, H. Miao, F. Wang and X. Li, Appl. *Catal., A, Gen.*, 2005, **292**, 223-228.
148. X. Q. Li, L. P. Zhou, J. Gao, H. Miao, H. Zhang and J. Xu, *Powder Technol.*, 2009, **190**, 324-326.
149. H. Ma, J. Xu, C. Chen, Q. Zhang, J. Ning, H. Miao, L. Zhou and X. Li, *Catal. Lett.*, 2007, **113**, 104-108.
150. V. Polshettiwar, R. Luque, A. Fihri, H. Zhu, M. Bouhrara and J. M. Basset, *Chem. Rev.*, 2011, **111**, 3036-3075.
151. X. Li, Z. Ju, F. Li, Y. Huang, Y. M. Xie, Z. P. Fu, R. J. Knize and Y. Lu, *J. Mater. Chem. A*, 2014, **2**, 13366-13372.
152. S. Shi, M. Wang, C. Chen, J. Gao, H. Ma, J. Ma and J. Xu, *Chem. Commun.*, 2013, **49**, 9591-9593.
153. C. Chen, S. Shi, M. Wang, H. Ma, L. Zhou and J. Xu, *J. Mater. Chem. A*, 2014, **2**, 8126-8134.
154. T. Kamegawa, Y. Shimizu and H. Yamashita, *Adv. Mater.*, 2012, **24**, 3697-3700.
155. B. Sreedhar, A. S. Kumar and P. S. Reddy, *Tetrahedron Lett.*, 2010, **51**, 1891-1895.
156. B. Sreedhar, A. S. Kumar and D. Yada, *Tetrahedron Lett.*, 2011, **52**, 3565-3569.
157. B. Sreedhar, A. S. Kumar and D. Yada, *Synlett.*, 2011, **8**, 1081-1084.
158. H. Aliyan, R. Fazaeli and R. Jalilian, *Appl. Surf. Sci.*, 2013, **276**, 147-153.
159. Y. Qiu, Z. Ma and P. Hu, *J. Mater. Chem. A*, 2014, **2**, 13471-13478.
160. Z. Y. Deng, W. Wang, L. H. Mao, C. F. Wang and S. Chen, *J. Mater. Chem. A*, 2014, **2**, 4178-4184.

161. P. Ragesh, S. V. Nair and A. S. Nair, *RSC Adv.*, 2014, **4**, 38498-38504.

162. S. Afzal, W. A. Daoud and S. J. Langford, *J. Mater. Chem. A*, 2014, **2**, 18005–18011.

163. K. Liu, M. Cao, A. Fujishima and L. Jiang, *Chem. Rev.*, 2014, **114**, 10044-10094.

164. P. -Z. Li, A. Aijaz and Q. Xu, *Angew. Chem. Int. Ed.*, 2012, **51**, 6753-6756.

165. H. Li, J. Liao, Y. Du, T. You, W. Liao and L. Wen, *Chem. Commun.*, 2013, **49**, 1768-1770.

166. I. Koh and L. Josephson, *Sensors*, 2009, **9**, 8130-8145.

167. F. Han, X. Qi, L. Li, L. Bu, Y. Fu, Q. Xie, M. Guo, Y. Li, Y. Ying and S. Yao, *Adv. Funct. Mater.*, 2014, **24**, 5011-5018.

168. J. Zhao, L. M. Wei, C. H. Peng, Y. J. Su, Z. Yang, L. Y. Zhang, H. Wei and Y. F. Zhang, *Biosens. Bioelectron.*, 2013, **47**, 86-91.

169. C. Pang, G. Y. Lee, T. I. Kim, S. M. Kim, H. N. Kim, S. H. Ahn and K. Y. Suh, *Nat. Mater.*, 2012, **11**, 795-801.

170. M. Yoon, Y. Kim and J. Cho, *ACS Nano*, 2011, **5**, 5417-5426.

171. M. I. Rial-Hermida, N. M. Oliveira, A. Concheiro, C. Alvarez-Lorenzo and J. F. Mano, *Acta Biomater.*, 2014, **10**, 4314-4322.

172. J. K. Bronk, B. H. Russell, J. J. Rivera, R. Pasqualini, W. Arap, M. Höök and E. M. Barbu, *Acta Biomater.*, 2014, **10**, 3354-3362.

173. M. S. Moorthy, M. J. Kim, J. H. Bae, S. S. Park, N. Saravanan, S. H. Kim and C. S. Ha, *Eur. J. Inorg. Chem.*, 2013, **17**, 3028-3038.

174. J. Lee, B. S. Kang, B. Hicks, T. F. Chancellor, B. H. Chu, H. T. Wang, B. G. Keselowsky, F. Ren and T. P. Lele, *Biomaterials*, 2008, **29**, 3743-3749.

175. H. Y. Wang, D. T. K. Kwok, M. Xu, H. G. Shi, Z. W. Wu, W. Zhang and P. K. Chu, *Adv. Mater.*, 2012, **24**, 3315-3324.

176. R. B. Pernites, C. M. Santos, M. Maldonado, R. R. Ponnapati, D. F. Rodrigues and R. C. Advincula, *Chem. Mater.*, 2012, **24**, 870-880.

177. W. Song, A. C. Lim and J. F. Mano, *Soft Matter*, 2010, **6**, 5868-5871.

178. W. Song, M. B Oliveira, P. Sher, S. Gil, J. M. Nóbrega and J. F. Mano, *Biomed. Mater.*, 2013, **8**, 045008 (1-8).

179. J. Nie, Y. Zhang, H. Wang, S. Wang and G. Shen, *Biosens. Bioelectron.*, 2012, **33**, 23-28.

180. J. Khandurina and A. Guttman, *J. Chromatogr. A*, 2002, **943**, 159-183.

181. L. Y. Yeo, H. -C. Chang, P. P. Y. Chan and J. R. Friend, *Small*, 2011, **7**, 12-48.

182. D. B Weibel and G. M Whitesides, *Curr. Opin. Chem. Biol.*, 2006, **10**, 584-591.

183. A. H. Diercks, A. Ozinsky, C. L. Hansen, J. M. Spotts, D. J. Rodriguez and A. Aderem, *Anal. Biochem.*, 2009, **386**, 30-35.

184. C. S. Zhang, J. L. Xu, W. L. Ma and W. L. Zheng, *Biotechnol. Adv.*, 2006, **24**, 243-284.

185. Q. Zhang and R. H. Austin, *Bionanoscience*, 2012, **2**, 277-286.

186. B. Ziaie, A. Baldi, M. Lei, Y. Gu and R. A. Siegel, *Adv. Drug Deliv. Rev.*, 2004, **56**, 145-172.

187. C. Kleinstreuer, J. Li and J. Koo, *Int. J. Heat Mass Tran.*, 2008, **51**, 5590-5597.

188. H. B. Yin and D. Marshall, *Curr. Opin. Biotechnol.*, 2012, **23**, 110-119.

189. C. Hansen and S. R Quake, *Curr. Opin. Struct. Biol.*, 2003, **13**, 538-544.

190. G. M. Whitesides, Nature, *2006*, **442**, 368-373.

191. F. Mumm, A. T. J. van Helvoort and P. Sikorski, *ACS Nano*, 2009, **3**, 2647-2652.

192. O. I. Vinogradova and A. L. Dubov, *Mendeleev Commun.*, 2012, **22**, 229-236.

193. E. Bormashenko, R. Pogreb, Y. Bormashenko, A. Musin and T. Stein, *Langmuir*, 2008, **24**, 12119-12122.

194. A. A. García, A. Egatz-Gómez, S. A. Lindsay, P. Domínguez-García, S. Melle, M. Marquez, M. A. Rubio, S. T. Picraux, D. Yang, P. Aella, M. A. Hayes, D. Gust, S. Loyprasert, T. Vazquez-Alvarez and J. Wang, *J. Magn. Magn. Mater.*, 2007, **311**, 238-243.

195. K. S. Seo, R. Wi, S. G. Im and D. H. Kim, Polym. Adv. Technol., 2013, **24**, 1075-1080.

196. V. Rastogi, A. A. García, M. Marquez and O. D. Velev, *Macromol. Rapid Commun.*, 2010, **31**, 190-195.

197. X. F. Ding, S. X. Zhou, G. X. Gu and L. M. Wu, *J. Coat. Technol. Res.*, 2011, **8**, 757-764.

Table caption

Table 1. Collective survey in the recent developments of superhydrophobic surface based magnetic materials (SSBMMs) and their properties.

Figure captions

Fig. 1 Instant superhydrophobic properties of the polymethylhydroxysiloxane/nature leaf powder hybrids on a range of substrates, (a) glass, (b) flexible laminating film, (c) tree leaf and (d) hand glove. (e and f) hand glove immersed in water before and after casting (attraction and reflection of uncasted and casted finger in water). (g) stainless steel plate, (h) paper, (i) cotton cloth, (j) cement floor, (k) wooden board, (l) cherry tomato and (m) fibreglass mesh (pore diameter, 1.5 mm). (n) Superhydrophobicity of the dip-coated hybrid/polydimethylsiloxane (PDMS) sponge dried at room temperature. (o and p) Superoleophilicity of the hybrid casted glass substrate for dodecane and soybean oil from ref.1. Reproduced with permission. Copyright 2013, Royal Society of Chemistry.

Fig. 2 Various ways of preparing superhydrophobic surface based magnetic materials (SSBMMs) and their potential applications.

Fig. 3 Number of papers published from 2004-2014 under the topic of (A) superhydrophobic surfaces, and (B) magnetic superhydrophobic surfaces (Source: ISI Web of Science).

Fig. 4 Pictorial representation of the methodology for producing Fe_3O_4@SiO_2@POTS magnetic microspheres from ref. 50. Reproduced with permission. Copyright 2013, Elsevier Ltd.

Fig. 5 Schematic diagram of polystyrene/silica/maghemite (PSVSF) preparation from ref. 52. Reproduced with permission. Copyright 2012, Elsevier Ltd.

Fig. 6 Scanning electron microscopy (SEM) images of Cu-ferrite films for different crystal growth times of (a) 1 h; (b) 3 h; (c) 8 h; and (d) 24 h from ref. 53. Reproduced with permission. Copyright 2007, American Chemical Society.

Fig. 7 Pictures of (a) water/oil separation and (b) an "oil marble" under water from ref. 54. Reproduced with permission. Copyright 2012, American Chemical Society.

Fig. 8 Synthetic route for surface-functionalised Fe_3O_4 nanoparticles from ref. 55. Reproduced with permission. Copyright 2010, American Chemical Society.

Fig. 9 (a) Preparation of a liquid marble with a particulate monolayer. (i) Rolling a droplet on PMSQ particle's bed. (ii) Surface cleaning of liquid marbles on clean OTS-modified substrate. (b−d) Optical micrograph of a liquid marble: (b) whole image, (c) magnified image of the as-prepared surface, and (d) magnified image after surface cleaning. (e) Confocal laser scanning microscopy images of bottom area of the liquid marble (5 μL of 1-ethyl-3-methylimidazolium tetrafluoroborate (EMIMTFB) containing 0.1 mg/mL rhodamine B dye). The observation position is depicted by the blue line in the z-axis from ref. 63. Reproduced with permission. Copyright © 2014, American Chemical Society.

Fig. 10 (a) Schematic diagram showing the preparation strategy for core/shell structured responsive magnetic particles. (b–e) transmission electron microscopy (TEM) images of Fe_3O_4 particles (b), Fe_3O_4@nSiO_2@mSiO_2 particles (c), and stimuli-responsive magnetic nanoparticles (RMPs) (d,e). Inset in (b): Enlarged TEM image of a single Fe_3O_4 particle. TEOS: Tetraethyl orthosilicate from ref. 74. Reproduced with permission. Copyright 2012, Wiley-VCH (Weinheim, Germany).

Fig. 11 a) Digital graphic images of liquid marbles produced from different liquids and FD-POSS powder (droplet size 3 μ L). For easy observation, a small amount of dye was added to the

liquid and the existence of the dye has no influence on the stability of the liquid marbles. b) Liquid marbles floating on water and hexadecane surfaces (droplet size 3 μ L). c) Magnet opened liquid marbles (droplet size 7 μ L). d) Magnet-driven motions of a FD-POSS-stained FD-POSS/Fe_3O_4 hexadecane marble on a glass slide (top) and water surface (bottom) (droplet size 7 μ L). e) Magnet opened hexadecane marbles with different numbers of coloured water droplets added (overall droplet size 10 μ L). f) A chemiluminescence reaction that occurs as a result of the coalescing of two magnetic liquid marbles that contain different reagents (top), and the same chemiluminescence reaction occurring within a single liquid marble (bottom) (droplet size 10 μ L). g) Chromatography analysis of a liquid in the opened liquid marble (droplet size 10 μ L). Scale bar: 1 mm from ref. 76. Reproduced with permission. Copyright 2010, Wiley-VCH (Weinheim, Germany).

Fig. 12 Photographs of multicompartment particles: (a) four compartment particles with red, blue, and green structural colours and a grey magnetic component; (b, c) three-compartment particles; (d−f) Janus particles. Scale bars are 100 μm from ref. 80. Reproduced with permission. Copyright 2013, American Chemical Society.

Fig. 13 Photographic and schematic diagrams of the PPy−PTES sponge fabrication process from ref. 87. Reproduced with permission. Copyright 2013, American Chemical Society.

Fig. 14 Expanded and contracted states of the magnetic sponge. Upper panel: Geometrical relation of two dipoles, μi at site i (located at the origin) and μ_j at site j. The vector r_{ij} connects i and j and makes an angle θ with respect to the X axis. Lower panel: the orange spheres represent the nanomagnet particles of a 3 nm Co-Pd alloy, and the blue spheres represent the nitrogen molecules. The black arrow represents the direction of the applied magnetic field. An expanded state with the nanopores filled with nitrogen is formed in the absence of a magnetic field (0 T), in

which the magnetic dipoles of the constituent nanomagnets are oriented randomly. A contracted state from which nitrogen has been expelled is formed upon the application of a magnetic field (7 T), in which all of the dipoles are oriented along the field direction. The two states are reversibly transformed by switching the magnetic field on/off. The nitrogen molecules serve to maintain the structure in the contracted/expanded state from ref. 91. Reproduced with permission. Copyright 2011, American Chemical Society.

Fig 15 Optical image (a), XRD pattern (b), TG curve (c), and room-temperature magnetisation hysteresis curve (d) of the as-prepared ultralight Fe_2O_3/C foams. The density of the foam was 3.9 mg cm^{-3}. A piece of ultralight Fe_2O_3/C foam could be manipulated by a magnet bar (e) and stand on a dandelion (f) from ref. 94. Reproduced with permission. Copyright 2013, American Chemical Society.

Fig. 16 Vibrating sample magnetometry measurements of γ-FeO*x* aerogel powders with various thermal treatments. The measurements were performed at ambient temperature from ref. 99. Reproduced with permission. Copyright 2004, American Chemical Society.

Fig. 17 (a) Coloured water droplets are laid onto the area of a cellulose sheet treated with poly(ethyl-2-cyanoacrylate) (PECA) (defined by the red line), whereas they are absorbed by its untreated area. (b) Optical microscopy image showing surface roughness generation on cellulose fibres by impregnating them with nanocomposite 10.0 wt.% carnauba wax in PECA to render them highly hydrophobic. (c) SEM image showing the surface of a cellulose fibre roughened by sub-micrometre (<200 nm) PTFE particles mixed with PECA (20.0 wt.% PTFE in PECA) to fabricate super water repellent cellulose sheets. (A) Photograph showing the difference in the wetting properties between the corner of a sheet treated with nanocomposite of 5.0 wt.% $MnFe_2O_4$ NPs in PECA (hydrophobic) and the untreated inherently hydrophilic part (a).

Magnetic actuation of the treated sheet: A simple magnet attracts the corner of the cellulose sheet treated with the magnetic nanocomposite causing the elevation of the whole piece (b-e) from ref. 117. Reproduced with permission. Copyright 2011, American Chemical Society.

Fig. 18 No lost transport processes of a superparamagnetic microdroplet in alternating magnetic fields (for movie, see Supporting Information). (a) A magnetic microdroplet was placed on an ordinary superhydrophobic surface, which was positioned above the PS nanotube layer with the distance of 2 mm. Magnets A and B were assembled outside. (b) When magnet A was switched on, the microdroplet was magnetised and attracted to fly upward. (c) Microdroplet was stuck to the surface of PS nanotubes due to strong adhesion between them. (d) When magnet A was switched off and magnet B was switched on, the direction of magnetic force was reversed and the microdroplet fell down the initial surface. (e) When both magnets were switched off, transport was stopped. (f) The superparamagnetic microdroplet was reversibly transported upward and downward by alternating magnetic fields from ref. 122. Reproduced with permission. Copyright 2007, American Chemical Society.

Fig. 19 Schematic diagram of the interactions between the superhydrophobic iron surface and the superparamagnetic microdroplet. Before the iron surface is magnetised, or after demagnetisation, the magnetic domains of iron surface are disordered, such a surface cannot lead to the magnetisation of Fe_3O_4 nanoparticles in the microdroplet, so there is no magnetic force between them, and the microdroplet resides in the low adhesive Cassie state with a layer of air below (left). After the iron plate is magnetised, the magnetic domains of iron are arrayed in orderly manner, and such surface can induce the magnetisation of Fe_3O_4 nanoparticles, so a magnetic force is produced. Meanwhile, the microdroplet would reside in the high adhesive Wenzel state

as a function of the magnetic force (right) from ref. 124. Reproduced with permission. Copyright 2008, Wiley-VCH (Weinheim, Germany).

Fig. 20 Schematic diagram (a) and sequence of frames from a video (d–e) showing a drop rotating due to the action of spinning the magnetic field. M, magnet; S, superhydrophobic surface; D, drop. The aligned particle clusters are seen to rotate counter clockwise with perspective looking down at the drop from above from ref. 125. Reproduced with permission. Copyright 2008, Elsevier Ltd.

Fig. 21 (a) Absorption of various oils and organic solvents by the superhydrophobic hybrid/PDMS sponge cured at room temperature (RT) and 100 °C. (b) Optical image of the hybrid/PDMS sponge after the absorption of diesel oil. The complete superhydrophilic properties of the pristine sponge illustrated at the right corner of the inset figure and at the bottom (black dotted circle) of the water bath. The left corner inset figure shows the complete superhydrophobic properties of the hybrid/PDMS sponge when immersed in water (silvery shine). (c, d) Graph of the absorption capacity to various oils (soybean (●), corn (◆), canola (✸), diesel (▼) and decane oils (■)) and various solvents (benzene (■), toluene (●) and chloroform (▲)) of the hybrid loaded and surface treated sponge cured at room temperature from ref. 1. Reproduced with permission. Copyright 2013, Royal Society of Chemistry.

Fig. 22 Illustration of the Removal of Oil from Water Surface through Highly Hydrophobic Fe_2O_3@C Nanoparticles under External Magnetic Field from ref. 135. Reproduced with permission. Copyright 2011, American Chemical Society.

Fig. 23 Schematic diagram of the recycling of Me-CNT sponges used for spilled oil sorption. (I) sprinkled on oil; (II) adsorb spilled oil; (III) collected by magnet; (IV) regeneration; (V) reuse from ref. 142. Reproduced with permission. Copyright 2013, American Chemical Society.

Fig. 24 Optical images for the removal of hexadecane spreading over the water surface using the as-prepared bulk material (a)–(c). The oil-absorbed bulk material can be removed easily from water under a magnetic field (d). Hexadecane absorbed in the bulk material can be removed directly by burning in air, allowing the bulk material to exhibit superhydrophobicity again (e) and (f) from ref. 143. Reproduced with permission. Copyright 2013, Elsevier Ltd.

Fig. 25 Field emission (FE-SEM) images of (a) structured Ti substrate, (b) PTFE/Ti, (c) TiO_2-PTFE/Ti and (d) TiO_2-PTFE/Ti with high magnification. The inset of (a,b) is also magnified images from ref. 154. Reproduced with permission. Copyright 2012, Wiley-VCH (Weinheim, Germany).

Fig. 26 Photographs of magnetic separation of Fe_3O_4/PS[im-C_6TEMPO]Cl in the Montanari oxidation of benzyl alcohol (the excess hypochlorite was destroyed by drops of saturated Na_2SO_3) from ref. 165. Reproduced with permission. Copyright 2014, Wiley-VCH (Weinheim, Germany).

Fig. 27 Superhydrophobicity of PAMA/BMPA nanoparticle multilayer-coated colloidal films. Water droplet on (A) silica colloidal films without nanoparticles and (B) (BMPA-Fe_3O_4/PAMA/BMPA-QDgreen/PAMA)$_3$ multilayer-coated silica colloidal films. In this case, the water contact angles obtained from bare and multilayer-coated colloidal films were approximately (A) 118° and (B) 153°, respectively. (C) Photographic image of a superhydrophobic surface prepared from magnetic luminescent colloidal films. Note that for samples in (A-C), the outermost surface of colloidal films was coated with fluoroalkylsilane polymer from ref. 170. Reproduced with permission. Copyright 2011, American Chemical Society.

Fig. 28 Picture of 24-well SSAP made of 24 superhydrophobic PC-modified polypropylene tubes each of which has specific dimensions of 1.5 cm (inner diameter) by 1.5 cm (height) (left) and the schematic representation of the SSAP-based magnetic electrochemical immunoassay for SjAb detection (right). (A) Capture of the SjAb analyte to the SjAg-immobilised magnetic particles (MP–SjAg); (B) binding of AuNP-labelled secondary antibodies (AuNP–Ab); (C) catalytic enlargement of AuNPs in the copper enhancer solution; (D) dissolution of copper metal deposited on the AuNPs in an acid; and (E) square-wave stripping voltammetry (SWSV) detection of the released copper ions from ref. 179. Reproduced with permission. Copyright 2012, Elsevier Ltd.

Fig. 29 (A) Microfluidic device based on marbles. (B) Rotation of the upper PP film (A→B→C subsequent stages). The black ball is the ferrofluidic marble from ref. 193. Reproduced with permission. Copyright 2008, American Chemical Society.

Fig. 30 (a) When a droplet is placed in the middle of a concave-shaped bowl with superhydrophobic surface, the droplet rolls off toward the centre due to the gravitational force. (b) Schematic diagram of single droplet transportation on a superhydrophobic magnetic elastomer. (c) A series of images showing fast droplet transportation of a 25 μL methyl orange indicator on the superhydrophobic magnetic elastomer from ref. 195. Reproduced with permission. Copyright 2013, Wiley-VCH (Weinheim, Germany).

Fig. 31 Schematics of the assembly configuration, optical micrographs and simulation patterns of applied external magnetic fields for a) single patch magnetic supraparticles, b) bi-patch magnetic supraparticles, and c) tri-patch or the so-called ‘‘Mickey Mouse’’ magnetic supraparticles. The scale bars are 500 mm in length. The magnetic simulation pattern is drawn to scale; one square

on the grid represents an area of 1 mm^2 from ref. 196. Reproduced with permission. Copyright 2010, Wiley-VCH (Weinheim, Germany).

Table 1.

No.	Basic materials	Superhydrophobic magnetic substrate/surface	Magnetic property	Contact angle (degree)	Ref.
1.	Metallic magnetic nanoparticles	Polymethylpetene substrate	-	153°	48
2.	PVA and $FeAc_2$	Carbon nanofibers	Ferromagnetism	156° ± 2.6°	49
3.	Fluorinated core/shell magnetic microsphere/PVDF	Nanofibers	Superparamagnetism	152.4° ± 0.4°	50
4.	Fe_3O_4@SiO_2@MPS/HFBA	Copper wafer substrate	Superparamagnetism	154.6°	51
5.	Polystyrene/silica/ maghemite film	Silicon wafer substrate	Superparamagnetism	157°	52
6.	Fluorinated copper-ferrite nanorods	Copper substrate	-	156.5° ± 2.1°	53
7.	Fluorinated carbonyl iron particles	-	-	159.6°	54
8.	Fluorinated magnetic nanoparticles	-	-	172.8° ± 0.2°	55
9.	FD-POSS/Fe_3O_4 magnetic liquid marble	-	-	171.1°	76
10.	PU foam/Fe_3O_4/ PTFE	Foam	Superparamagnetism	>160°	93
11.	PU sponge/ $Fe(NO_3)_3$ or $Co(NO_3)_2$ or $Ni(NO_3)_2$	Foam	Superparamagnetism	152°	94
12.	TEOS/ HDTES/ Fe_3O_4	Polyester surface	Paramagnetism	>150°	112
13.	Metal nano particles/ octadecylthiol	Sponges/textile fabrics	-	>150°	113
14.	ECA/$MnFe_2O_4$/ PTFE	Cellulose fabrics	Superparamagnetism	>150°	117
15.	Spherical magnetic fluid	Nanowire surface	Paramagnetism	145° to 160°	118
16.	Superparamagnetic microdroplet	Aligned polystyrene surface	Superparamagnetism	~160°	122
17.	Ferrofluid	Aluminum or Al alloy substrate	Ferromagnetism	162°	123

18.	Superparamagnetic fluid	Polystyrene nanotube surface	Ferromagnetism	157°	124
19.	Paramagnetic fluid	LDPE surface	Paramagnetism	>160°	125
20.	Ferrofluid	Copper substrate	Ferromagnetism	~175°	127
21.	Ferrocene and dichlorobenzene	CNT sponge	Ferromagnetism	>145°	142
22.	PTFE with MWCNT/Fe_3O_4	Bulk material	Superparamagnetism	~158°	143
23.	Co, Ni and CoNi alloy	Nanoparticles/NPs alloy films	Ferromagnetism	~152-157°	166
24.	Fe_3O_4/BMPA/QD/PAMA	Nanoparticles	Superparamagnetism	>153°	170
25.	Magnetic hydrogel beads	Polystyrene substrate	-	>150°	177
26.	Polysiloxane/ Fe_3O_4 nanocomposite	Glass or polycarbonate substrate	-	156-158°	197

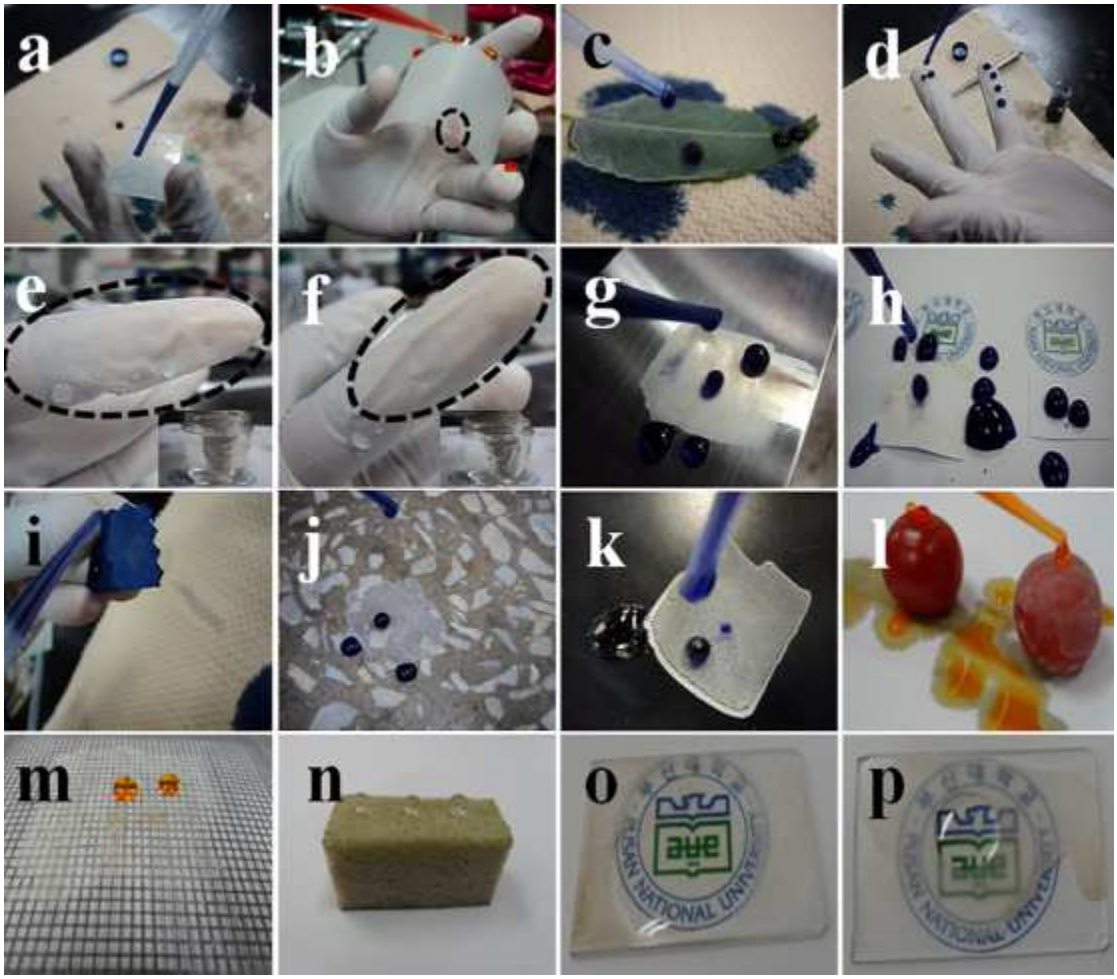

Fig. 1

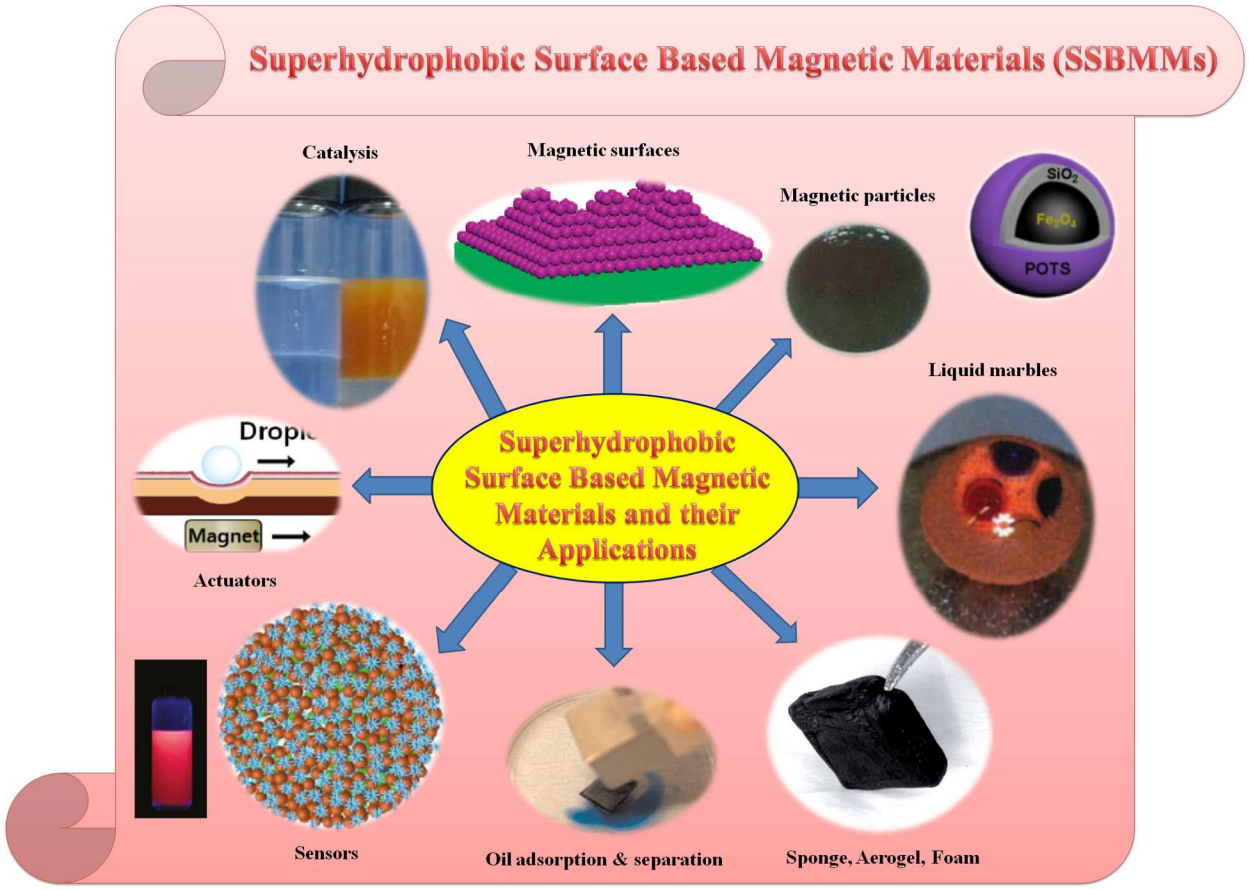

Fig. 2

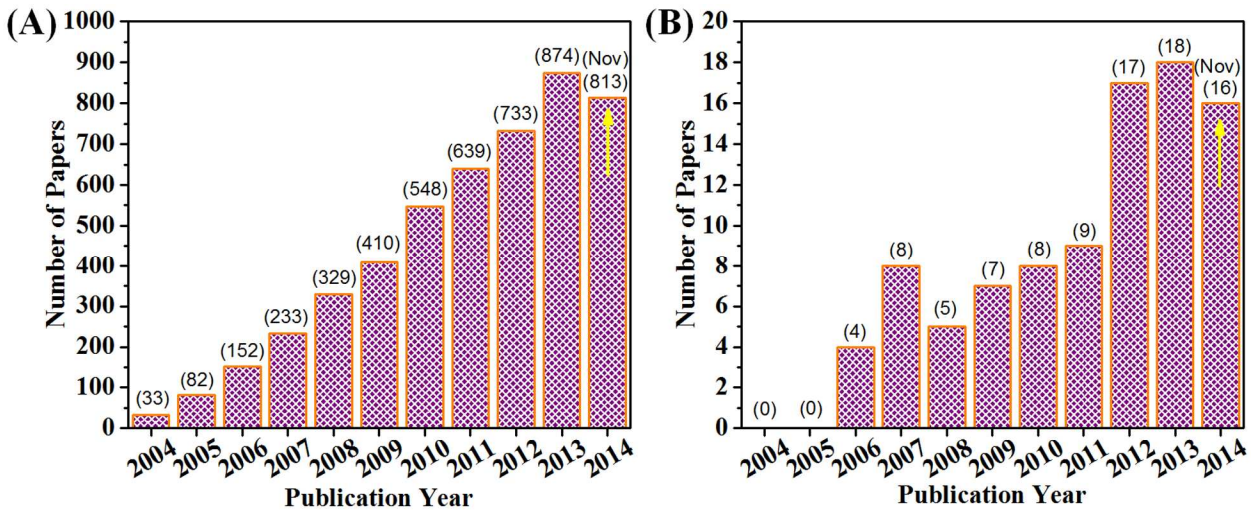

Fig. 3

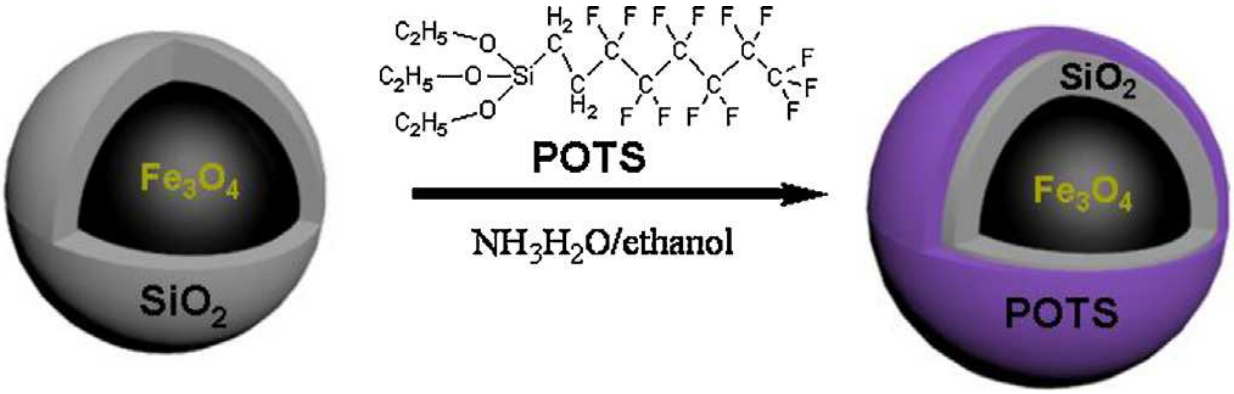

Fig. 4

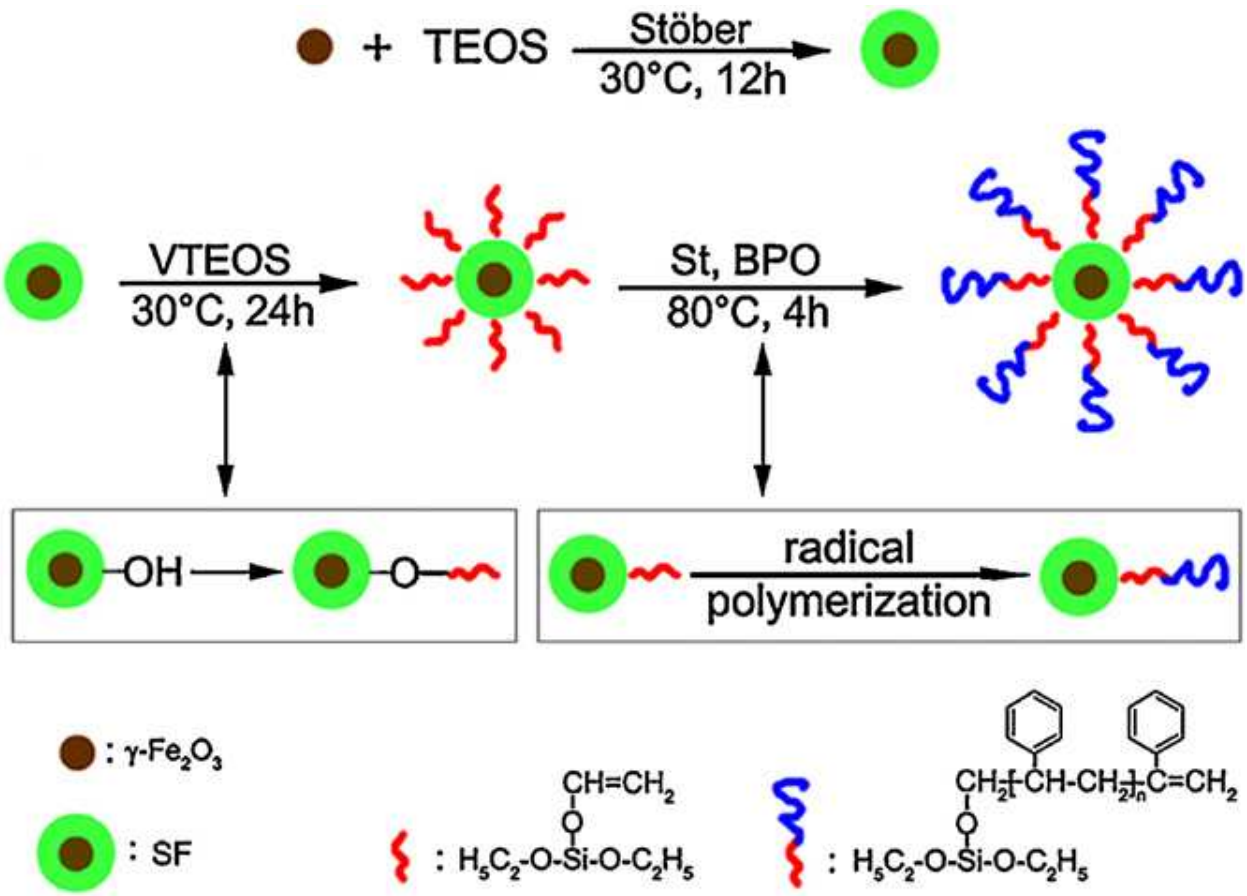

Fig. 5

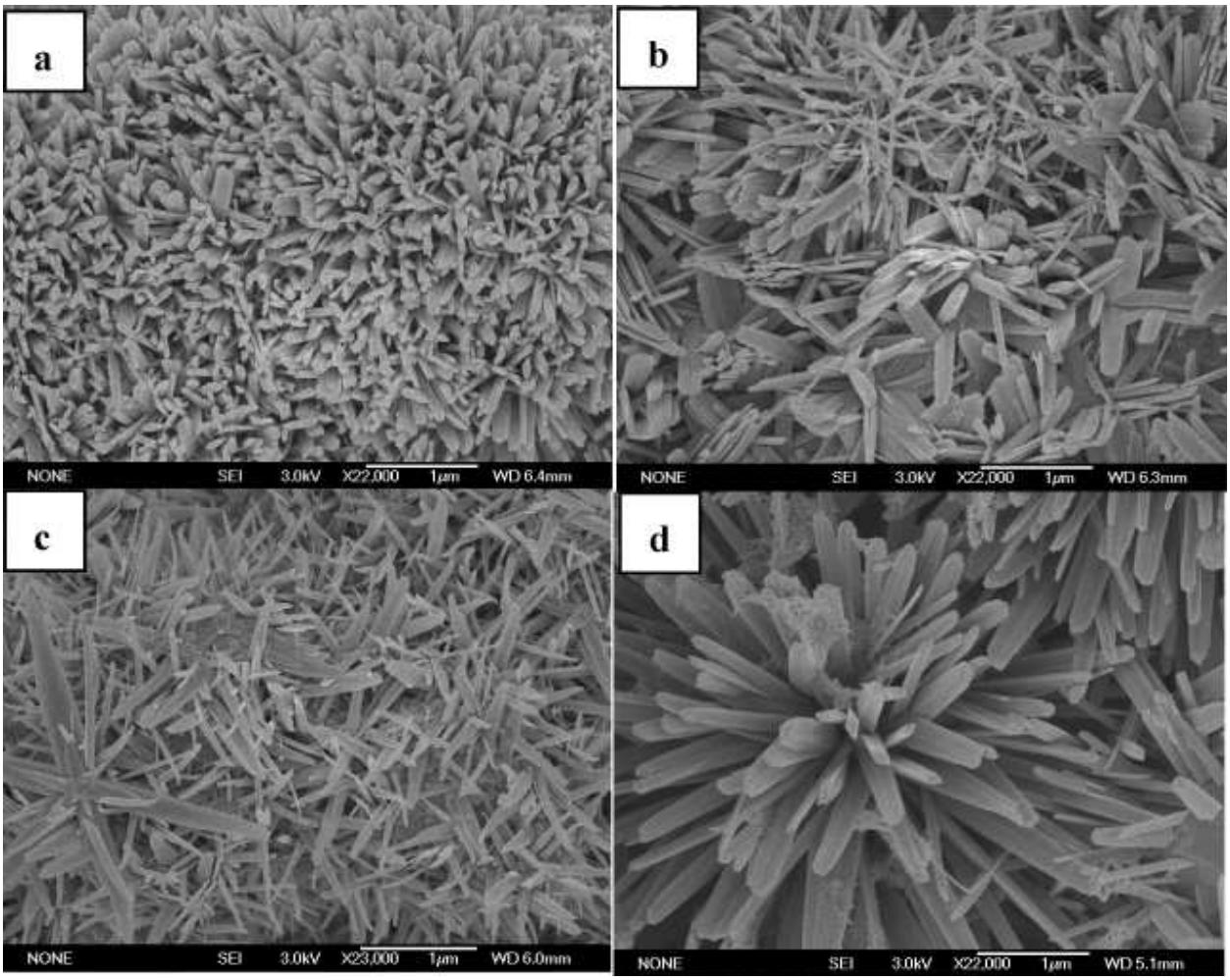

Fig. 6

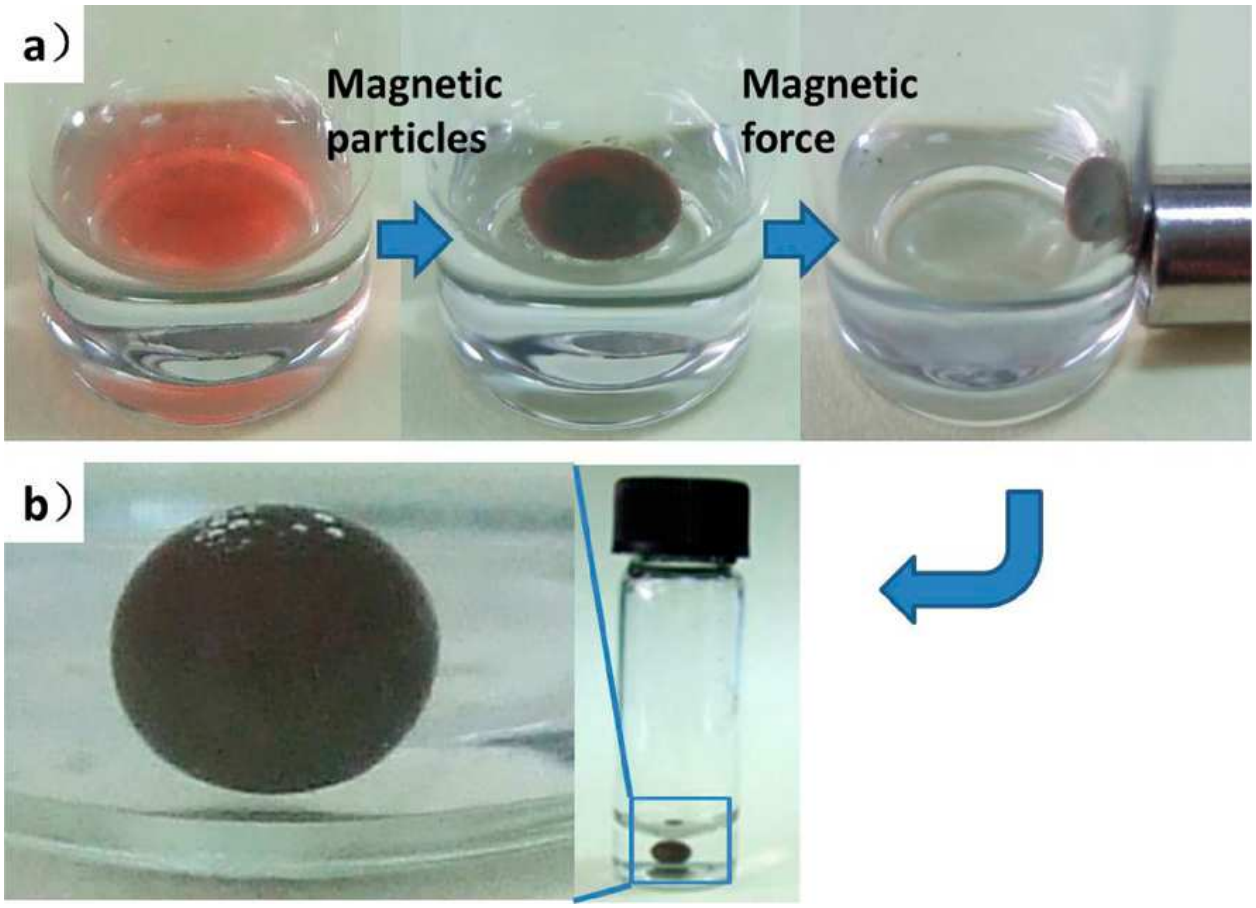

Fig. 7

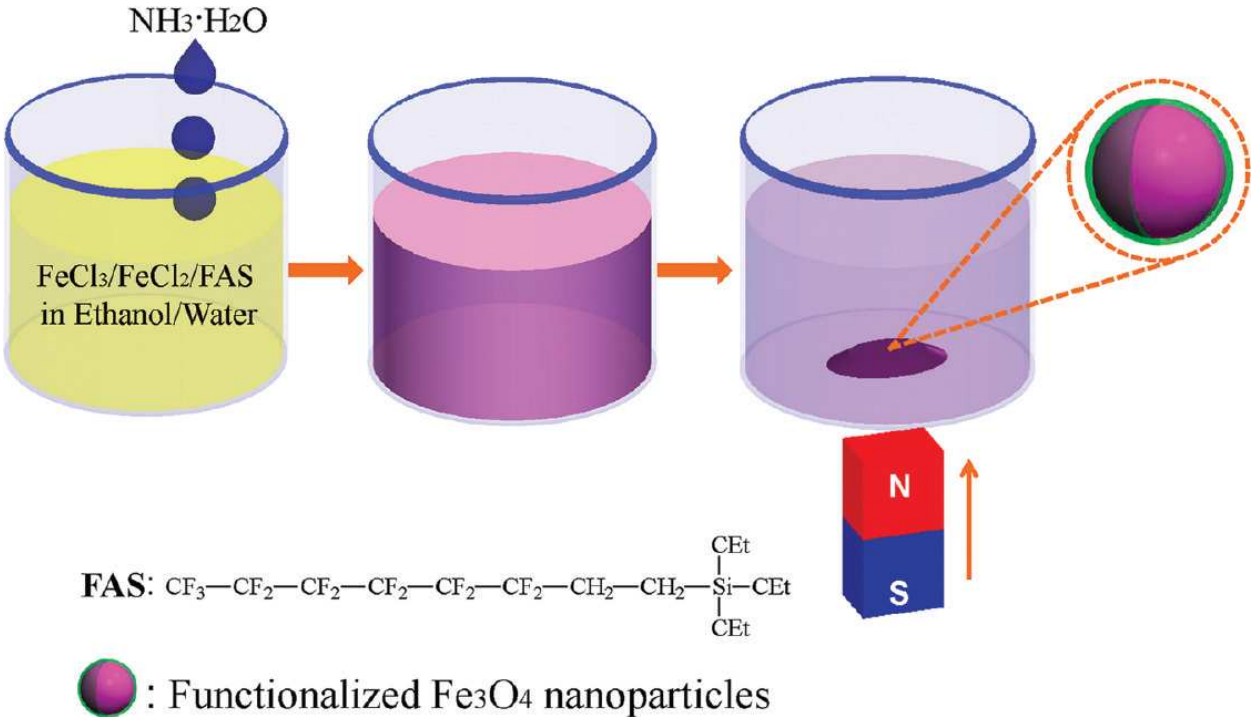

Fig. 8

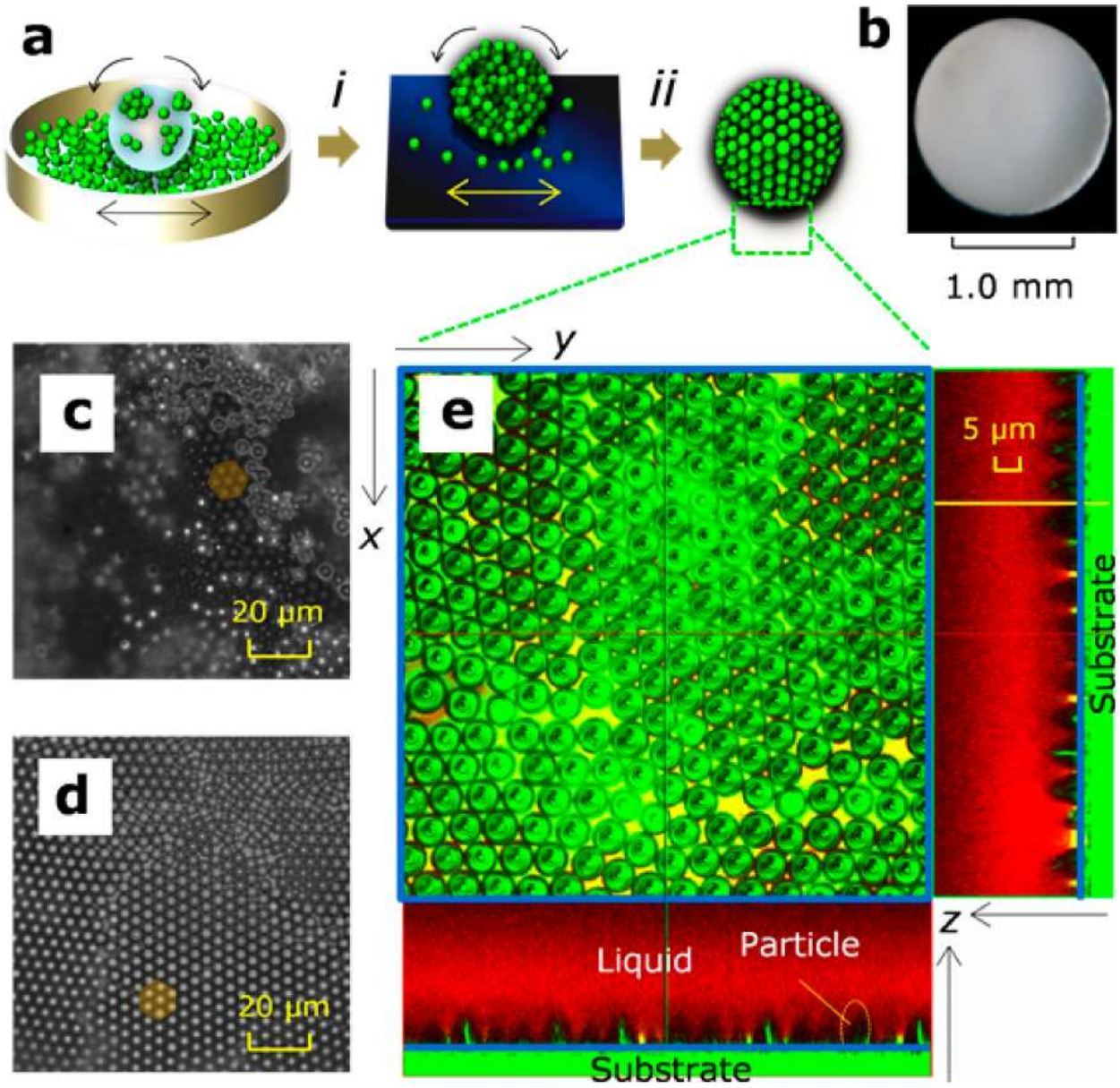

Fig. 9

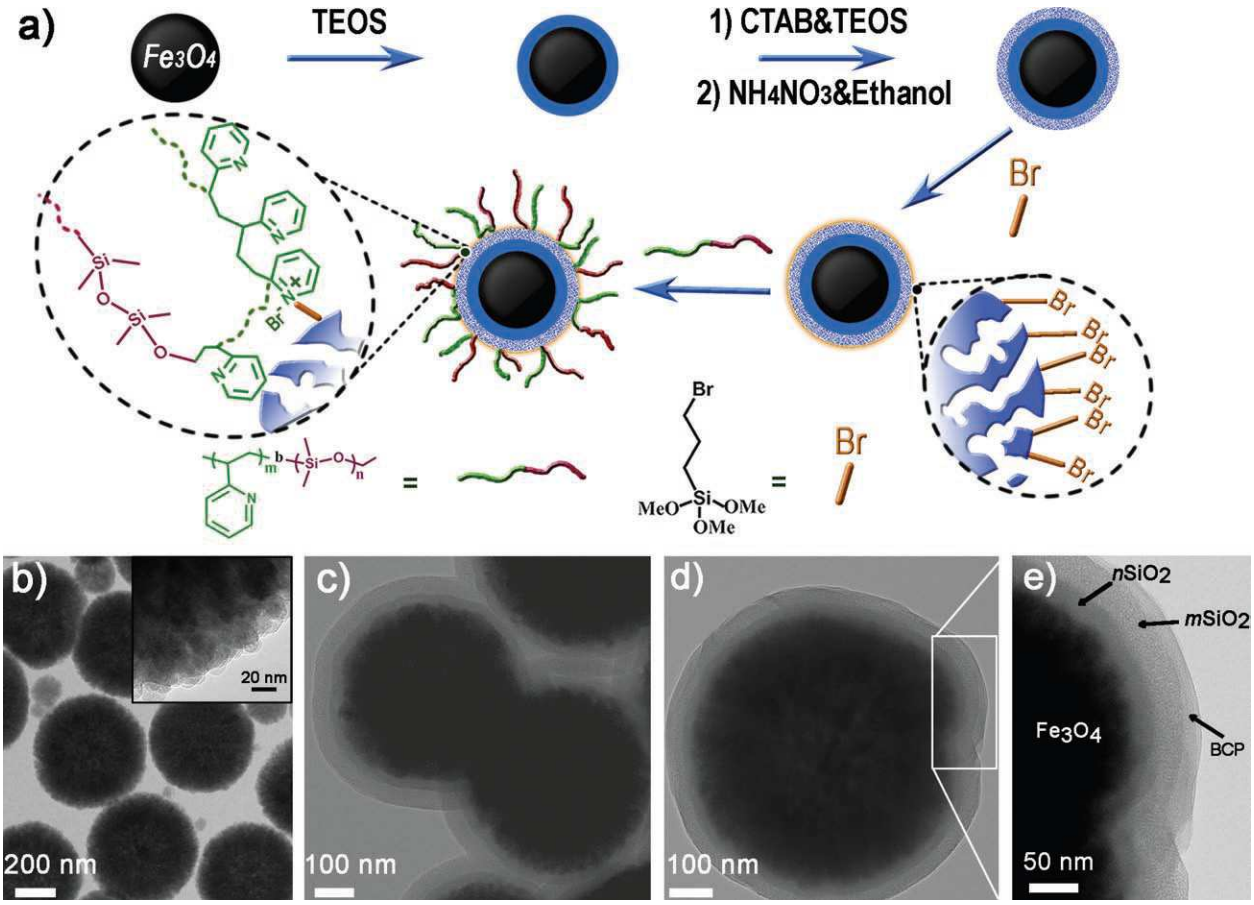

Fig. 10

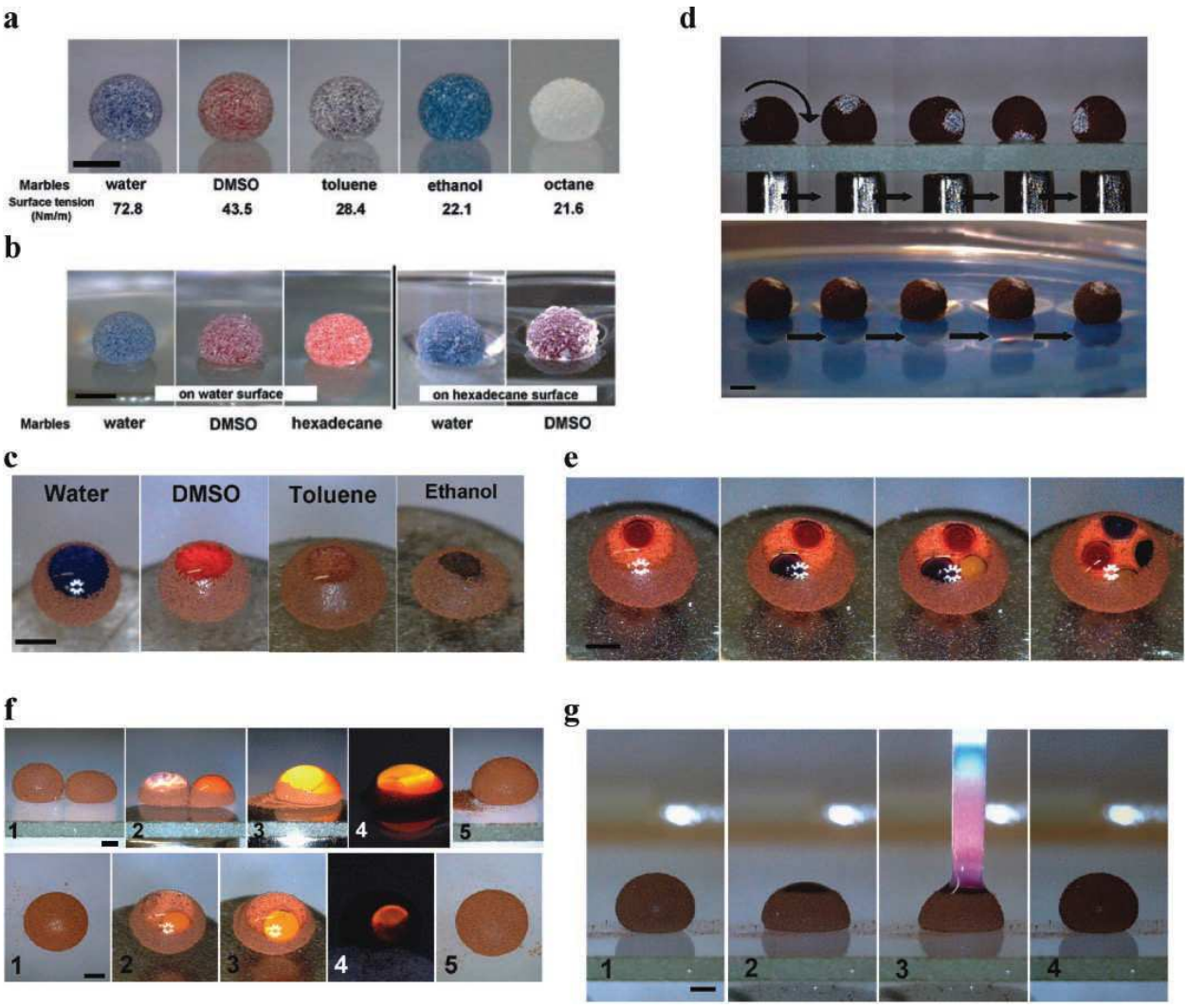

Fig. 11

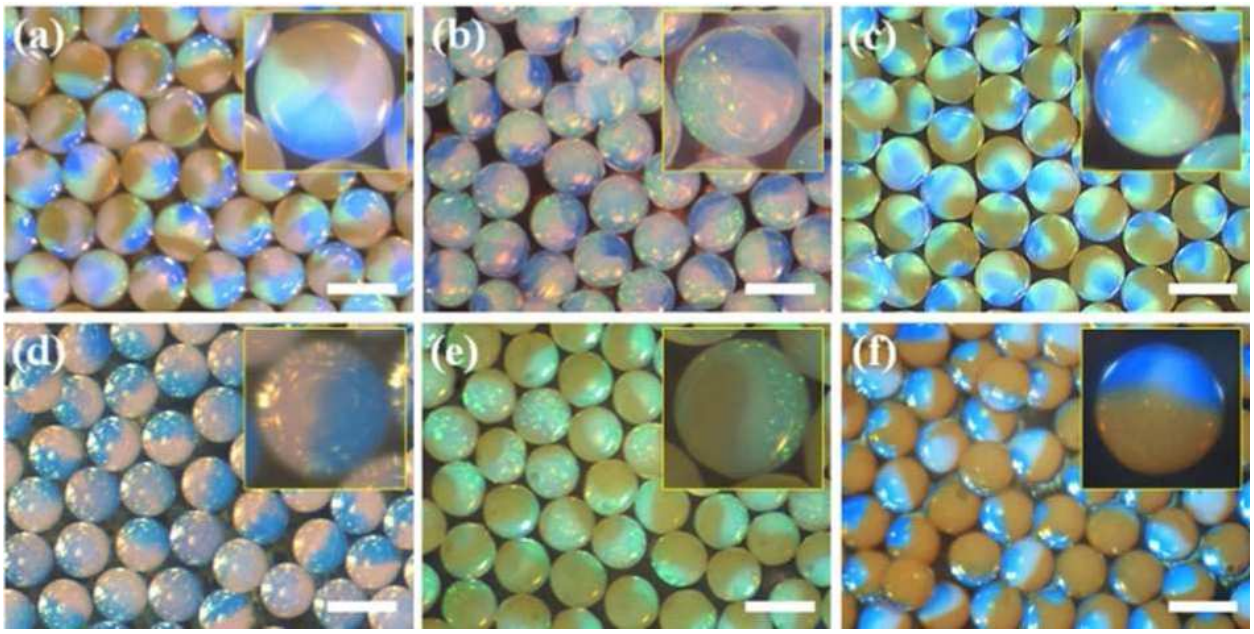

Fig. 12

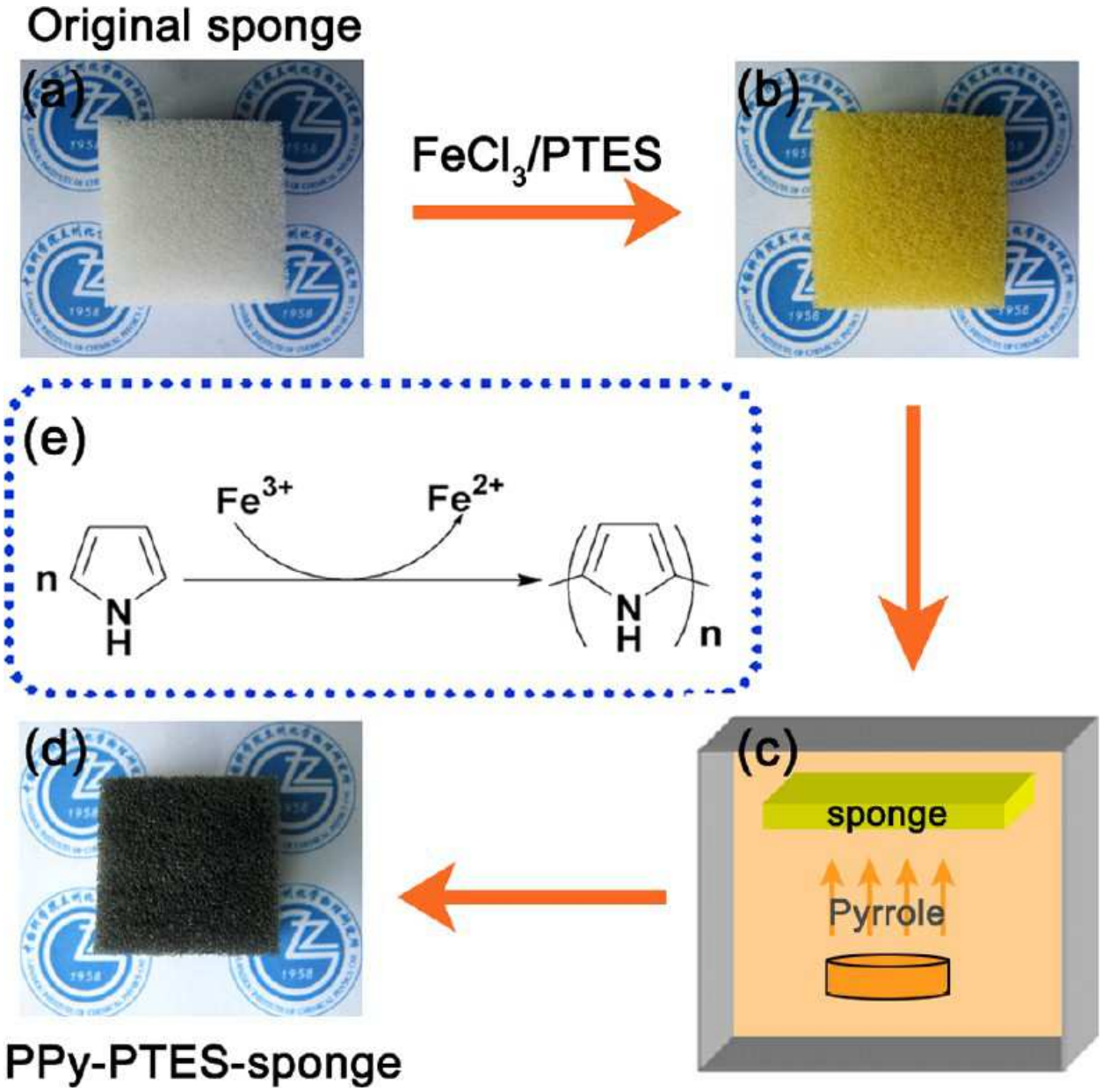

Fig. 13

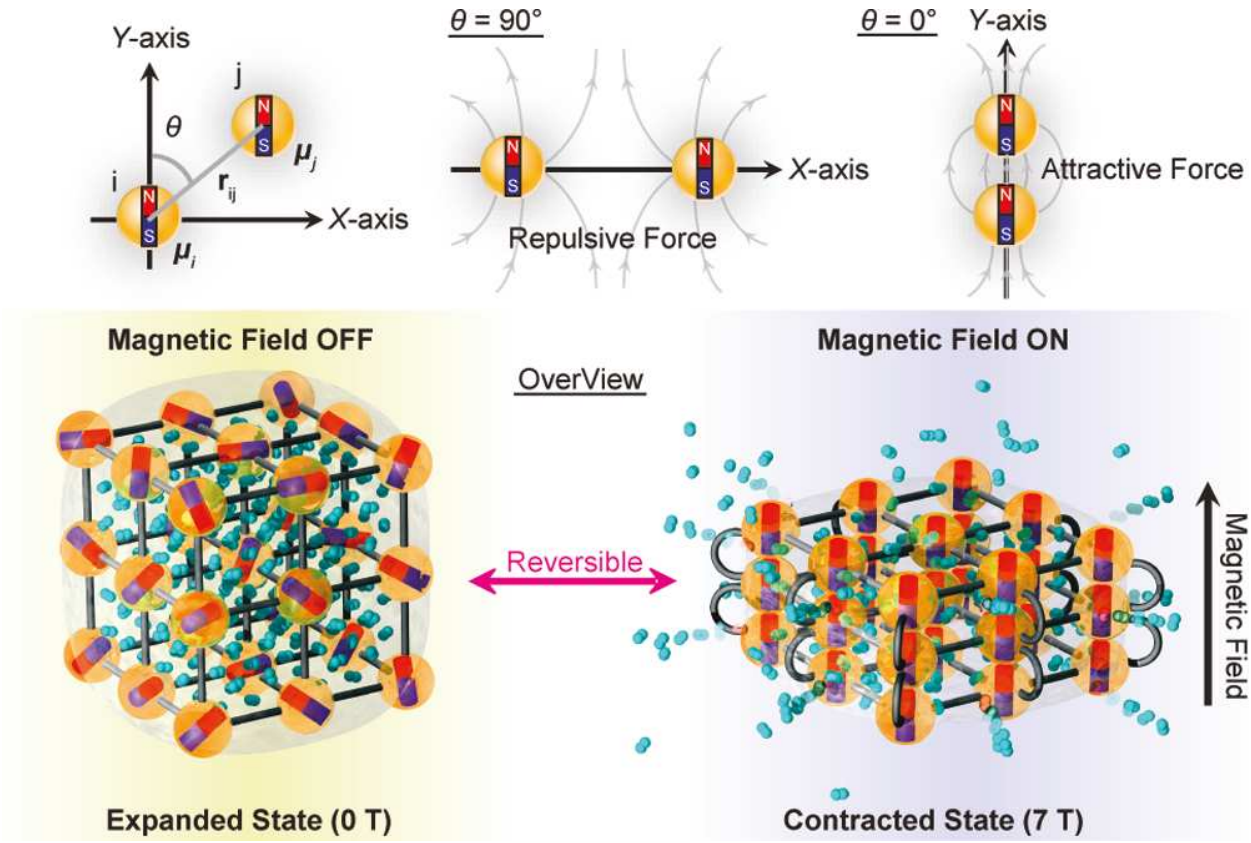

Fig. 14

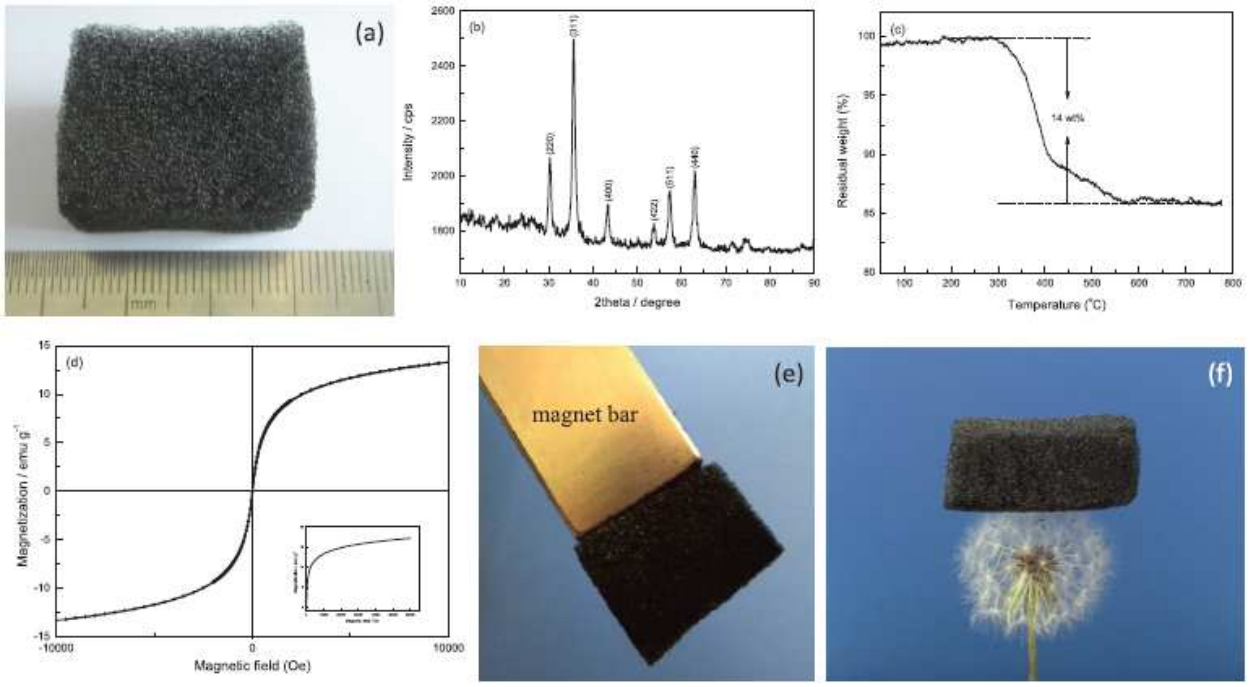

Fig 15

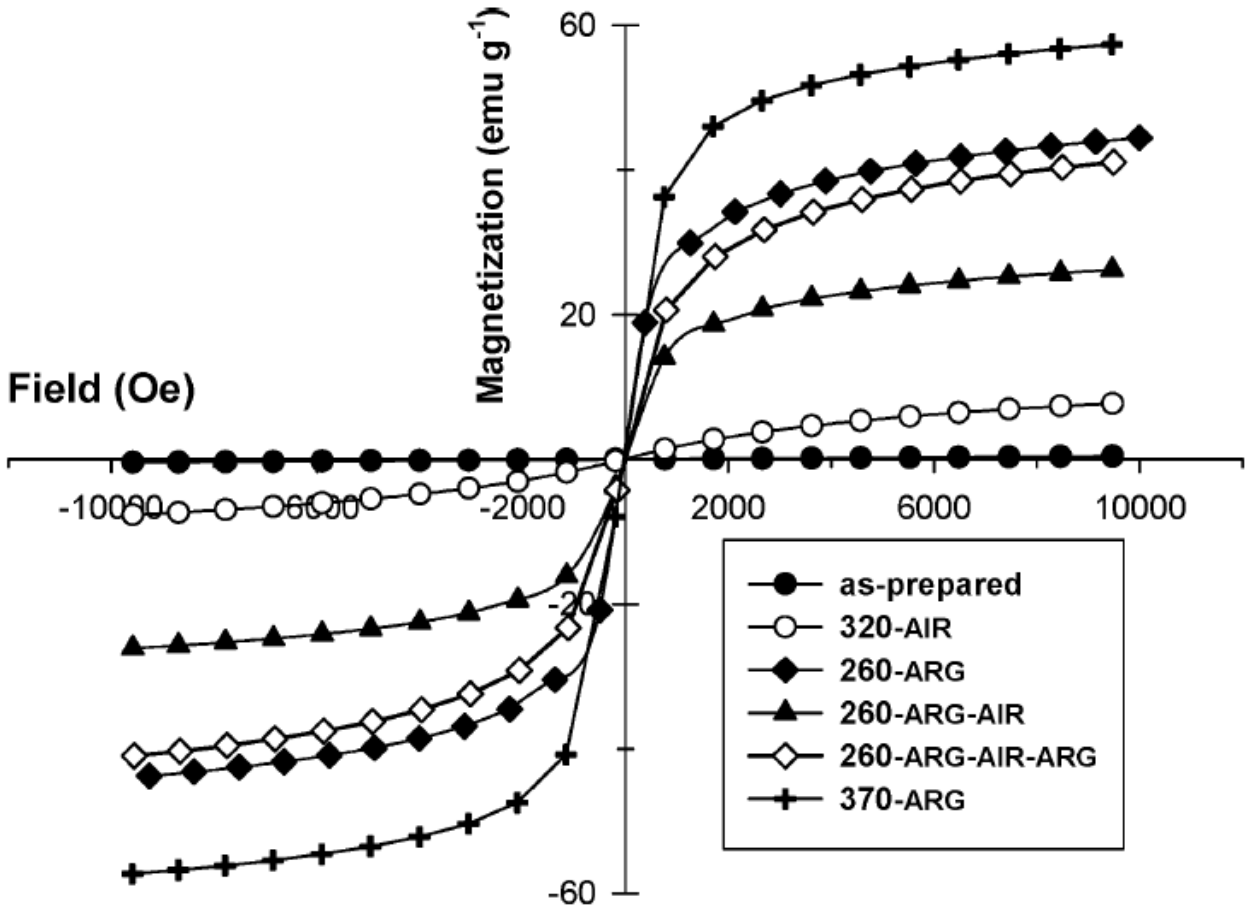

Fig. 16

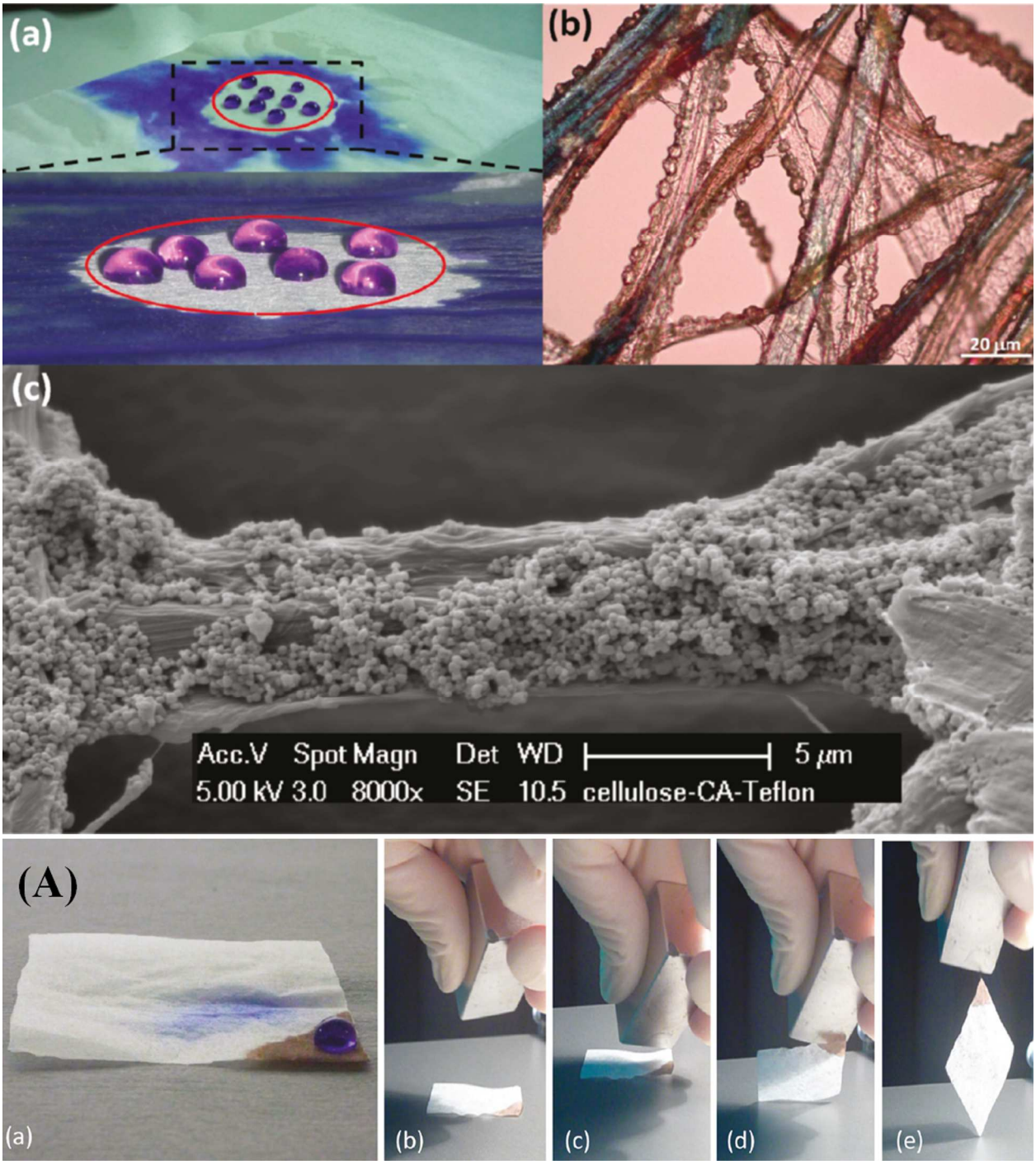

Fig. 17

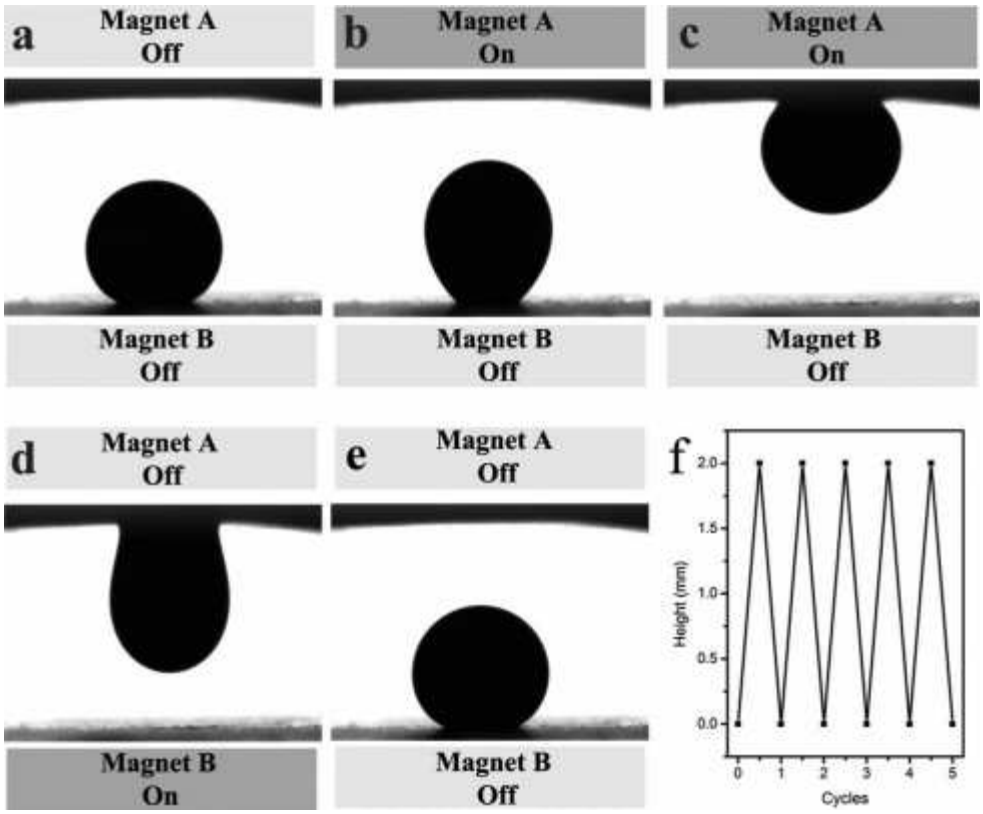

Fig. 18

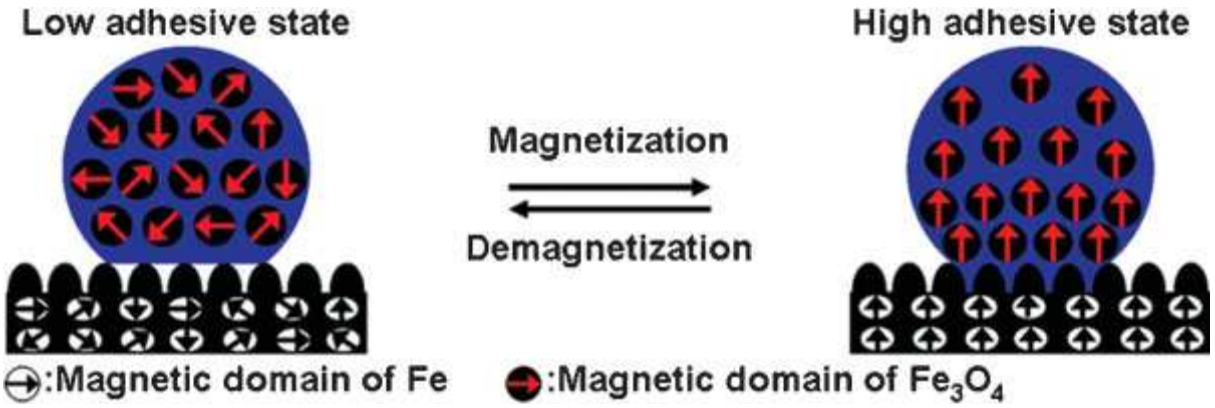

Fig. 19

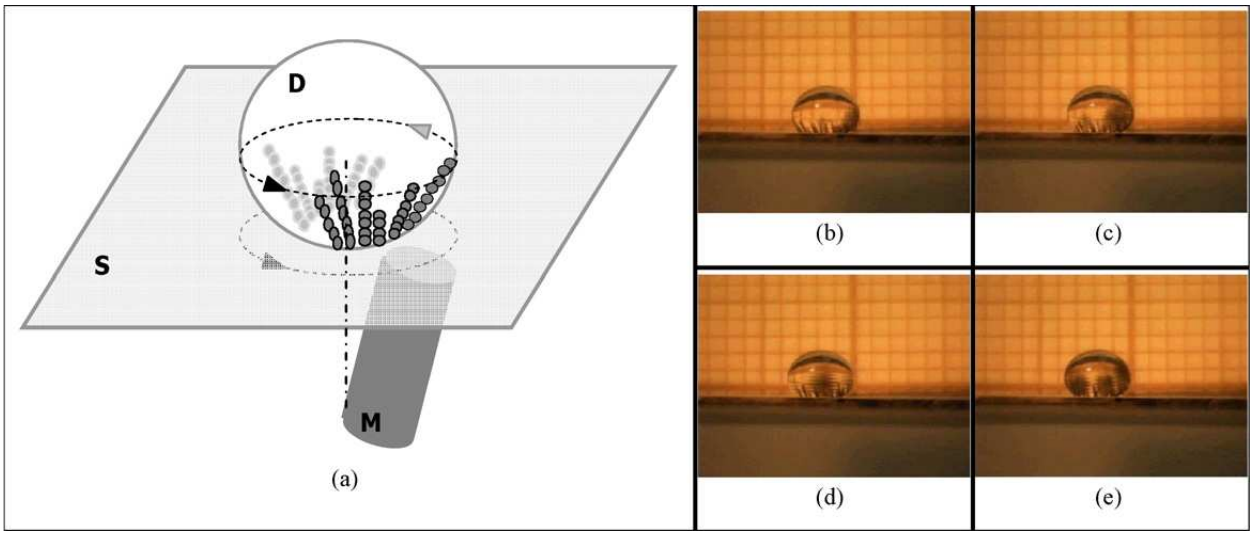

Fig. 20

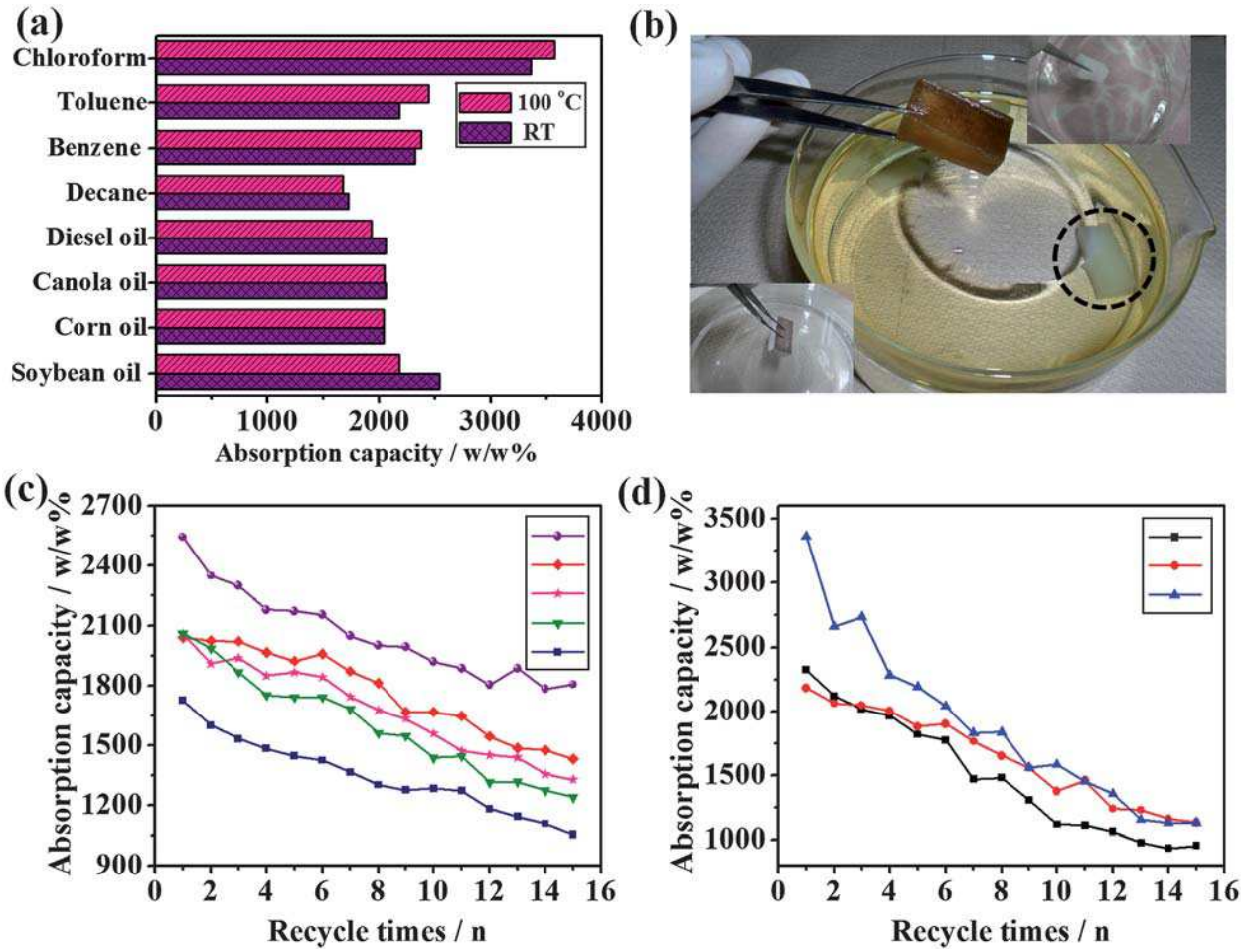

Fig. 21

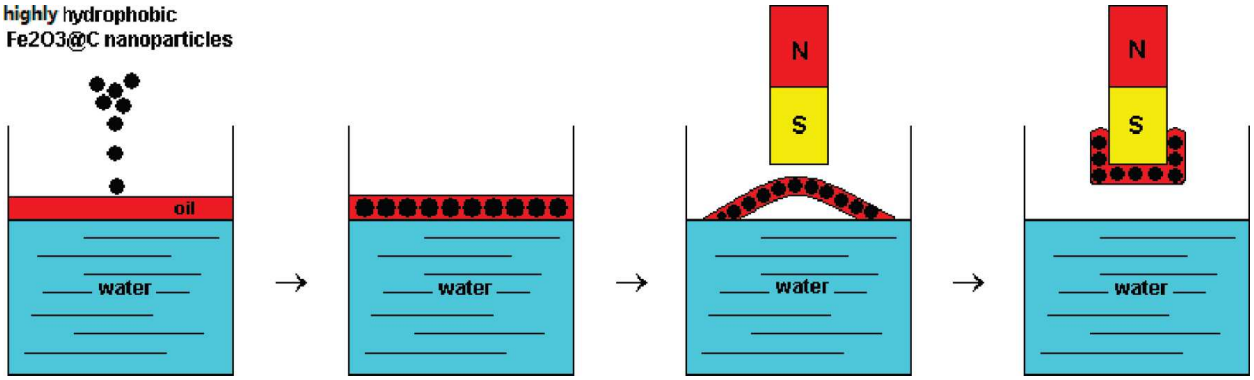

Fig. 22

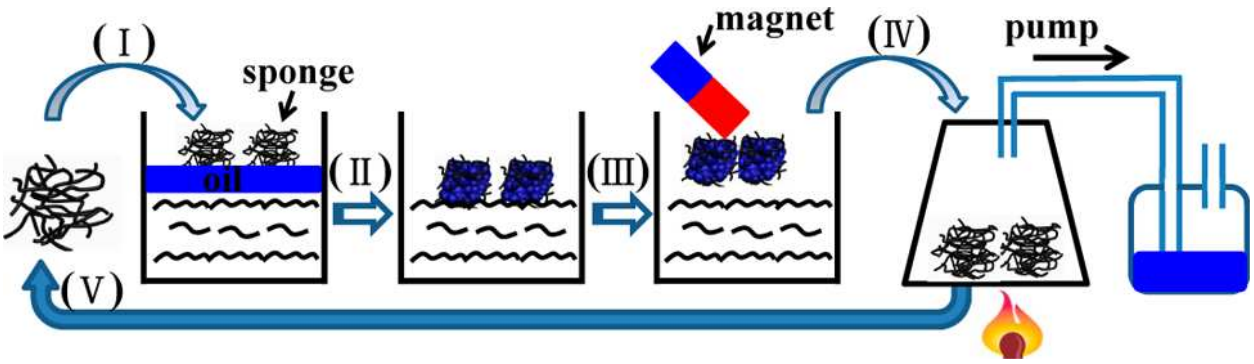

Fig. 23

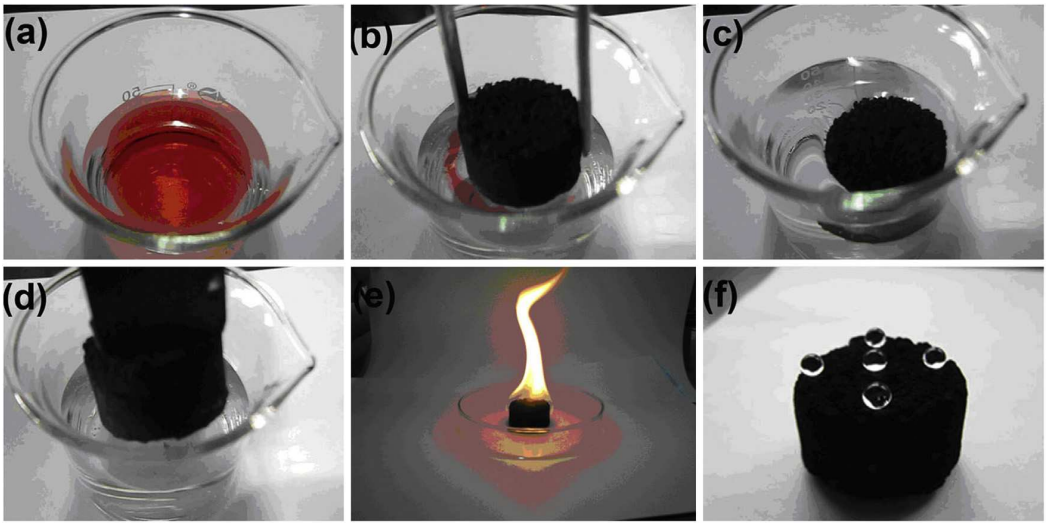

Fig. 24

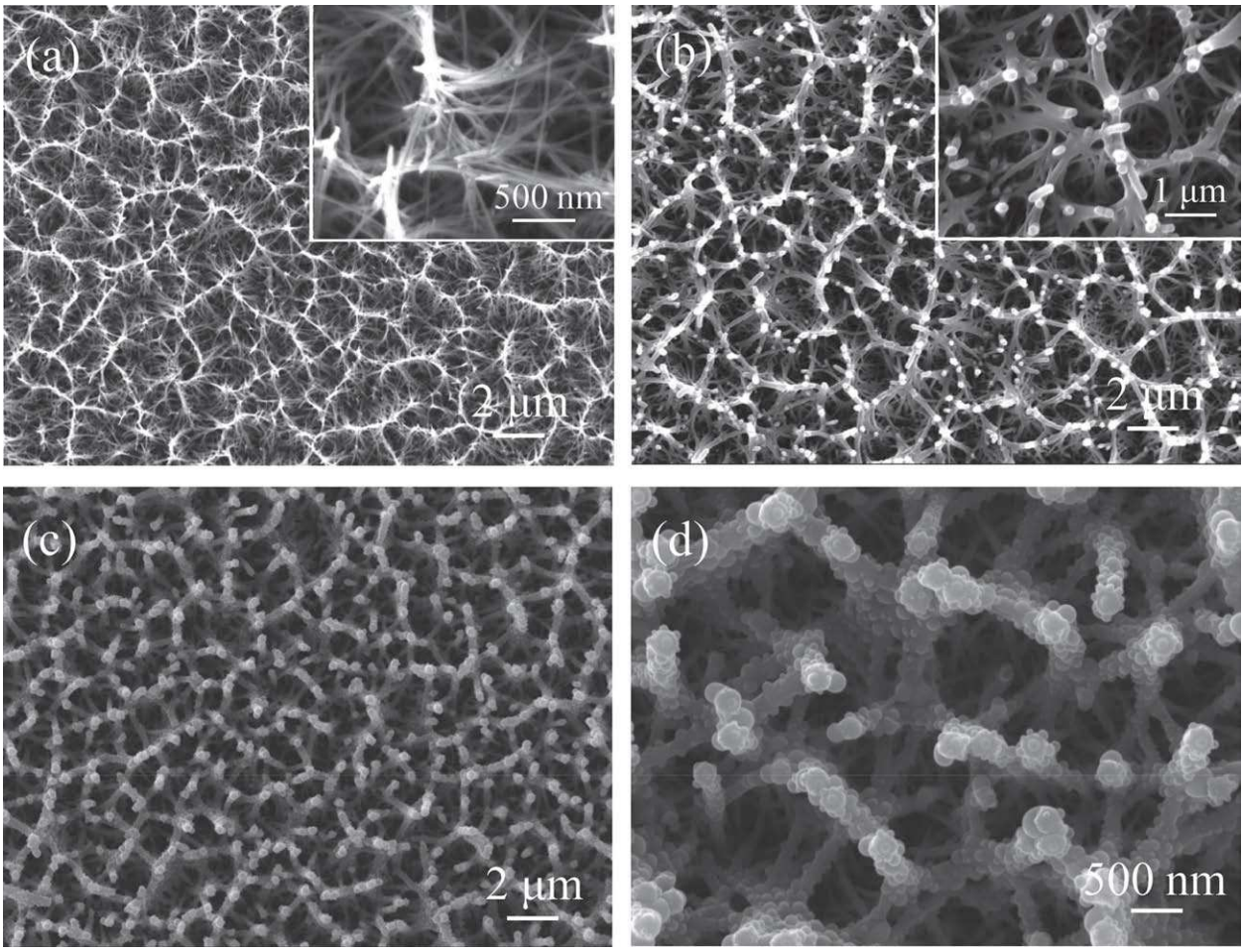

Fig. 25

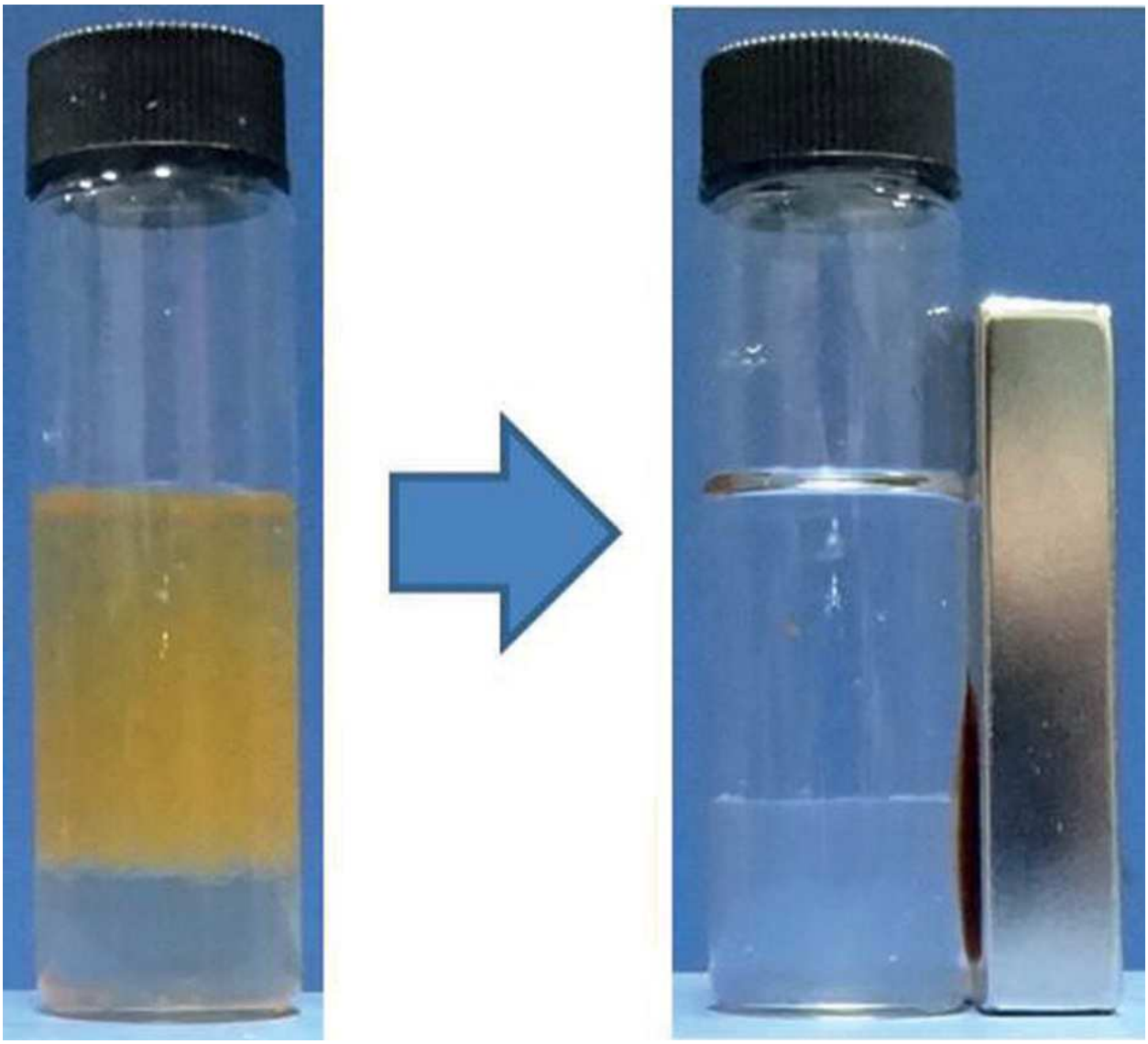

Fig. 26

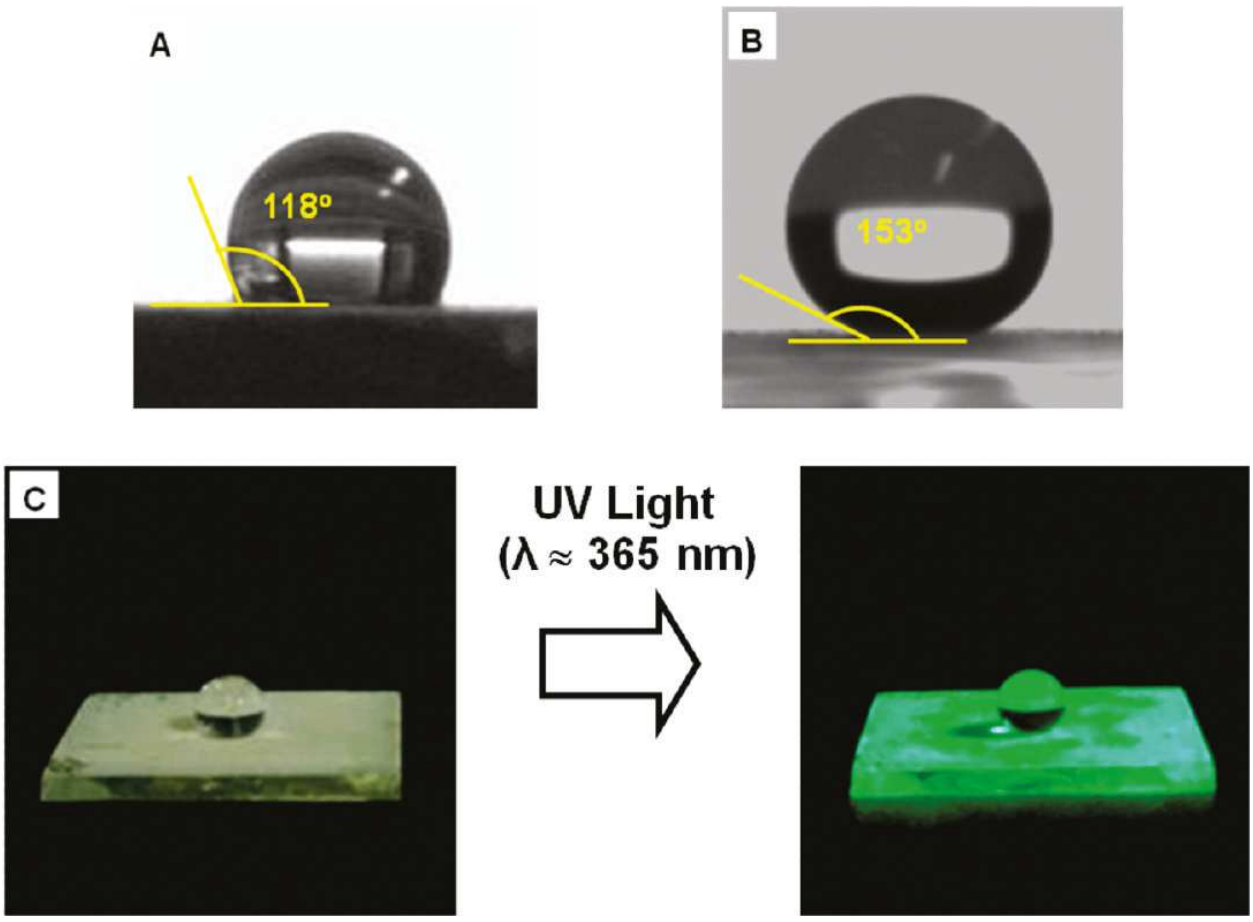

Fig. 27

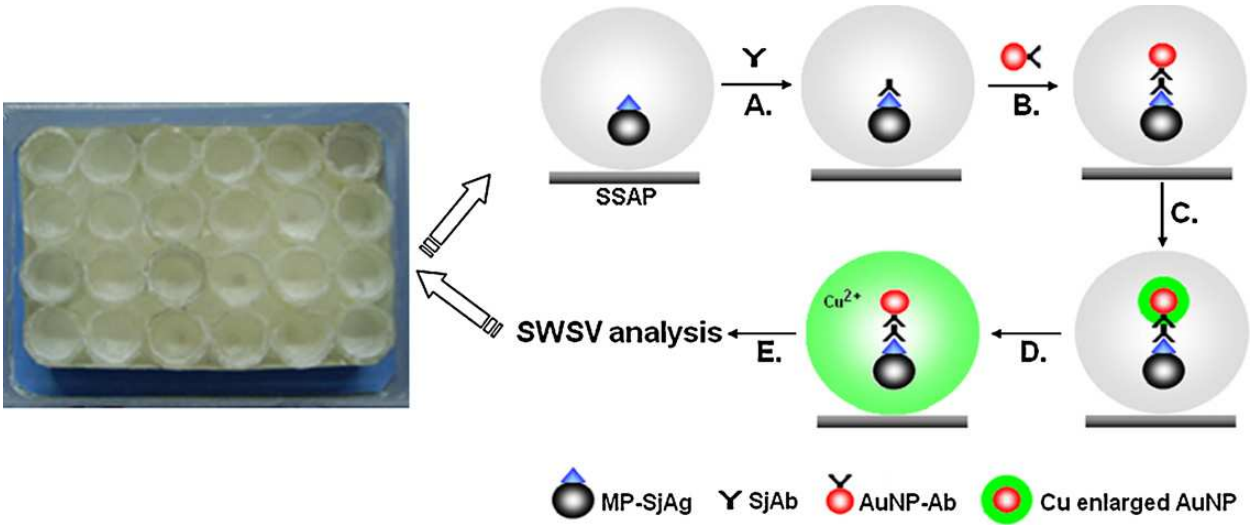

Fig. 28

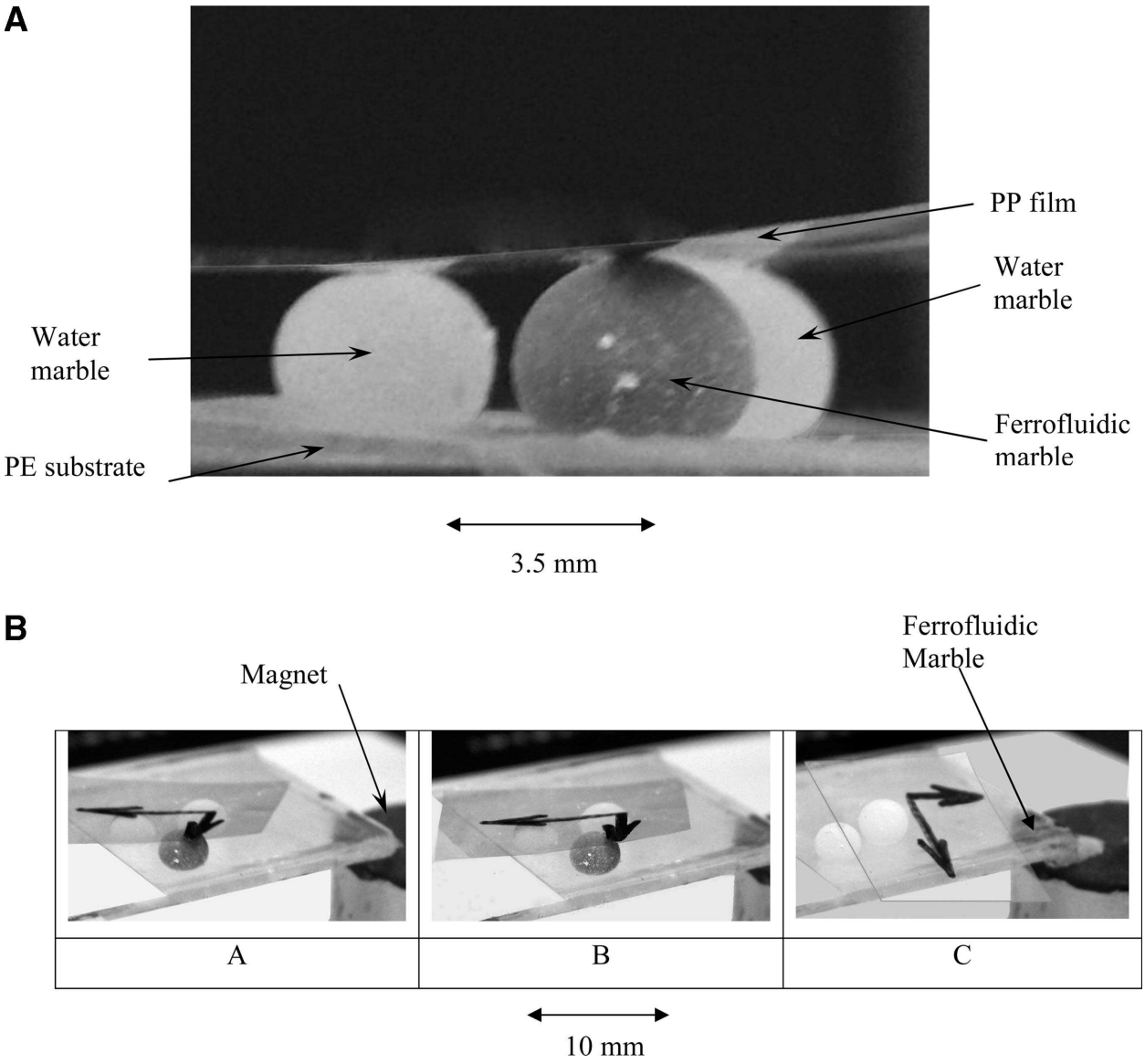

Fig. 29

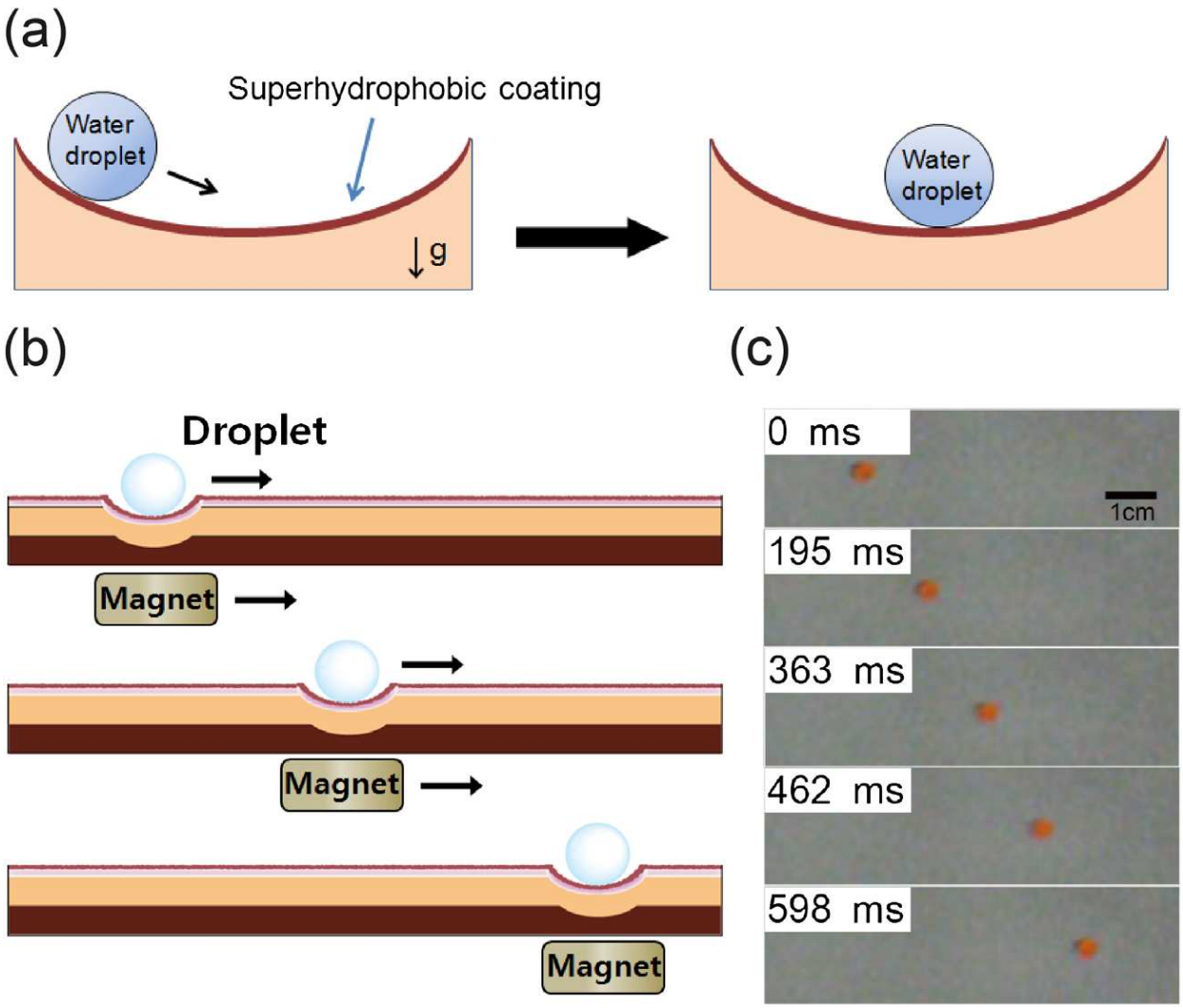

Fig. 30

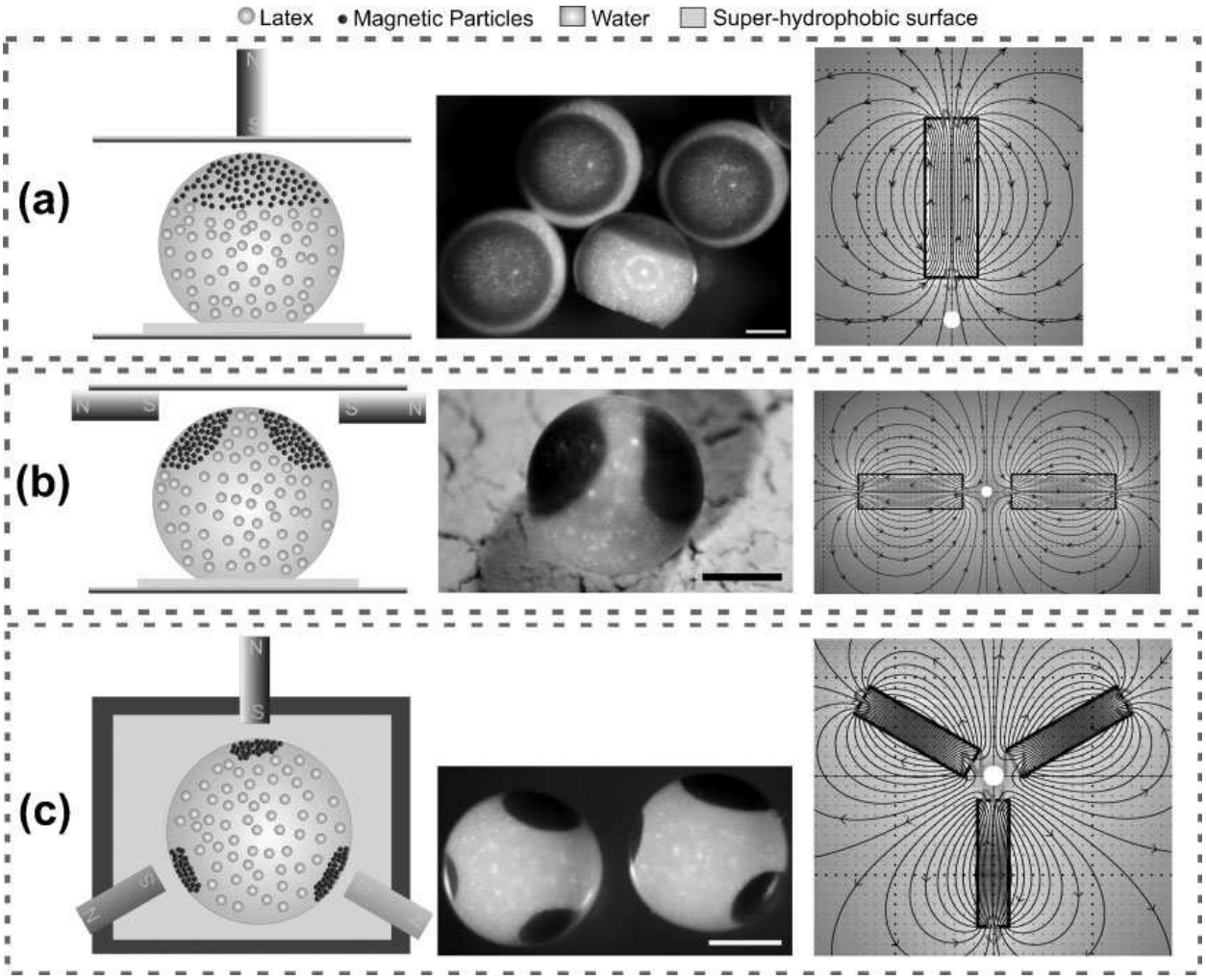

Fig. 31